AMERICAN UNIVERSITY OF BEIRUT

THERMALLY ACTIVATED PERSULFATE AS AN
EFFICIENT AND SUSTAINABLE SOLUTION FOR THE
REMOVAL OF PHARMACEUTICAL COMPOUNDS FROM
WATER: APPLICATION TO HOSPITAL EFFLUENTS

by
AL-MUTHANNA FAWWAZ TUQAN

A thesis
Submitted in partial fulfillment of the requirements
for the degree of Master of Science
to the Department of Chemistry
of the Faculty of Arts and Sciences
at the American University of Beirut

Beirut, Lebanon
February, 2015

AMERICAN UNIVERSITY OF BEIRUT

THERMALLY ACTIVATED PERSULFATE AS AN EFFICIENT AND SUSTAINABLE SOLUTION FOR THE REMOVAL OF PHARMACEUTICAL COMPOUNDS FROM WATER: APPLICATION TO HOSPITAL EFFLUENTS

by
AL-MUTHANNA FAWWAZ TUQAN

Approved by:

_____

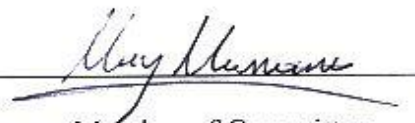Dr. Antoine Ghauch, Associate Professor
Chemistry

Advisor

_____

Dr. Faraj Hasanayn, Associate Professor
Chemistry

Member of Committee

_____

Dr. May Massoud, Associate Professor
Environmental Health

Member of Committee

_____

Dr. Walid Saad, Assistant Professor
Chemical Engineering Program

Member of Committee

Date of thesis defense: February 4, 2015

AMERICAN UNIVERSITY OF BEIRUT

THESIS, DISSERTATION, PROJECT RELEASE FORM

Student Name: _____TUQAN_____AL-MUTHANNA_____FAWWAZ_
                             Last   First   Middle

⬤ Master's Thesis   ◯ Master's Project   ◯ Doctoral Dissertation

☐   I authorize the American University of Beirut to: (a) reproduce hard or electronic copies of my thesis, dissertation, or project; (b) include such copies in the archives and digital repositories of the University; and (c) make freely available such copies to third parties for research or educational purposes.

☒   I authorize the American University of Beirut, **three years after the date of submitting my thesis, dissertation, or project,** to: (a) reproduce hard or electronic copies of it; (b) include such copies in the archives and digital repositories of the University; and (c) make freely available such copies to third parties for research or educational purposes.

_____February 6, 2015_____

Signature   Date

ACKNOWLEDGMENTS

AN ABSTRACT OF THE THESIS OF

Al-Muthanna Fawwaz Tuqan   for   Master of Science
                                                   Major: Chemistry

Title: Thermally activated persulfate as an efficient and sustainable solution for the removal of pharmaceutical compounds from water: Application to hospital effluents.

Thermally activated persulfate (TAP) has been recently introduced as an advanced oxidation process (AOP) for water treatment. In this thesis, we study the feasibility and efficiency of TAP for the removal of pharmaceutical compounds from water. In order to study the ability of TAP to remove pharmaceuticals from aqueous solutions, three different active ingredients from two commonly used pharmaceutical classes have been chosen to be studied in this thesis. Experimental studies were performed on non-steroidal anti-inflammatory Naproxen and Ibuprofen, as well as on Beta-Blocker Bisoprolol Fumarate. Reaction rates were calculated alongside with studying factors affecting reaction rates such as temperature, pH, concentrations and inorganic additives effect. Furthermore reaction activation energies and reaction stoichiometric efficiency (RSE) were calculated. Moreover, degradation of pharmaceuticals and their % mineralization have been monitored, as well as by-product evolution and degradation in an attempt to propose degradation pathways and determine by-product identity. Matrix effect was studied in the form of hospital effluent spiked with pharmaceuticals and treated with TAP. Overall, this thesis aims to show the importance of TAP as an advanced oxidation process, using advanced analytical techniques, for the removal of pharmaceuticals whether in lab induced contamination of ultra-pure water, or in a matrix of collected hospital effluents.

TABLE OF CONTENTS

LIST OF ILLUSTRATIONS

X

LIST OF TABLES

LIST OF SCHEMES

CHAPTER I

INTRODUCTION

It is no doubt that water is one of the most vibrant elements needed to sustain humanity. Its uses and benefits are endless whether it was in domestic, agricultural or industrial fields of use. In recent years, the scientific community drew attention to a raising problem threatening our water sources. Pharmaceutical and personal care products (PPCPs) wastes have been recently considered as a great threat to our water recourse due to their high toxicity and resistivity to currently used waste water treatment methods. Although the problem of pharmaceutical wastes in water sources has been an issue for a couple of decades, it wasn't until recently that its toxicological effect has been established on humans and the environment [1-4]. Recent studies have shown that these pharmaceuticals and their metabolites are still found in treated waste water that is used in our daily lives. Moreover, contaminants found in treated water were not restricted to pharmaceuticals and also included other organic wastes such as PCPs, fire retardants and fragrance compounds. Pharmaceutical residues in treated waste water are yet to be fully understood in term of their Eco toxicological effects although scientists are arguing their long term effect on both humans and the environment, for example, the emerging of antibiotic resistant bacteria, as well as abnormal physiological effects on humans [5]. Furthermore, governments did not legally regulate a maximum allowed concentration for pharmaceutical residues in treated waste water [6]. Given what has been mentioned and the inefficiency of today's wastewater treatment plants (WWTPs) and current used water treatment methods, such as, filtration, coagulation and reverse osmosis (RO) [7], a new approach to remove these PPCPs

1

from wastewater have emerged in the form of advanced oxidation processes (AOPs) [8,9]. In these AOPs, active radicals, such as the sulfate radical SO_4^- and the hydroxyl radical $OH^{\cdot-}$, are generated and are highly reactive with organic molecules. These AOPs were found to be very efficient in terms of cost and time in comparison to conventional water treatment methods which deals better with inorganic wastes [8,10,11]

A. *Literature review*

1. *Pharmaceutical Compounds*

Pharmaceutical compounds have been recently placed on top of the emerging environmental contaminants list. These chemical molecules are synthesized for specific purposes and most of them are meant to be rather persistent molecules. Given their persistent nature, pharmaceuticals molecules remain in water even after treatment with currently used methods at wastewater treatment plants [7]. For that reason pharmaceuticals and their residues are being treated as environmental threats with great effect on both humans and the wildlife. Recently scientists have become more and more interested in identifying, as well as quantifying, these pharmaceuticals in water sources [1].

The toxicological effect of these pharmaceuticals in our different water sources is yet to be fully understood. However, scientists have associated these pharmaceutical compounds with several serious dangers such as the potential to create pathogens with antibiotic resistant strains. This particular form of hazard can be a threat in cases where waste water contaminated with antibiotics is used for agricultural and marine purposes, fish farms for example [12]. Although a lot of pharmaceuticals found in wastewater are in rather low concentrations (ng.l^{-1} – µg.l^{-1}) mixture toxicity needs to be taken into account. In mixture toxicity the additive effect of contaminants is taken into consideration. When one pharmaceutical alone in low concentration

can be harmless, a group of pharmaceuticals below their effective concentrations can be very hazardous when taking their cumulative concentration into account [12,13]. Table 1 lists some of the most common pharmaceuticals used today with their different therapeutic properties, and the range of concentrations they are found in [14-16].

Table 1. Most frequently present pharmaceuticals in wastewater and their concentrations [14-16]

Pharmaceutical type	Pharmaceutical name	Concentration ($\mu g.l^{-1}$)
Antiphlogistics / NSAIDs	Naproxen	1.12-5.22
	Ibuprofen	0.05-7.11
	Ketoprofen	0.01-1.62
	Diclofenac	0.68-5.45
β-Blockers	Bisoprolol	0.01-0.98
	Propranolol	0.79-2.84
	Metoprolol	0.08-0.39
	Acebutolol	0.06-0.13
Antibiotics	Sulfamethoxazole	0.05-0.09
	Ofloxacin	0.33-0.58
	Ciprofloxacin	0.06-0.07
	Lomefloxacin	0.19-0.32
Lipid regulators	Gemfibrozil	0.84-4.76
	Clofibric acid	0.01-0.68
	Clofibrate	0.01-0.80
	Fenofibrate	0.14-0.16

2. Pharmaceutical route into the environment

Pharmaceuticals find their way to the environment via two possible routes. The first route is the unchanged molecules passing throw the human body wither via urination or with feces. The concentration of these pharmaceuticals depends on the type and dose of drug consumed. Once the drug leaves the body it is introduced in to the municipal sewage as it travels to the wastewater treatment facilities where they are absorbed on sludge or diluted in water. The second route for pharmaceuticals into wastewater is industrial from pharmaceutical manufacturers disposing of unused or expired medication, in addition to waste generated from the production process [17-18].

3. Fate of the pharmaceuticals in the environment

Different pharmaceuticals face different fates once discharged into the environment. Several factors play a role in the fate which a certain pharmaceutical faces such as the molecular weight of the drug's molecule. Pharmaceuticals molecules with higher molecular weights tend are more likely to be adsorbed on sludge or removed via coagulation processes. On the other hand, pharmaceutical molecules with lighter molecular weight are more likely to move down the waste treatment line and remain in the water [19].

Another factor playing a role in the fate of a pharmaceutical present in wastewater is its biodegradability. As mentioned earlier most pharmaceutical molecules are persistent and therefore are not readily biodegradable and may take several months to degrade. The presence of oxygen can also affect biodegradation, where pharmaceuticals are more easily biodegraded under aerobic conditions. Additionally, the location of the drug down the waste treatment line can

affect its removal percent. sludge adsorbed pharmaceutical molecules are more easily degraded than those which make it further down the line. This can be attributed to the presence of microorganisms in the sludge which in their turn are key players in the biodegradation reactions [20-21].

One more important aspect to conceder when studying the fate of pharmaceuticals in the environment is photodegradation. During the process of photodegradation a pharmaceutical molecule can undergo several direct and indirect photo induced reactions [22]. However, studies have shown that photo degradation is rather inefficient in the removal of pharmaceuticals from water and the removal percent depends on structure if each molecule and in some case its transformation products [20,23].

The inadequacy of currently used wastewater treatment methods used at WWTPs imposes a serious threat to both humans and their surrounding environment. These threats can range anywhere between intoxication from direct consumption of treated water to Eco toxicological hazards affecting both flora and fauna.

4. Characteristics of pharmaceuticals under study (BIS, IBU, NAP)

4.1 Bisoprolol (BIS):
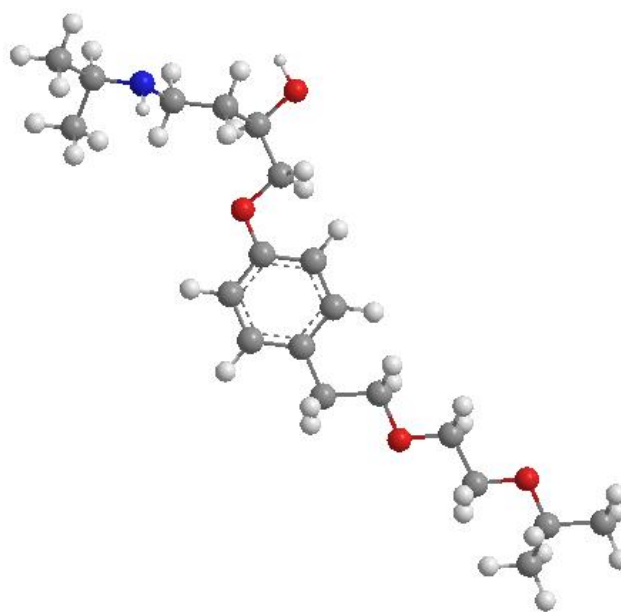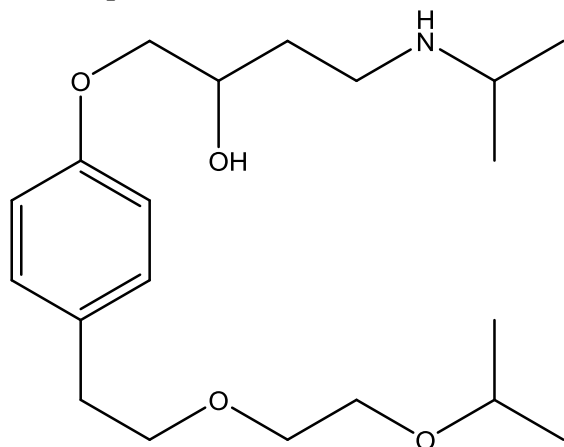
Bisoprolol
Chemical Formula: $C_{20}H_{35}NO_4$
Molecular Weight: 353.50

Scheme 1. 2D and 3D structure of BIS molecule

Bisoprolol (BIS) is a medicine belonging to the β-Blockers family; it is mainly used in the treatment of cardiovascular diseases worldwide. BIS has been approved by the Food and Drug Administration (FDA) since 1992 and has been available commercially since then. Due to its cheap price and availability, BIS has been widely used worldwide and placed on the World Health Organization's (WHO) list for essential medications. Bisoprolol has a melting point of 100 °C, and a solubility of 2240 mg.l^{-1}.

4.2 Ibuprofen (IBU):

Ibuprofen
Chemical Formula: $C_{13}H_{18}O_2$
Molecular Weight: 206.29
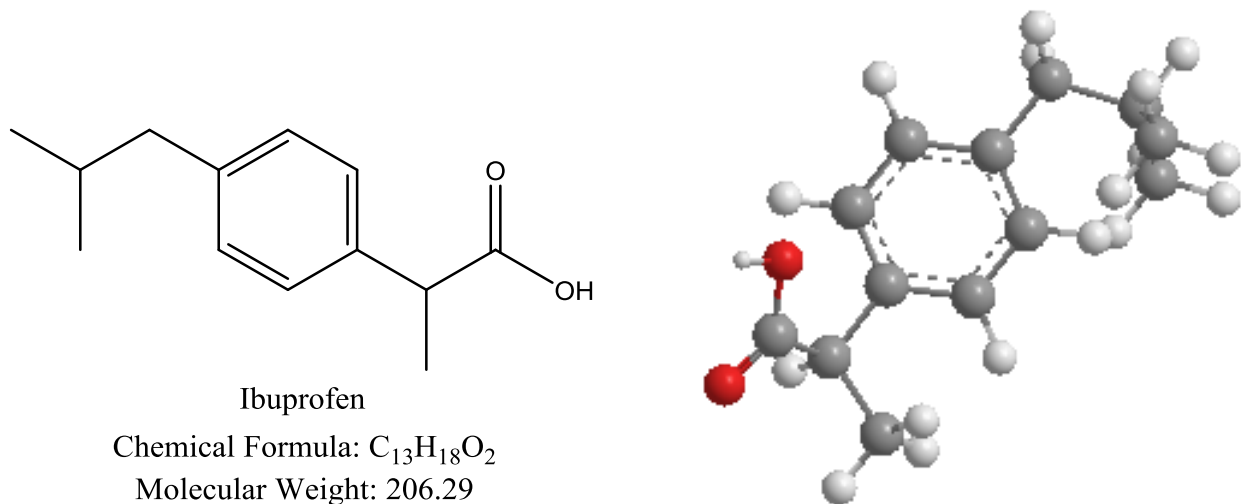
Scheme 2. 2D and 3D structure of BIS molecule

Ibuprofen (IBU) is a non-steroidal anti-inflammatory drug (NSAID). It has a range of uses with the most common being the reduction of fever, relieving pain and reducing inflammations. IBU tablets contain both optically active isomers of the drug, R and S-isomers, however it is the S-isomer that is more biologically active and is responsible of the anti-inflammatory properties of the pharmaceutical. IBU has been discover in the 1960s and has been widely used since then. It has been present for many years on the annual list of essential medication placed by the WHO. Ibuprofen has a melting point of 75-77.5 °C, and a solubility of 21 mg.l^{-1}.

4.3 Naproxen (NAP):
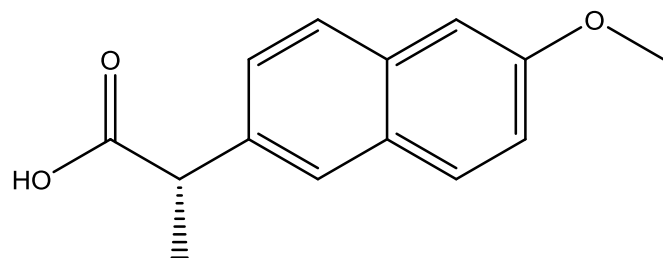
Naproxen

Chemical Formula: $C_{14}H_{14}O_3$
Molecular Weight: 230.26
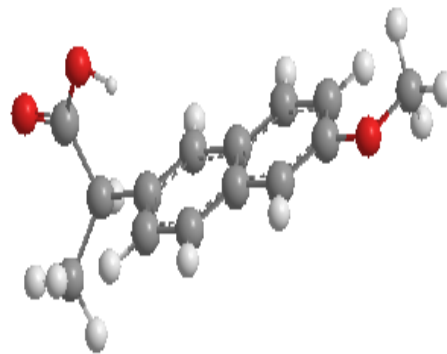
Scheme 3. 2D and 3D structure of NAP molecule

Naproxen is a pharmaceutical compound belonging to the same family of NSAIDs as IBU. It has also been known for its ability to relief pain and swelling. NAP is used as a replacement for IBU in the cases of long term treatment with NSAIDs due to its reduced risk of causing stomach ulcers and in the cases of patients having a history of cardiovascular diseases [24]. Bisoprolol has a melting point of 155 °C, and a solubility of 15.9 mg.l⁻¹ in its Naproxen Sodium form.

5. Advanced oxidation processes (AOPs)

In recent years, wastewater treatment plants (WWTPs) found the need to add advanced technologies as a tertiary treatment step in order to fully mineralize micropollutants, or at the least convert those into less harmful materials before discharging them back into the environment. Following this need, research started moving towards chemical oxidation process which will degrade harmful organic material [25].

AOPs were found to be clean and efficient technologies to be used in the treatment of wastewater. These processes revolve around the production of the highly reactive hydroxyl radical ($OH^.$). These radicals are not only highly reactive, but they are also very strong oxidants having an $E^0 = 2.80\ V$ and are unselective. The previously mentioned properties of the hydroxyl radical make it a great candidate to be used in the mineralization of organic waste. $OH^.$ can be generated via several methods via different AOPs such as ozonation and Fenton processes [26].

One method used for the generation of $OH^.$ is the Fenton process which uses hydrogen peroxide (H_2O_2) and its high oxidation potential ($E^0 = 1.78V$) as a source of $OH^.$ generation (Eq.1) which is known as the Fenton reagent (FR).

$$H_2O_2 + Fe^{2+} \longrightarrow Fe^{3+} + OH^\bullet + OH^- \qquad \text{(Eq. 1)}$$
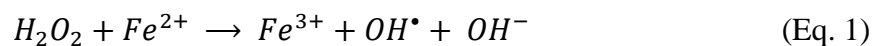
The limitation of this AOP is that it can only function in a very limited acidic range of pH, as well as having very slow transformation rate for the generation and regeneration of the ferrous ion. It also requires high initial iron concentration to achieve an efficient system [27].

Currently used AOPs such as the Fenton reaction were found to be very energy demanding reactions, expensive, and catalyst consuming. Because of these short comings, the need for a more efficient, economical and more oxidative AOP raised [27,28]. This need has diverted the attention to the sulfur-oxygen radicals SO_n^- (where n= 3, 4, 5).

6. The Chemistry of Persulfate

Even though AOPs demonstrated great results in removing organic contaminants from wastewater, however the need for a more efficient and less expensive AOP emerged. In recent years the process of in situ chemical oxidation (ISCO) became a very promising solution to the treatment of wastewater. ISCO is the process of adding chemical oxidants, such as ozone, hydrogen peroxide, and persulfate, to the polluted soil or water [29]. Regardless of their performance, all the above-mentioned treatment methods are expensive [30] and not very practical for large scale and on-field applications since continuous feeding of reagents is necessary. A novel method has shown the possibility of applying activated persulfate as an excellent choice of advanced oxidation processes (AOPs) for the treatment of organic solvents. Persulfate ($S_2O_8^{2-}$) is a very strong oxidant having a redox potential of $E^0 = 2.01V$, while at the same time being highly soluble in water at room temperature (556g/L at STP) [31]. Even with its high redox potential, the rate of organic material removal via persulfate at room temperature is rather low, however when activating persulfate it produces the much more reactive sulfate radical SO_4^- having a redox potential of $E^0 = 2.60V$ which is much higher than that of persulfate, yet lower than that of the hydroxyl radical $OH^{\cdot-}$ which has a redox potential of $E^0 = 2.70V$.

There are various methods used to activate persulfate into the more reactive sulfate radicals such as the use of transition metals [32], UV light [33], and heat [10].

$$S_2O_8^{2-} \xrightarrow{\Delta} 2SO_4^{\cdot-} \qquad (30\ C^0 < T < 99\ C^0) \qquad\qquad \text{(Eq. 2)}$$

$$S_2O_8^{2-} \xrightarrow{UV} 2SO_4^{\cdot-} \qquad\qquad\qquad\qquad\qquad \text{(Eq. 3)}$$

$$S_2O_8^{2-} + Fe^{2+} \xrightarrow{\text{Chemical activation}} SO_4^{2-} + SO_4^{\cdot-} + Fe^{3+} \qquad \text{(Eq. 4)}$$
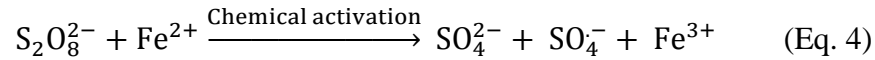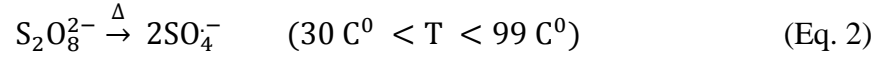
Unlike$OH^{\cdot-}$, which when degrading organic molecules tend to remove a hydrogen atom from a C-H bond or add to a carbon-carbon double bond (C=C), the sulfate radical is more likely to abstract an electron from the probe molecule converting it into its radical cation form:

$$SO_4^{\cdot-} + CH_3\,CO_2^- \longrightarrow SO_4^{2-} + CH_3\,CO_2^{\cdot} \qquad\qquad \text{(Eq. 5)}$$
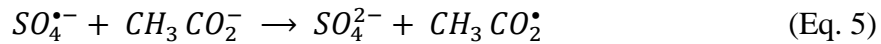
Similar to other radical reactions, the sulfate radical, operates in solution on the basis of a kinetic competition between organic and inorganic molecules in solution. Carbonate ions, Bicarbonates, and chlorides, are examples of inorganic substances which could have a scavenging effect on the sulfate radicals in solution, and hence lower the efficiency of oxidation of the targeted organic probe [34,35]. For this reason, reactions done in this thesis, were performed using deionized water (DI), however additional experiments were performed to test the effect of these scavengers on the reaction rates, as well as the application of using sulfate radicals in cleaning hospital waste water as a method to study the matrix effect.

B. Objectives

Both pharmaceutical and personal care products have been increasingly found in water sources. This has led to an increase is interest by the scientific community towards the issue. AOPs were found to be a feasible solution to the problem. In this thesis, thermally activated persulfate was used to remove 3 active pharmaceuticals separately. The three pharmaceuticals tested were Bisoprolol (BIS), Ibuprofen (IBU), and Naproxen (NAP). Work done in thesis was done on three stages. Chapter II shows the feasibility of using thermally activated persulfate (TAP) in the removal of pharmaceuticals with BIS used as the testing probe. Chapter III of this thesis represents a testing module of TAP on the IBU molecule. Finally chapter IV demonstrates real life application of using TAP in the removal of pharmaceuticals from hospital effluents were the probe being tested was the NAP molecule.

During experimentation, several parameters that may affect the rate of reaction and the removal percent were studied. These parameters consisted of (i) probe concentration, (ii) persulfate concentration, (iii) temperature level, (iv) pH of the system, and (v) effect of inorganic material and scavengers on the reaction. These parameters were tested in order for us to find the optimum reaction conditions which were determined via calculating the stoichiometric efficiency of the reaction (%RSE). Analysis of the solution was performed via HPLC-MSD as a mean of tracking the probe molecule concentration, evolution of possible reaction by-products, and identification of emerging reaction by-products. Identification of the emerging by-products was also used in proposing a degradation mechanism of the probe molecule.

CHAPTER II
DEGRADATION OF BISOPROLOL FUMARATE VIA HEATED PERSULFATE IN AQUEOUS SOLUTION

A. Materials and Methods

1. Chemicals

Bisoprolol Fumarate was obtained from Tabuk pharmaceutical manufacturing company (KSA). Sodium Persulfate (SPS) ($Na_2S_2O_8$, 99+%) was purchased from Chem-Lab (Belgium); Sodium dihydrogen phosphate dihydrate ($NaH_2PO_4 \cdot 2H_2O$, >99%) and ammonium acetate ($C2H_7NO_2$, >98%) (puriss ACS reagent) from Fluka (Netherlands). Di-Sodium hydrogen phosphate anhydrous (Na_2HPO_4) was purchased from Merck (Germany). Potassium iodide (KI) (puriss, 99–100.5%) was purchased from Riedel-de-Haen (Germany). Calcium sulfate ($CaSO_4$), calcium chloride ($CaCl_2$), sodium chloride (NaCl), magnesium nitrate ($Mg(NO_3)_2$) and sodium hydrogen carbonate ($NaHCO_3$) are all of analytical grade and acquired from Prolabo (France).

2. Experimental setup

High concentration stock solutions were prepared for all reagents used in the batch experiments. For the case of BIS, 77 mg of BIS standard were dissolved in 1 L of deionized (DI) water producing a 200 µM BIS stock solution. The volumetric flask was left to stir over night and then filtered using a 0.45 µm PTFE filter to insure the removal of any non-dissolved particles. The buffer solution is a phosphate buffer (PB) prepared by dissolving 3.2025 g of Na_2HPO_4 and 5.3038 g of NaH_2PO_4 in 100 mL of DI water. The resulting PB solution has a pH of 7 and a concentration of 200 mM. Reaction was carried out in 10 mL Pyrex vials were appropriate volumes of the stock solutions prepared were added to achieve the final desired concentration i.e.

$[BIS]_0 = 50$ µM; $[SPS]_0 = 1.0$ mM and $[PB]_0 = 50$ µM. Vials were then immersed in a temperature controlled water bath set at the desired temperature (40-70 °C). Sample vials were removed from the water bath at the desired time intervals and immersed in an ice bath (approximately 4 °C) to quench the heat activated reaction. After BIS and SPS measurements samples were discarded. The pH was measured at the beginning and by the end of each experiment using a pH/Ion meter (Thermo Orion, USA) equipped with an ultra-combination pH electrode (Ross). Reaction was monitored over 2 h with sampling at every 5 min interval until 1 h then every 30 min; this was done in order to also study the effect of SPS on the transformation products. For the monitoring of SPS, 0.5 g of sodium bicarbonate and 25 g of KI were dissolved in 250 mL of DI water and the resulting solution was mixed in 1:1 ratio with the sample and left to complex for 15 min. Control tests were conducted in parallel in the absence of SPS for each experiment. Data presented are averaged value of 4 replicate samples.

3. Chemical Analysis

All analyses were performed in duplicate on an Agilent 1100 Series LC/MS system consisting of a quaternary pump, a vacuum degasser, an autosampler and a thermostated column compartment. Two detectors were also used in series: a diode-array detector for BIS quantification as well as a MSD extra capacity ion trap mass spectrometer detector for the identification of intermediates and transformation products. The MSD is equipped with a PhotoMate orthogonal atmospheric pressure photoionization (APPI) spray source (Syagen Technology) based on a radio frequency discharge of a gas mixture consisting primarily of Kr and operates on the atomic emission lines at 10.0 and 10.6 eV. The liquid chromatography column was a C18 reversed phase column (5 µm; 4.6 mm i.d.×250 mm long) coupled to a security guard column HS C18 (5 µm; 4.0 mm i.d.× 20 mm long) (Discovery, Supleco, USA) all maintained at 30 ∘C.

For BIS isocratic elution conditions were as follow: the eluent was a mixture of 50:50 methanol/ammonium acetate 10 mM (v/v) with a flow rate of about 1.0 mL min^{-1}. BIS is eluted under these conditions at a retention time of about 6.1 min. A calibration curve was done for every set of analysis over the range of 10–100 µM. Under our experimental conditions, the limit of detection of BIS obtained was <0.05 µM. The system was controlled by the LC/MSD ChemStation software version A.09.03.

The persulfate anions were spectrophotometriclly determined using a Nanodrop 2000c UVVIS Spectrophotometer (Thermo Scientific) in accordance with the procedure developed by Liang et al. [35]. The absorbance of the SPS complex was measured at 352 nm based on a calibration curve having a linear dynamic range extending from 1 to 1000 µM.

B. Results and discussion

1. Temperature effect, kinetics and stoichiometric efficiency

Fig.1a shows the effect of temperature on BIS oxidation over a range of 40–70 °C at a pH of 7.0 (phosphate buffer). In all experiments, the BIS remaining concentration plotted vs reaction time (min) exhibits a good fit of the experimental data to a pseudo-first-order model by exponential regression analysis. This is evidenced by the very high correlation coefficient ($R^2 > 0.99$ except for 40 °C where $R^2 = 0.95$) obtained from the linear plots of Ln[BIS]/[BIS]$_0$ vs Time (min) (Fig. 1b; Table 2). One can also notice from the decline curves that as the temperature increases from 40 °C to 70 °C, the degradation rate constant increases from $(0.74 \pm 0.05) \times 10^{-2}\,min^{-1}$ to $(35.5 \pm 2.46) \times 10^{-2}\,min^{-1}$, respectively (Fig. 1b). Complete BIS disappearance occurs after 15, 25 and 45 min of reaction at 70, 65 and 60 °C respectively while partial degradation is obtained for lower temperatures e.g. 50 °C and 40 °C yielding only 61% and 38% respectively. However, at these temperatures, BIS can be completely oxidized over an extended reaction time e.g. >2 h (data are not shown). The calculated half lives ($t_{1/2}$) as well as the observed degradation rates constants (k_{obs}) are summarized in Table 2. $t_{1/2}$ were calculated upon the use of the pseudo-first order equation over different reaction times. $t_{1/2}$ reached less than 2 min for the reaction undertaken at 70 °C and is about 93.7 min for that at 40 °C. One can also notice from the data assembled in Table 2 that the overall consumption of SPS varies depending on the reaction temperature. For example, full BIS degradation is obtained at 60 °C where only 5.0% of the initial SPS concentration was consumed after only 45 min of reaction. However, 8.8% and 9.2% of SPS were consumed at 65 °C and 70 °C and this for a reaction time of about 25 and 15 min respectively. The last column of Table 2 shows the SPS consumption over 1 h of time interval. It is obvious that more SPS is consumed yielding 5.3%, 19.2% and 42.5% for reactions undertaken

at 60 °C, 65 °C and 70 °C respectively. As for the lower temperatures (e.g. 40 °C and 50 °C), the consumption rate of SPS is similar to the one reported for the maximum of BIS disappearance because the maximum degradation (partial) is reached after 1 h of reaction. As a result, we decided to more investigate the oxidation of BIS with TA-SPS at 60 °C being the optimum temperature yielding full degradation within a reasonable time and a very well acceptable reaction stoichiometric efficiency (RSE). The latter is defined as the number of BIS moles degraded vs the number of SPS moles consumed over a specific time interval (Δ[BIS]/Δ[SPS]).

Table 2 Comparison of BIS degradation as a function of temperatures

Temp (°C)	k_{obs}[a] x 10^{-2} (min^{-1})	$t_{1/2}$[b] (min)	R^2	%SPS consumption at maximum BIS disappearance [c]	%SPS consumption at 1 h
40	0.74 ± 0.05	93.7 ± 6.3	0.95	2.3 (38%)[d]	2.3 (38%)
50	1.56 ± 0.03	44.4 ± 4.8	0.99	2.5 (61%)	2.5 (61%)
60	8.47 ± 0.31	8.2 ± 0.3	0.99	5.0 (100%)	5.3 (100%)
65	18.4 ± 0.29	3.8 ± 0.1	0.99	9.15 (100%)	19.2 (100%)
70	35.5 ± 2.46	1.9 ± 0.1	0.99	8.8 (100%)	42.5 (100%)

[a] obtained from the slope of the plots of Fig. 1b. The associated uncertainties are obtained from the standard deviation on the slope determined after using the LINEST function of Microsoft excel.

[b] calculated from the pseudo-first order equation where $t_{1/2} = \ln2/k_{obs}$

[c] 50 ᴓM BIS and 50 ᴓM phosphate buffered solution

[d] numbers in brackets represent the % degradation of the initial BIS concentration (~ 50 ᴓM)
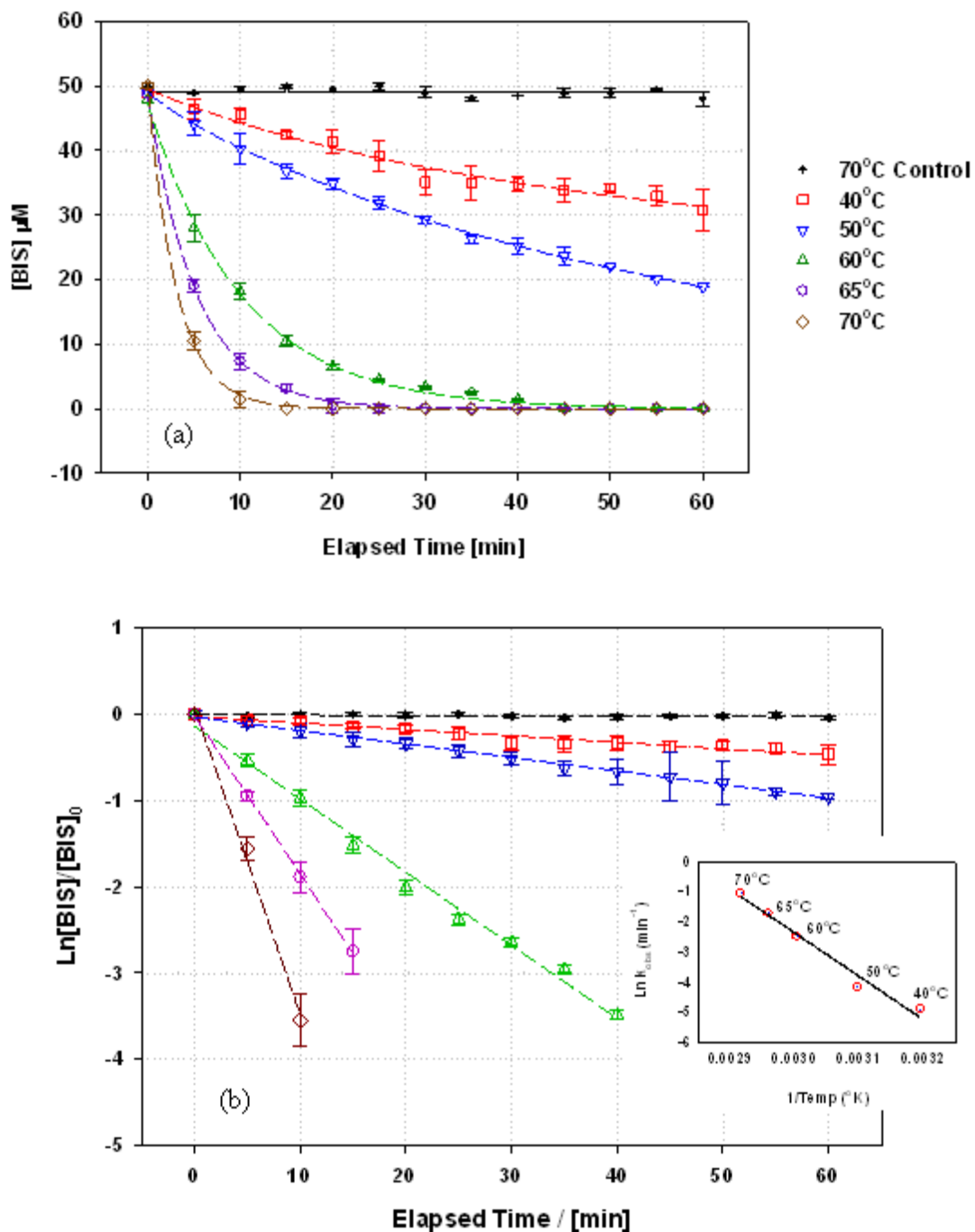
Fig. 1. (a) Influence of temperature on SPS oxidation of BIS and (b) the corresponding pseudo-first order disappearance profiles. The inset is the Arrhenius plot for BIS degradation. Experimental conditions: phosphate buffer 50 μM, pH = 7.0, $[BIS]_0$ = 50 μM, [SPS] = 1 mM. The control was done at 70°C without SPS. The error bars represent the standard deviation of four replicate samples.

Fig. 2 shows all calculated RSE at all temperatures over 1 h of reaction or less. As it can be noticed, the best RSE determined (RSE = 1) is for reaction occurring at 50 °C. At this temperature, only 61% of BIS have been degraded. The lowest RSE ($\approx$0.17) is obtained for reaction occurring at 40 °C accompanied with only 38% of BIS degradation. However, for reactions at 65 °C and 70 °C with 100% BIS degradation, the calculated RSE were about 0.45 and 0.82 respectively.
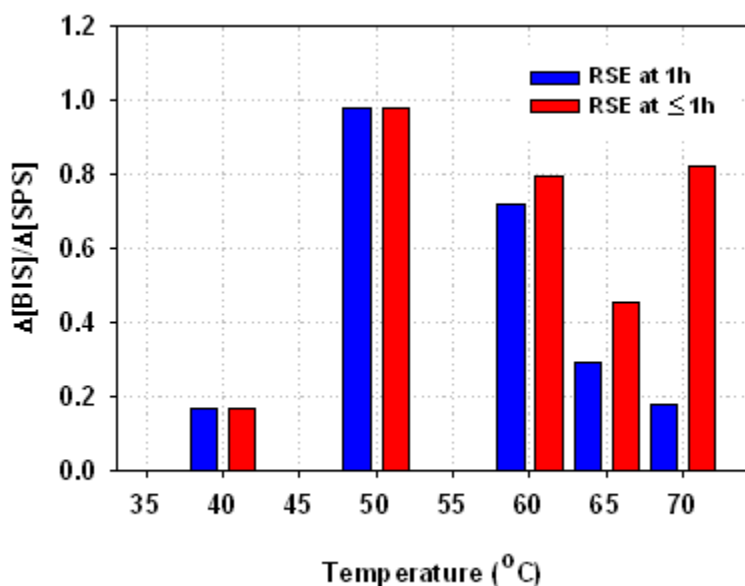
Fig. 2. Reaction stoichiometric efficiency (RSE) at different temperatures. The experimental conditions are the same as of Fig. 1.

The temperature dependency of the kinetics constant was further evaluated using the Arrhenius equation. It has been shown that for the different temperatures investigated, $Ln(k_{obs})$ decreased linearly with $1/T$ (inset Fig.1b) and, therefore, fit well to the Arrhenius type model:

$$Ln(k_{obs}) = LnA - \frac{E_A}{RT} \qquad \text{(Eq. 6)}$$

Where A is the pre-exponential factor, EA is the apparent activation energy, R is the universal gas constant (8.314 J mol^{-1} K^{-1}), and T is the absolute temperature. The fitting parameters from this linear plot of correlation coefficient $R^2 > 0.97$ showed activation energy of 119.8 (± 10.8) kJ mol^{-1} and an Arrhenius constant of 40.8. The calculated EA is within the range of those obtained for example during the persulfate thermal oxidation of chlorinated ethenes: 108 and 144 kJ mol^{-1} for trichloroethylene and *cis*-dichloroethylene respectively [36], [37] and [38], making thermal oxidation of pharmaceutical compounds easily applicable.

2. Buffering effect on the reactivity of SPS toward BIS at 50 °C

In order to determine the optimum conditions for BIS degradation through SPS oxidation, we carried out two experiments at 50 °C in the presence and in the absence of phosphate buffer (50 μM). The latter has been used since phosphate species showed a slow kinetics with sulfate radicals (e.g. $k = 1.2 \times 10^6$ M^{-1} s^{-1} for $SO_{4\bullet}{}^-/HPO_4{}^{2-}$ and 7.0×10^6 M^{-1} s^{-1} for $SO_{4\bullet}{}^-/H_2PO_4$) compared to a fast kinetics reported between $SO_{4\bullet}{}^-$ and organic contaminants ($k\sim 1.0 \times 10^9$ M^{-1} s^{-1}) [39]. As it can be noticed (Fig. 3), the degradation of BIS is more

supported in a PB medium than in a non-buffered solution. This can be explained by the drop in

the pH of the non-buffered BIS solution reaching 4.90 after 1 h of reaction. The pH lowering is

due to the formation of acidic species (e.g. H^+, HSO_5^-) after SPS thermal activation

(Eqs. (7) and (8)).

$$SO_4^{-\cdot} + H_2O \leftrightarrow OH^\cdot + SO_4^{-\cdot} \qquad \text{(Eq. 7)}$$

$$SO_4^{-} + OH^\cdot \leftrightarrow HSO_5^{-} \qquad \text{(Eq. 8)}$$
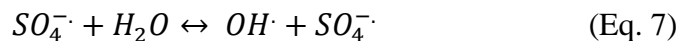
At such low pH, the hydroxyl radicals formed (Eq. 7) are rapidly consumed by sulfate radicals

after radical with radical reaction or radical with radical scavenging reactions (Eq. 8). This could

disfavor radical organic reactions (e.g. BIS) [36] and [37] showing only 26% BIS degradation

(Fig. 3 upper curve). However, at near neutral pH value, hydroxyl radicals can be formed and do

participate actively in the oxidation of BIS (63% degradation) as it can be observed in the

buffered solution where the pH dropped by only 0.4 unit (pH 6.70 at 1 h reaction, Fig. 3 lower

curve). At the same time, the calculated RSE showed clearly the advantage of buffering the

medium (inset of Fig. 3) to keep a near neutral pH. In fact, the RSE in the presence of PB is close

to 1.0 while in the absence of PB it drops to 0.12 which is considered very low in TA-SPS

oxidation processes. Another feature confirming the negative effect of acidic conditions on the

degradation of BIS comes also from Fig. 3. As it can be seen, the two decline curves started with

almost the same initial degradation rates until only 10 min. However, with time running, the BIS

degradation rate conserves the same order of magnitude for the PB solution while it totally

vanished for the PB free system. This can be explained by a drop in the pH of the PB free

solution after 10 min of reaction at 50 °C yielding therefore less available reactive radicals to

oxidize BIS.
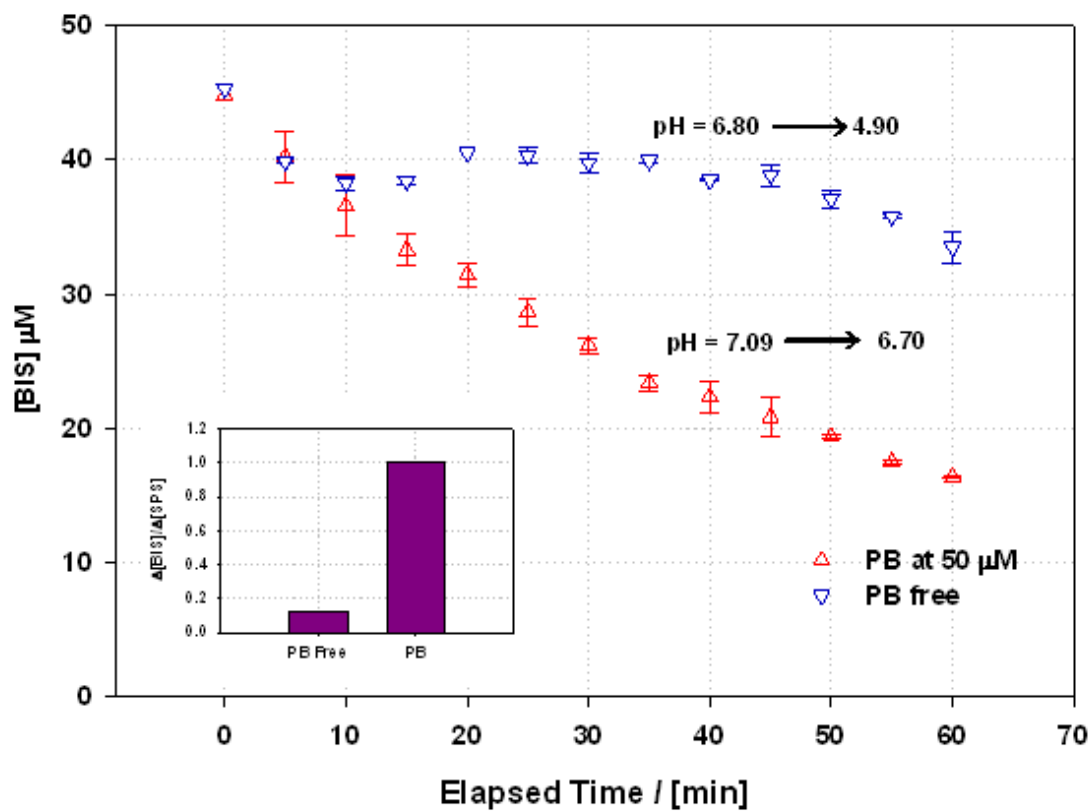
Fig. 3. Buffer effect on the degradation of BIS by SPS at $50^{o}C$. Experimental conditions: $[BIS]_0$ $= 50$ μM, $[SPS] = 1$ mM. The inset shows the reaction stoichiometric efficiency in the presence and in the absence of buffer.

3. Identification of predominate radical species under neutral pH

The above results showed clearly the degradation of BIS upon reaction with thermally activated SPS. A total degradation is reached in less than 1 h at 60 °C. However, in order to better elucidate the degradation mechanism and identify the predominant radical $(OH^{\cdot}, SO_4^{-\cdot})$ responsible of BIS oxidation, we investigated the BIS oxidation at neutral pH and 60 °C after spiking the reactive medium with an excess of EtOH or t-BuOH (TBA). In all experiments, the initial Scavenger/SPS/BIS molar ratio was about 8000/20/1 in order to have always a great excess of alcohol. EtOH and t-BuOH are known by their potential to quench $OH^{\cdot}$ and $SO_4^{-\cdot}$ radicals however at different rates. For example the reported second order rate constants of the alcohols with those radicals are as follow [40]:

$$t-BuOH + OH^{\cdot} \sim 3.8 - 7.6 \times 10^8 \ M^{-1}s^{-1}$$

$$t-BuOH + SO_4^{-} \sim 4.0 - 9.1 \times 10^5 \ M^{-1}s^{-1}$$

$$EtOH + OH^{\cdot} \sim 1.2 - 2.8 \times 10^9 \ M^{-1}s^{-1}$$

$$EtOH + SO_4^{-} \sim 1.6 - 7.7 \times 10^7 \ M^{-1}s^{-1}$$
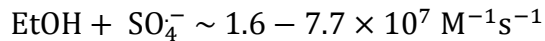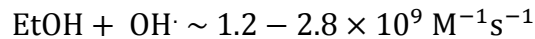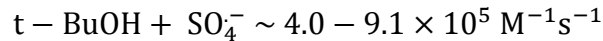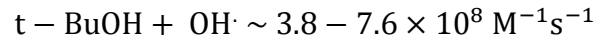
Fig. 4 shows clearly that after adding alcohols, a significant decrease in the oxidation rate of BIS occurs. For example, the maximum of BIS degradation reached over 1 h of reaction after the addition of TBA is about 51%. However, only 18% of BIS disappeared under similar conditions after adding EtOH while full degradation is obtained in the absence of any scavenger. Based on the above mentioned second order rate constants of EtOH and t-BuOH, one can explain the observed results as follow: in TBA system, $SO_4^{-\cdot}$ was degrading BIS while in EtOH system, both

23

radicals were scavenged, which resulted in much lower degradation efficiency (18%). $SO_4^{-\cdot}$ radicals are known to be more selective for electron transfer reactions while $OH^{\cdot}$ species can rapidly undergo by hydrogen addition or abstraction [41] and [42]. The calculated k_{obs} obtained with EtOH and TBA upon the pseudo-first order decay plots are summarized in Table 3. As it can be noticed, the % change in k_{obs} (($k_{obs\ (with\ alcohol)}$)/$k_{obs\ (alcohol\ free)} - 1) \times 100$) noticed for reactions without scavengers is greater when EtOH is used (96.2%) instead of TBA (85.8%). This finding corroborates the reaction rate constants between either radicals ($OH^{\cdot}$ or $SO_4^{-\cdot}$) or the radical scavengers (EtOH or TBA) mentioned above. Similar results have been obtained by Liang et al. [36] where more inhibition is reported due to EtOH addition. The same authors also found that degradation inhibition is pH dependent based on the availability of $OH^{\cdot}$ or $SO_4^{-\cdot}$. For example, under more acidic conditions, less hydroxyl radicals are available than under neutral conditions. In fact, in the presence of EtOH, both generated radicals $OH^{\cdot}$ and $SO_4^{-\cdot}$ are quenched by the alcohol EtOH though at different rates; $OH^{\cdot}$ reaction rate being greater than that of $SO_4^{-\cdot}$ by 400–850 folds [26] and [30]. As a result, $OH^{\cdot}$ will mainly take part in EtOH oxidation while $SO_4^{-\cdot}$, considered as the predominant species at acidic pH, is in part responsible of the oxidation of EtOH and BIS as well. The rapid consumption of $OH^{\cdot}$ radicals yields more SPS degradation (85% of SPS consumption after 1 h of reaction). Consequently, more $SO_4^{-\cdot}$ are produced favoring therefore a more acidic solution responsible of the buffer capacity rupture with a final pH of about pH_f 3.64. This is most probably due to the release of protons when $SO_4^{-\cdot}$ radicals react with water (Eq. (7)). However, when TBA is added, the density of $SO_4^{-\cdot}$ radicals is greater because of its slower reaction with TBA. Therefore, $SO_4^{-\cdot}$ remains the predominant species able to oxidize more BIS molecules. In this case, a lesser decrease in the pH of the initial solution is noticed

24

(pH_f 4.80). This is probably due to the formation of less sulfate radicals since they are slowly consumed (5% of SPS consumption after 1 h of reaction). These results confirm the responsibility of both radicals in oxidizing BIS at neutral pH. However, if 51% of BIS removal has been attributed to $SO_4^{-\cdot}$ (mid curve of Fig. 4) and 100% to $SO_4^{-\cdot}$ and $OH^{\cdot}$ combined (lower curve of Fig. 4), this can explain the probability of $OH^{\cdot}$ to oxidize BIS to an extent of 49% at neutral pH.
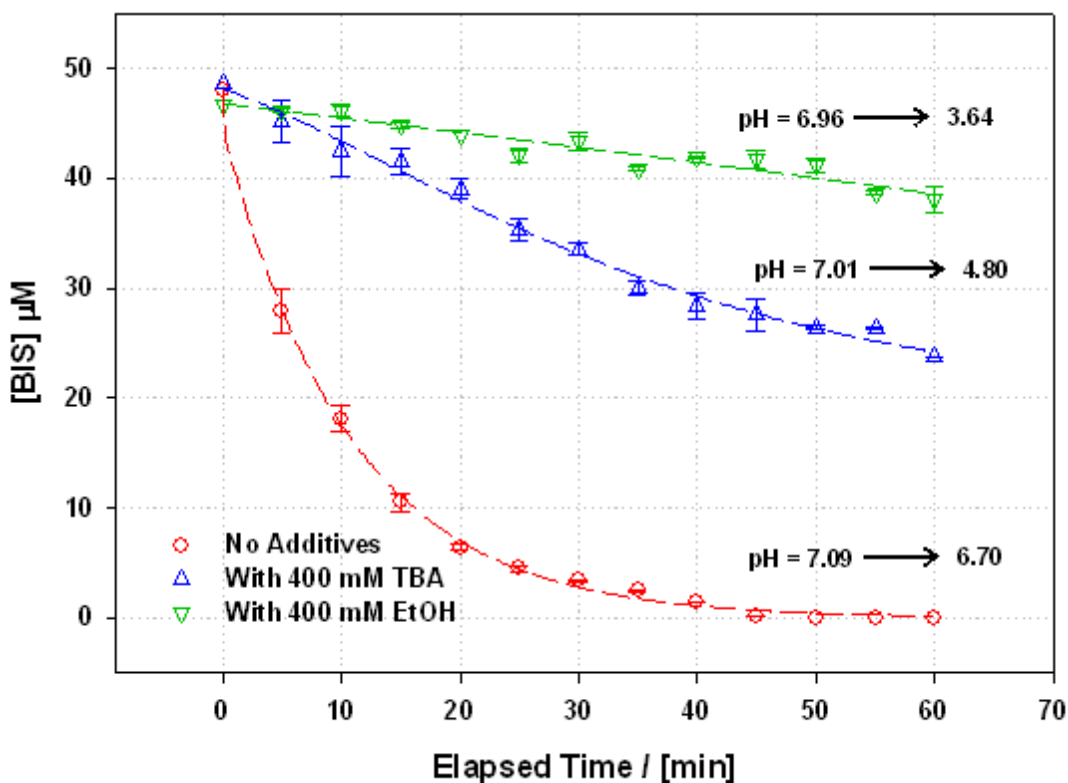
Fig. 4. BIS degradation in the absence and in the presence of radical scavengers under neutral pH at 60°C. The error bars represent standard deviation of four replicates. The dotted lines are fitting functions. Experimental conditions: $[BIS]_0 = 50$ μM, $[SPS] = 1.00$ mM and $[PB] = 50$ μM.

Table 3. Radical identification parameters

Additive	k_{obs}[a] x 10^{-2} (min^{-1})	R^2	% change in k_{obs}
Alcohol free solution	8.47 ± 0.31	0.99	
TBA	1.20 ± 0.04	0.98	$- 85.8 \pm 4.9$
EtOH	0.32 ± 0.03	0.91	$- 96.2 \pm 5.1$

[a] obtained from the slope of the plots $Ln[BIS]/[BIS]_0 = - k_{obs}$ x t (min). The associated uncertainties are obtained from the standard deviation on the slope determined after using the LINEST function of Microsoft excel.

4. Effect of inorganic additives: application to mineral drinking water

The application of a successful SPS thermal activation process to any effluent should take into consideration the effect of additives that might reduce the RSE. A series of experiments were carried out separately on BIS solution in the presence of $CaSO_4$ (5 mg L^{-1}), $CaCl_2$ (50 mg L^{-1}), NaCl (5 mg L^{-1}), $Mg(NO_3)_2$ (2.5 mg L^{-1}), and $NaHCO_3$ (160 mg L^{-1}) in order to account for their role in some possible side reactions decreasing thereby the oxidation reaction rate. The concentrations of all inorganic compounds have been chosen to represent those in typical underground or surface waters. Furthermore, a commercial mineral drinking water supposed to be free of organic carbon (composition in mg L^{-1}: $Ca^{2+} = 33$, $Mg^{2+} = 16$, $Na^+ = 2.3$, $K^+ = 0.3$, $HCO_3^- = 150$, $SO_4^{2-} = 12$, $Cl^- = 7$, $NO_3^- = 1.5$, $F^- = 0.1$ and $Fe^{2+} < 0.01$) has also been tested after being spiked with an adequate concentration of BIS to form a final solution concentration of 50 μM. All experiments were conducted at 60 °C in a 50 μM phosphate buffer solution over

1 h. As it can be noticed (Fig. 5), none of the additives showed a negative effect on the degradation of BIS except for bicarbonate. The latter is known by its capacity of quenching sulfate radicals and hydroxyl radicals as well with rate constants of about $2.8 \times 10^6 \ M^{-1} \ s^{-1}$ (Eq. (9)) [43] and $8.5 \times 10^6 \ M^{-1} \ s^{-1}$ (Eq. (10)) [44] respectively. Consequently this can explain the decrease in the oxidation rate constant of BIS by a factor of 31% (e.g. from $k_{obs} = 8.47 \ (\pm 0.31) \ min^{-1}$ to $k_{obs} = 6.06 \ (\pm 0.17) \ min^{-1}$ as shown in Table 4).

$$SO_4^{-\cdot} + HCO_3^- \rightarrow SO_4^{2-} + CO_3^{-\cdot} + H^+ \qquad \text{(Eq. 9)}$$

$$OH^\cdot + HCO_3^- \rightarrow CO_3^{-\cdot} + H_2O \qquad \text{(Eq. 10)}$$
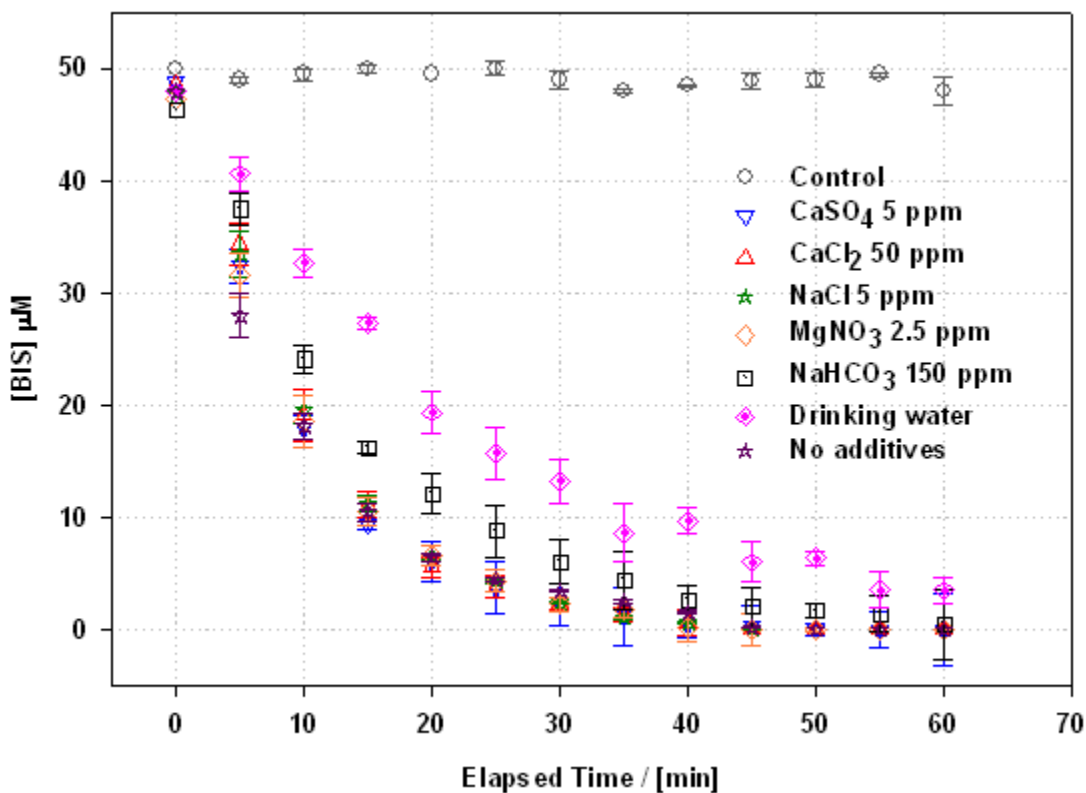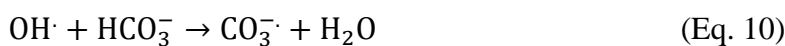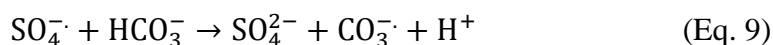
Fig. 5. BIS degradation in the absence and in the presence of additives (CaSO$_4$, CaCl$_2$, NaCl, Mg(NO$_3$)$_2$ and NaHCO$_3$) and in BIS spiked drinking water under neutral pH at 60°C. The error bars represent standard deviation of four replicates. Experimental conditions: [BIS]$_0$ = 50 μM, [SPS] = 1.00 mM and [PB] = 50 μM.

As for the other species, it seems that most of them are in favor of BIS oxidation due probably to the formation of new radicals that can be involved in oxidation reaction yielding more BIS degradation. The calculated k_{obs} for systems spiked with $CaSO_4$ ($k_{obs} = 8.97 \pm 0.31$ min^{-1}), $CaCl_2$ ($k_{obs} = 9.24 \pm 0.28$ min^{-1}), NaCl ($k_{obs} = 9.32 \pm 0.17$ min^{-1}) and $Mg(NO_3)_2$ ($k_{obs} = 9.46 \pm 0.40$ min^{-1}) are slightly greater than the k_{obs} for the system without any additive ($k_{obs} = 8.47 \pm 0.31$ min^{-1}). For systems containing chloride ions, the slight degradation enhancement can be explained according to Eqs. (11) and (12). In this case $SO_{4\bullet}^{-}$ reacts with a chloride anion to yield a chlorine radical $Cl^{\cdot}$ (k = 2.47×10^8 M^{-1} s^{-1}) (Eq. (11)). $Cl^{\cdot}$ reacts again with Cl^{-} (k = 8×10^9 M^{-1} s^{-1} [45] or 1.4×10^5 M^{-1} s^{-1} [46]) in order to form the dichlorine radical $Cl_2^{-\cdot}$ which can be involved in the oxidation of BIS (Eq. (12)). It has been demonstrated that $Cl_2^{-\cdot}$ presents rate constants upon reaction with oxygenated hydrocarbons ranging from 1.4×10^3 M^{-1} s^{-1} to 2.7×10^5 M^{-1} s^{-1} [35] and with amino acids from 1.2×10^5 M^{-1} s^{-1} to 1.4×10^7 M^{-1} s^{-1} [47]. This shows that sometimes $Cl_2^{-\cdot}$ can selectively react with an organic compound at comparable rates as $SO_4^{-\cdot}$ does (case of serine amino acid with 2.3×10^7 M^{-1} s^{-1}) [47].

$$SO_4^{-\cdot} + Cl^{-} \rightarrow Cl^{\cdot} + SO_4^{2-} \qquad \text{(Eq. 11)}$$

$$Cl^{\cdot} + Cl^{-} \leftrightarrow Cl_2^{-\cdot} \qquad \text{(Eq. 12)}$$
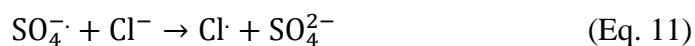
The solution containing $Mg(NO_3)_2$ showed the highest k_{obs} that can be attributed to the formation of nitrate radicals $NO_{3\bullet}$ (Eq. (13)) with a reported k_{obs} of about $(5.0 \pm 0.5) \times 10^4$ [48].

$$SO_4^{-\cdot} + NO_3^{-} \rightarrow NO_3 + SO_4^{2-} \qquad \text{(Eq. 13)}$$
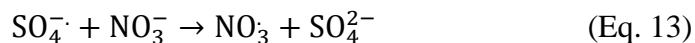
$NO_3\bullet$ has the ability to better oxidize BIS as $CO_3^{-\bullet}$, $Cl_2^{-\bullet}$ or $SO_4^{-\bullet}$ since it is characterized by the highest redox potential among all radicals (e.g. $E_{1/2}^{red}$ ($CO_3^{-\bullet}$) = 1.50; $E_{1/2}^{red}$ ($Cl_2^{-\bullet}$) = 2.09; $E_{1/2}^{red}$ ($SO_4^{-\bullet}$) = 2.43; $E_{1/2}^{red}$ (NO_3) = 2.50) [37] and [48]. Fig. 5 shows also that the removal rate of BIS is the smallest one for drinking water (k_{obs} = 4.41 ($\pm$0.17) $\times$ 10^{-2} min^{-1}). This observation can be explained by the interferences among all species present in the water matrix. For example, non-determined radical quenching processes are likely to occur between potential oxidative radicals. This will decrease the density of available oxidative radicals which could be responsible of a slower BIS oxidation rate. Although BIS oxidation in drinking water presented slower kinetics, almost 100% removal was achieved within 1 h.

Table 4. Comparison of BIS degradation as a function of additives

Additives (mg/L)	k_{obs}[b] $\times 10^{-2}$ (min^{-1})	$t_{1/2}$[c] (min)	R^2
$CaSO_4$ (5)[a]	8.97 ±0.31	7.73 ± 0.27	0.99
$CaCl_2$ (50)	9.24 ± 0.28	7.50 ± 0.22	0.99
NaCl (5)	9.32 ± 0.17	7.44 ± 0.14	0.99
$Mg(NO_3)_2$ (2.5)	9.46 ± 0.40	7.33 ± 0.31	0.98
$NaHCO_3$ (160)	6.06 ± 0.17	11.43 ± 0.31	0.99
No additive	8.47 ± 0.31	8.2 ± 0.30	0.99
Drinking water[d]	4.41 ± 0.17	15.70 ± 0.59	0.98

[a] numbers in brackets represent the concentration of additives in mg L^{-1}.

[b] k_{obs} are obtained from the slopes of the plots of Ln([BIS]/[BIS]$_0$) vs Time of Fig. 5. The associated uncertainties are obtained from the standard deviation on the slope determined after using the LINEST function of Microsoft excel.

[c] calculated from the pseudo-first order equation where $t_{1/2} = ln2/k_{obs}$

[d] Refer to the text for drinking water composition

5. Study of transformation and byproducts
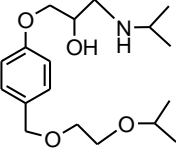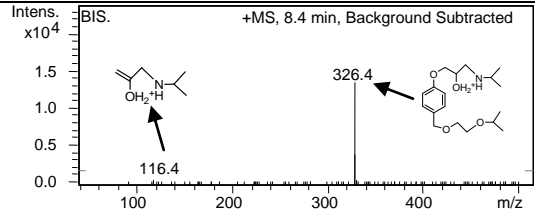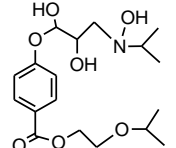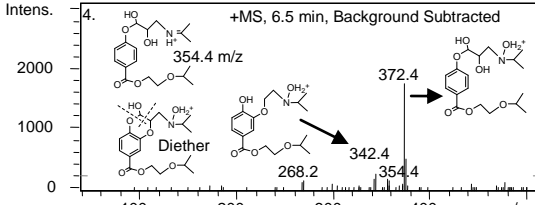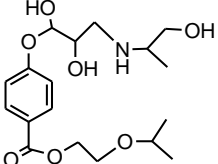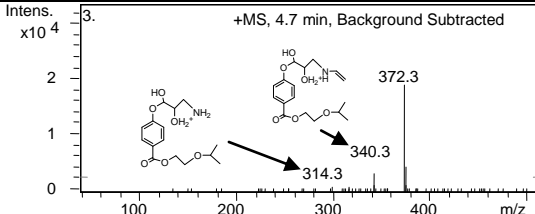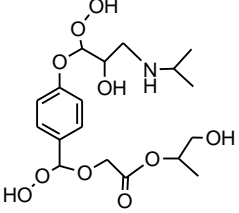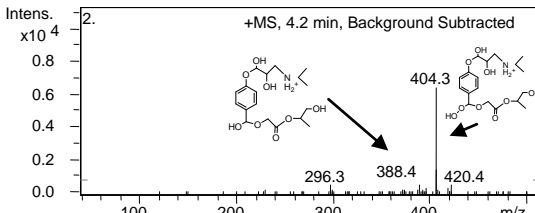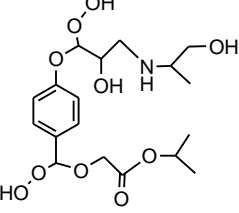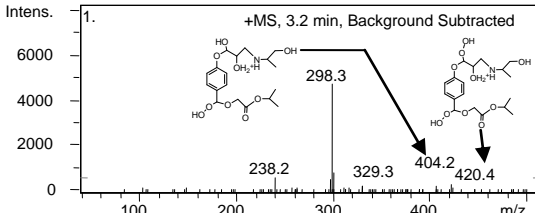
The degradation of BIS was accompanied by the appearance of oxidative products as it appears in the total ion chromatogram of Fig. 6. Under current experimental conditions, BIS is eluted at a retention time of about $Rt = 8.4$ min. As the degradation experiment moved forward, four transformation products (**1**-**4**) clearly showed up at different Rt, all of them having a Rt less than the one noticed for BIS. This observation makes sense since BIS exhibits oxidation reactions after the addition of hydroxyl radicals on different available sites of the original molecule. Such reactions will make the resulting molecules more polar and consequently eluted at lesser Rt than the original BIS molecule on the C_{18} non polar chromatographic column. Another feature of the thermally activated SPS/BIS system showed in Fig. 6 (inset A) is the time course plots of BIS and its transformation products. For example product **3** is the first one to disappear quickly (after 20 min) followed by products **2** and **4** (after 40 min). This can be due to the difference in stability of those products reacting in a powerful oxidative medium. However, product **1** seems to be the most resistant since its decline occurs after 50 min of reaction. In order to confirm the disappearance trend for all by-products noticed over 1 h of reaction, an additional experiment was carried out however over 2 h. The results were affirmative showing almost complete disappearance of BIS transformation products (data are not shown). Furthermore, an additional UV/Vis analysis done immediately on aliquots taken from the heated reactors at different time intervals showed a significant decrease in the absorbance band in the range of 190–240 nm in parallel to a slight increase in the region of 240-340 nm (inset B). This was ascribed to the oxidation of the aliphatic chains by the hydroxyl radicals followed by a possible loss of the resulting moieties yielding partial or total mineralization [49]. In order to better understand the oxidation mechanism of BIS by heated persulfate, HPLC/MS analysis was undertaken on a more

concentrated BIS solution (66.6 µM). An analysis of the chromatographic peaks and their corresponding mass spectra as well reveals the presence of hydroxylated and/or peroxylated compounds. Those are known by their typical signature in the HPLC/APPI/MS analysis. The hydroxylated species are characterized by the loss of 18 amu occurring after the addition of a proton to the molecule to form the molecular ion $[M+H]^+$ followed by the loss of a water molecule $[M+H-H_2O]^+$. However, the peroxylated species are characterized by the loss of 16 or 32 amu attributed to a single or two oxygen atoms respectively ($[M+H-O]^+$; $[M+H-O_2]^+$).

As it can be noticed (Fig. 6 and Table 5), BIS presents a molecular ion $[M+H]^+$ at 326.4 m/z with a fragment at 116.4 m/z ($C_6H_{14}NO^+$) resulting from the loss of a neutral $C_{12}H_{18}O_3$ moiety. The four transformation products detected at early time of the degradation process seem to have common functional groups most probably attributed to hydroxyls after oxidation of the original molecule by OH. (Eq. (7)). It is important to notice that the HPLC/MS total ion chromatograms did not show any mono hydroxylated BIS byproduct identified by a molecular ion of about 342.4 m/z $[M+H]^+$. This can be attributed to (i) the extremely high reaction rate of the oxidation process on hand and (ii) the high density of OH. yielding chemical attacks on many sites (symmetric or asymmetric) of the original molecule. This will result in the formation of multiple hydroxylated isomers. Consequently accurate structure elucidation of the intermediate by-products seems very difficult to accomplish especially in the absence of authentic standards. However, from some MS fragmentation patterns, one can determine the more favored carbon site exhibiting hydroxylation. For example, byproduct **1** eluted at 3.2 min shows the loss of 60 amu ($m = 298.3–238.3$ amu) that can be assigned a hydroxylated isopropyl group (C_3H_8O). Furthermore, the loss of 31 amu ($m = 329.3–298.3$ amu) can be attributed to an aminomethyl

group (CH_3NH_2) (Table 5). This fragmentation pattern indicates that hydroxylation occurred on the isopropylamino group and not on the isopropoxyethoxy group of the original BIS molecule. The fragmentation pattern of by-product **2** eluted at 4.2 min exhibits two successive losses of 16 amu (m = 420.4–404.3 amu and 404.3–388 amu). This could be ascribed to the loss of an oxygen atom from two peroxide functions formed on two separate sites of the BIS molecule. It is also important to notice that molecular ion 420.4 m/z being greater than the one reported for by-products **3** and **4** e.g. 372.4 m/zexplains well the more polar character of the resulting by-products **1** and **2** which could be attributed to more hydroxylation and/or peroxydation. Byproducts **3** and **4** eluted at higher Rt e.g. 4.7 and 6.5 min respectively are less hydroxylated (thus less polar) than by-products **1** and **2**. They are also isomers because of their common molecular ion $[M+H]^+$ at 372.4 m/z and different fragmentation patterns. For example, by-product **3**shows clearly the loss of CH_3OH (32 amu) moiety followed by C_2H_2 (26 amu) confirming the hydroxylation of BIS on the isopropylamino or the isopropoxyethoxy group (Table 5). By-product **4** shows the loss of (i) H_2O (m = 372.4–354.4 = 18 amu) through dehydration or (ii) CH_2O (m = 372.4–342.4 = 30 amu) through the formation of a cyclic diether followed by its rupture upon collision with ionized species into the heated ionization chamber. Probable structures of some fragments are proposed as inset to the MS spectra of Table 5.

Table 5. UV and MS data of BIS and its degradation products observed under thermal activated SPS oxidation. Transformation products are arranged by decreasing order of retention time.

Product	R_t (min)[a]	Proposed Structures[b]	Molecular Weight g mol^{-1}	UV data (λ_{max}, nm)	Molecular ion and Product ions (relative abundance %) (+) APPI	MS Spectra
BIS	8.4		325.23	198, 225, 275	$[M+H]^+$ 326.4 (100) $[M-C_{12}H_{18}O_3]^+$ 116.4 (2.4)	
4	6.5		371.4	206, 270	$[M+H]^+$ 372.4 (100) $[M+H^+-H_2O]^+$ 354.4 (8.9) $[M-CH_2O]^+$ 342.4 (14.1) $[M-CH_2O-74]^+$ 268.2 (7.8)	
3	4.7		371.4	200, 260	$[M+H]^+$ 372.3 (100) $[M-CH_3OH]^+$ 340.3 (15.6) $[M-CH_3OH-C_2H_2]^+$ 314.3 (2.7)	
2	4.2		419.4	204, 258	$[M+H]^+$ 420.3 (6.5) $[M-O]^+$ 404.3 (100) $[M-O_2]^+$ 388.4 (7.5) $[M-O_2-92]^+$ 296.3 (7.3) $[M-O_2-159]^+$ 228.9 (2.7)	
1	3.2		419.4	219, 275	$[M+H]^+$ 420.4 (5.9) $F_1 = [M-O+H]^+$ 404.2 (4.1) $F_2 = [F_1-75]^+$ 329.3 (3.9) $F_3 = [F_2-CH_2NH_2]^+$ 298.3 (100) $F_4 = [F_3-C_3H_8O]^+$ 238.2 (17.2)	

[a] R_t: Retention time; [b] Only one hydroxylated and/or peroxylated isomer is shown.

34
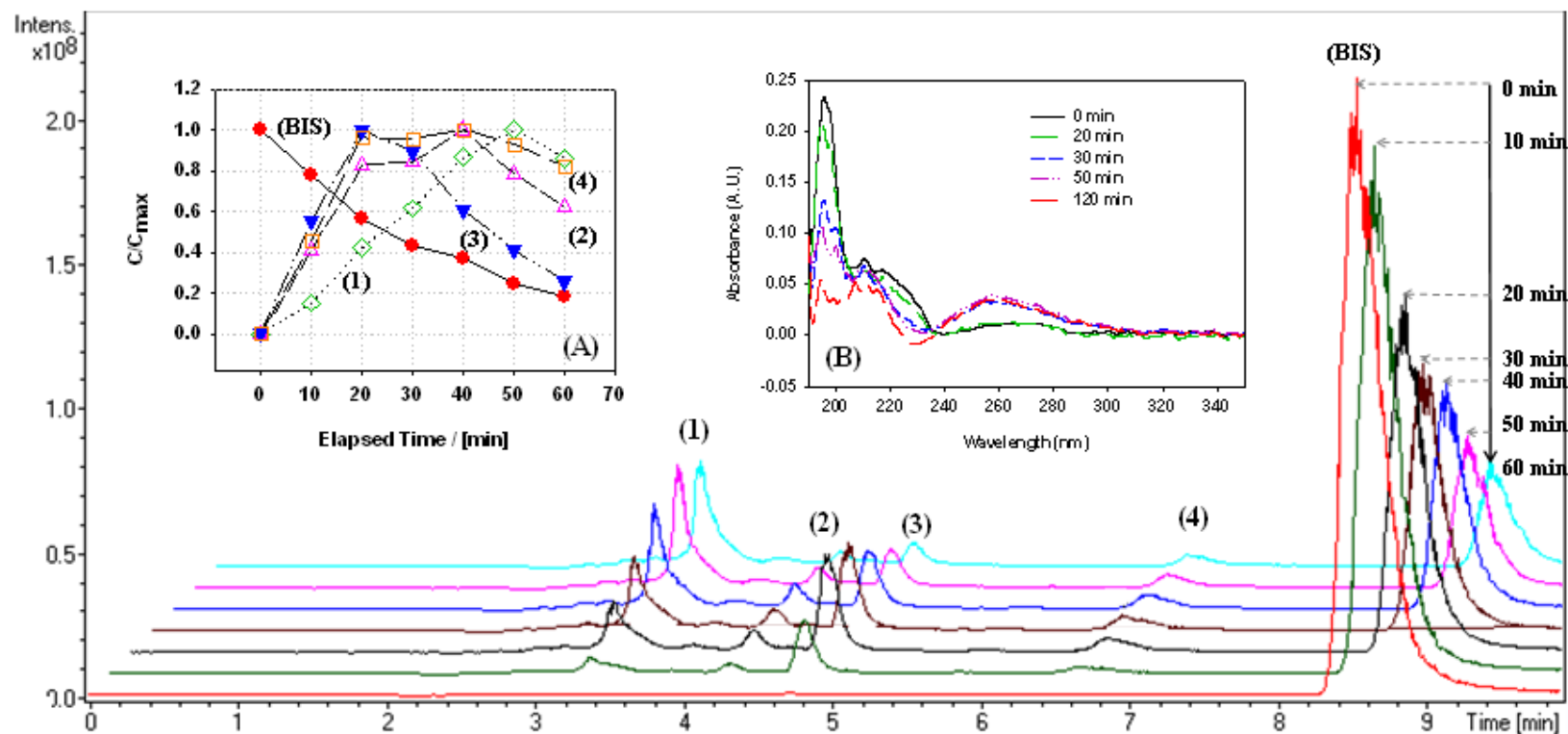
Fig. 6. HPLC/APPI/MS chromatograms of BIS solution during oxidation with thermally activated SPS over 60 min. BIS is detected at its $[M+H]^+$ 326.4 m/z molecular ion. Inset (A) is representing the time course of BIS and its transformation products as well over 1 h. Inset (B) represents the UV/Vis spectra of the whole solution taken at different time intervals over 2 h. Experimental conditions: $[BIS]_0 = 66.7$ μM, $[SPS] = 1.00$ mM, $[PB] = 50$ μM, $T = 60^\circ C$.

6. Chapter conclusion

In this study, BIS was successfully degraded within 1 h in aqueous solutions under thermal persulfate activation (40-70$^{\mathrm{o}}$C) through oxidation reactions involving different radicals. The calculated reaction stoichiometric efficiency was very satisfying at 50$^{\mathrm{o}}$C (RSE = 1.0) and 60$^{\mathrm{o}}$C (RSE > 0.8). The reaction kinetics was attributed pseudo-first order rate with respect to BIS. Results showed that high temperatures and neutral pH values e.g. 7.0 were more favorable than acidic solutions and low temperatures for complete BIS degradation. Alcohol additives demonstrated the responsibility of hydroxyl radicals $OH^{\bullet}$ as well as sulfate radicals $SO_4^{\bullet-}$ in oxidizing BIS. Among all inorganic additives, only HCO_3^- slightly influenced the observed degradation rates of BIS. Tests done on spiked BIS drinking water showed almost complete BIS degradation over 1 h of reaction regardless of a slight decrease in the observed degradation rate. The study of the total ion chromatograms obtained showed explicitly the formation of intermediate BIS oxidation products through hydroxylation and/or peroxydation. Oxidation reactions extended over 2 h confirmed the total disappearance of all byproducts. However, in order to confirm full mineralization, additional work should be undertaken using appropriate analytical techniques. The efficient oxidation of BIS can be considered as good indicator in order to extend this AOP to additional pharmaceutical persistent molecules dissolved in water or adsorbed on soils.

CHAPTER III
DEGRADATION OF IBUPROFEN VIA HEATED PERSULFATE IN AQUEOUS SOLUTION

A. Materials and methods

1. Chemicals

Ibuprofen of pharmaceutical grade was acquired from Tabuc industry (KSA). Sodium Persulfate (SPS) ($Na_2S_2O_8$, 99+ %) was purchased from Chem-Lab (Belgium); Sodium dihydrogen phosphate dihydrate ($NaH_2PO_4 \cdot 2H_2O$, >99%), hydrated tri-sodium phosphate Na3PO4 · 12H2O, phosphoric acid (H_3PO_4) and ammonium acetate ($C_2H_7NO_2$, >98%) (puriss ACS reagent) from Fluka (Netherlands). Di-Sodium hydrogen phosphate anhydrous (Na2HPO4) was purchased from Merck (Germany). Potassium iodide (KI) (puriss, 99–100.5%) was purchased from Riedel-de-Haen (Germany). Methanol and acetonitrile are of HPLC grade and purchased from Sigma.

2. Chemical analysis

For monitoring purposes, IBU analysis was performed with an Agilent 1100 Series liquid chromatograph (LC) system consisting of a quaternary pump, a vacuum degasser, an autosampler and a thermostated column compartment. The LC system is equipped with a diode array detector (DAD) configured in series with an ion trap MS detector (MSD). The DAD was used for the quantification of IBU while the MSD equipped with an electrospray ionization source (ESI) was for the identification of potential transformation products. IBU MS detection was done in (−) ionization mode. The LC column was a C18 reversed phase column (5 μm; 4.6 i.d. × 250 mm long) coupled to a security guard column HS C18 (5 μm; 4.0 i.d. × 20 mm long) (Discovery, Supleco, USA) all maintained at 30 °C during analysis. Additional details on this

equipment have been previously described [10]. The mobile phase consisted of 0.1% (v/v) formic acid (35%) and acetonitrile (65%) under isocratic mode. The flow rate and injection volume were about 1.0 mL min^{-1} and 50 μL respectively. The system was controlled by Agilent ChemStation software for LC and LC/MS systems version A.09.03. Under those conditions, IBU is eluted at 8.5 min, has a shoulder at 220 nm, a maximum absorbance at 196 nm and a limit of detection <0.05 μM. The persulfate anions were spectrophotometrically determined using a 1 mm path length Nanodrop 2000c UV–VIS Spectrophotometer (Thermo Scientific), in accordance with the procedure developed by Liang et al. [35]. The absorbance of the complex was measured at 352 nm for [SPS]0 < 1000 μM while for [SPS]0 > 1000 μM the wavelength 400 nm was used for SPS quantification. An absorbance UV/Vis spectrum of the complex SPS-KI is presented in Fig. 7. The limit of detection of SPS under those conditions was less than 5.0 μM. A calibration curve of SPS (5–500 μM). The same UV–VIS Spectrophotometer was also used for monitoring the overall absorbance spectrum of the IBU solution under analysis using a 10 mm quartz cell. Full scan measurement was also carried out on the range 200–400 nm as shown in Fig. 8. This was done in order to follow IBU characteristic absorbance bands and/or to identify any significant transformation (bathochromic, hypsochromic, hypochromic and/or hyperchromic shifts) in the absorbance spectrum of IBU.
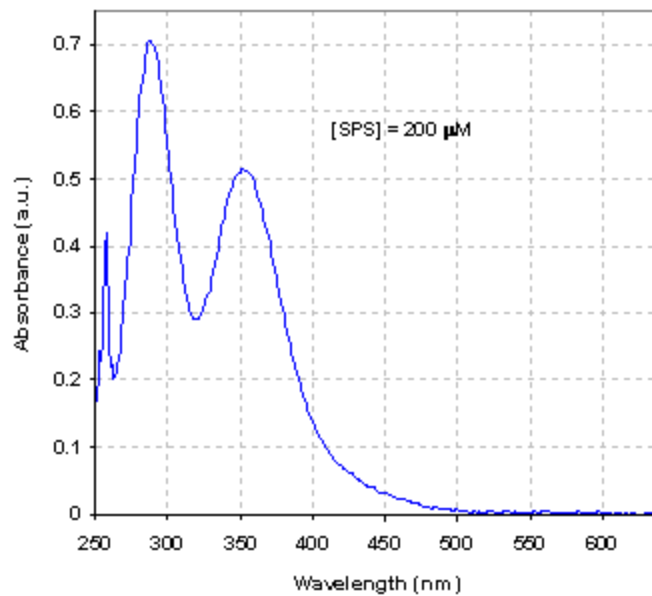
Fig. 7. UV/Vis absorbance spectrum obtained for the SPS-KI complex according to Liang et al. (2008). The wavelength $\lambda = 352$ nm is suitable for the range 20-1000 μM while $\lambda = 400$ nm was used for the upper limit range because of signal saturation at 1000 μM.
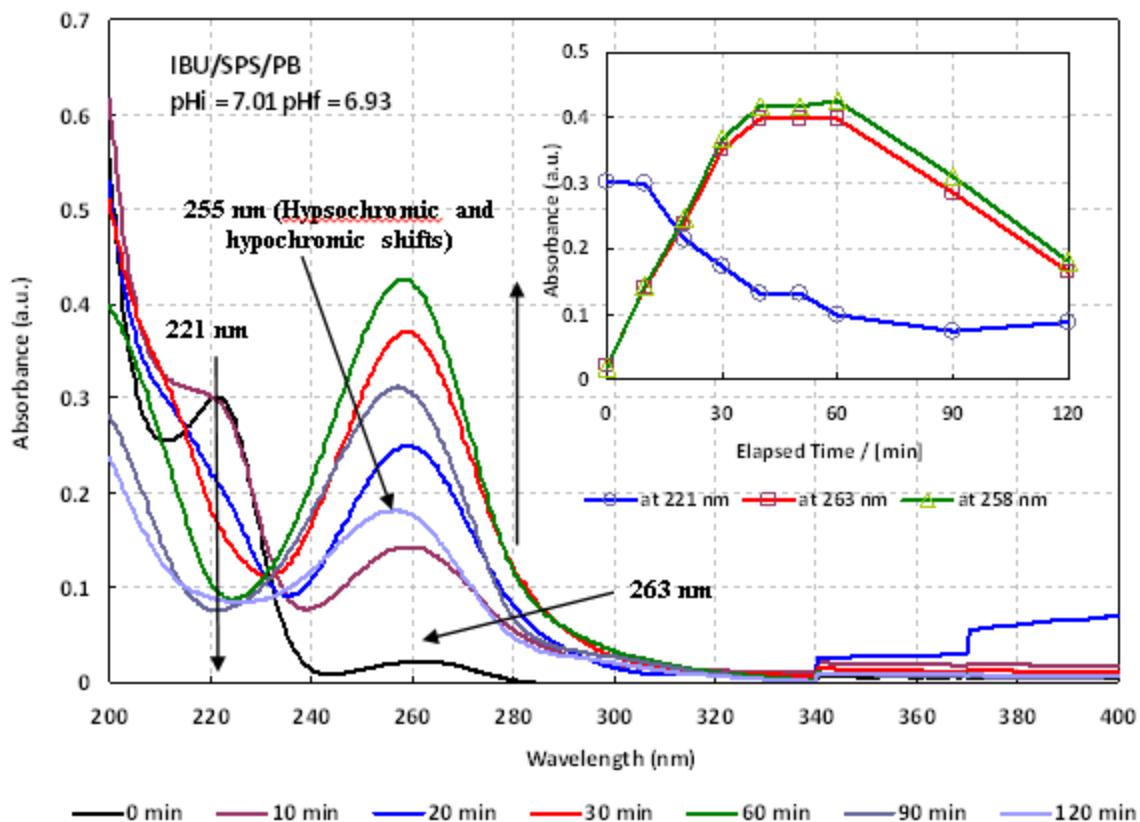
Fig. 8. Evolution of the UV/Vis spectra of IBU solution during TAP degradation process. The inset represents the evolution of the absorbance at specific wavelengths (221, 258 and 263 nm). Experimental conditions: $[IBU]_0 = 20.36$ μM, $[SPS]_0 = 1.0$ mM, $[I]_{PB} = 0.09$ M, T = 60°C.

3. Experimental setup

3.1. Solutions preparation

All reagents were prepared as stock solutions as follow: The IBU solution was prepared by adding 21 mg of IBU as maximum solubility at room temperature into deionized water (capped 1 L volumetric flask) to make a 102 μM stock solution. The latter was stirred overnight at room temperature until complete IBU dissolution and then filtered through a 0.45 m filter to remove any non-dissolved particles. Before each experiment, an SPS stock solution (200 mM) was freshly prepared in order to always have the same SPS concentration for starting solutions in all

40

conducted experiments [26]. For SPS residual analysis, KI stock solution was also freshly prepared and used for persulfate complexation reactions. In order to not affect the kinetics study of IBU degradation during the oxidation process, all experiments were carried out at fixed ionic strength ([I]PB) obtained after adding adequate amounts of phosphate buffer (PB) maintaining thereby constant pH. During thermal activation (e.g. T $>$ 40 °C), $SO_4^{\bullet-}$ are rapidly produced which can greatly influence the pH of the solution if not buffered. PB have been largely used by many authors for their low reactivity with $SO_4^{\bullet-}$ and $OH^{\cdot}$ as well [10], [36], [74], [75] and [76]. Those radicals are much more reactive with organic compounds than with phosphate species. The reaction rate constants of phosphate species with sulfate and hydroxyl radicals are as follows: $SO_4^{\bullet-}/HPO_4^{2-}$ ($k = 1.2 \times 10^6 \, M^{-1}s^{-1}$), $SO_4^{\bullet-}/H_2PO_4^-$ ($k = 7.0 \times 10^6 \, M^{-1}s^{-1}$), $OH^{\cdot}/_{HPO_4}^{\quad 2-}/H_2PO_4^{2-}$ ($k < 3.0 \times 10^6 \, M^{-1}s^{-1}$)). However, the rate constants of those radicals with organic compounds are estimated to more than >109 M−1 s−1 [36], [74], [75] and [76]. PB stock solution of pH ∼ 6.8–7.0 was prepared by mixing 6.6860 g Na2HPO4 with 6.3396 g NaH$_2$PO$_4$ · 2H$_2$O in 200 mL double distilled water (DDW) so as to obtain an ionic strength [I]PB = 0.9 M. For stock solution of pH 4.0, 0.081 mL of concentrated H3PO4 was mixed with 15.383 g of NaH$_2$PO$_4$ · 2H$_2$O in 100 mL DDW yielding [I]PB = 1.6. For pH 9.0 stock solution, 14.196 g of Na2HPO4 were mixed with 0.0171 g of Na$_3$PO$_4$ in 100 mL DDW yielding [I]PB = 2.5. All PB stock solutions were stored in the refrigerator at 4 °C prior to experiments.

41

3.2. IBU oxidation

The aqueous thermal oxidation reactions were conducted in a set of 10 mL Pyrex vials at 50–70 °C. Adequate volumes of the prepared stock solutions and DDW were added together into vials in the following order: IBU, PB, DDW. Before introducing SPS solution, vials (in duplicate) were immersed into the thermal bath until reaching the working temperature (e.g. 50–70 °C). The water bath was covered in order to minimize photo-catalyzed oxidation of IBU. Thereafter, vials were spiked with the appropriate volumes of SPS so as to obtain final concentrations of all reactants in the reactors as follows: $[IBU]0 = 7.33\text{-}20.33$ μM and $[SPS]0 = 1.0\text{-}2.8$ mM. Control experiments were done in 2.0 mM SPS PB solutions at $[I]PB = 0.09$ M in the absence and in the presence of IBU (systems: IBU/SPS/PB and SPS/PB) and in water-only solutions (system: SPS/H_2O) in order to check if more SPS are being consumed by dissolved phosphate species. The results presented in Fig. 9 showed clearly a non-significant difference between the three systems. This observation demonstrated that organic compounds react much more quickly than phosphate species with sulfate and hydroxyl radicals. Accordingly, one can assume that no serious competition between radical-organic and radical-phosphate occurred as long as the organic contaminant is present into the solution. As for the PB content, several attempts were made in order to choose the most appropriate $[I]_{PB}$ able to maintain constant pH value and high RSE after 1 h of reaction at 60 °C. Results showed excellent buffer capacity and a very acceptable RSE (>0.6) at $[I]PB = 0.09$ M. Accordingly adequate volumes of PB were added to all reactors so as to obtain an ionic strength due to PB of about $[I]PB = 0.09$ M. This value is greater than the one previously used for bisoprolol degradation at 50 °C [10] however close to the one reported by Liang and co-workers on the degradation of TCE at 40 °C [74] and by

Costanza and collaborators [76] on the degradation of PCE whose PB solution's ionic strength was about 0.1 M.
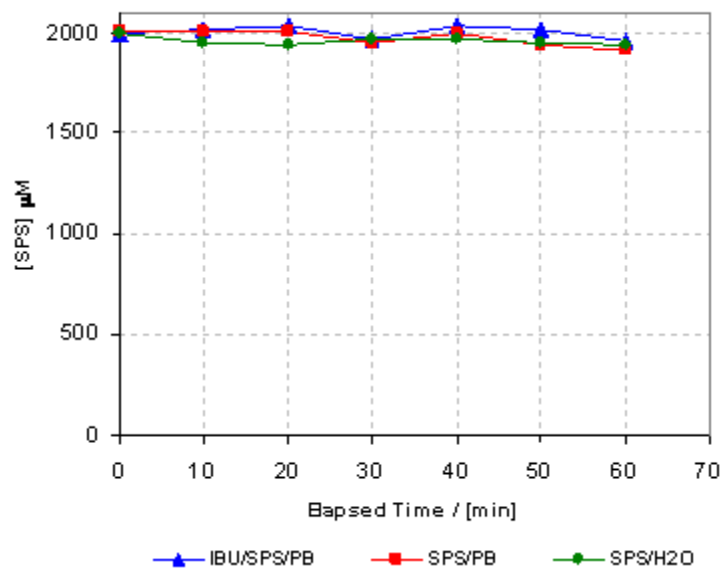
Fig. 9. Control experiments showing no significant difference in the number of micro moles of SPS remaining into the solution among three systems: IBU/SPS/PB, SPS/PB and SPS/H_2O. Experimental conditions: $[IBU]_0 = 20.36$ μM, $[SPS]_0 = 2.0$ mM, $[I]_{PB} = 0.09$ M, T = 60°C.

3.3. IBU sampling

In order to avoid any SPS and IBU concentrations' change during sampling, at each designated time interval (5 min each) two reactors were removed from the water bath, chilled at 4 °C in an ice bath for about 5 min to quench the oxidation reaction and then sacrificed for IBU and SPS analysis. The chilling process has been successfully used to quench persulfate reactions [10], [36], [75] and [77]. However in order to insure that the reaction stopped, IBU and SPS were monitored in ice-chilled and non ice-chilled (room temperature) samples. The results did not show any significant difference in the residual SPS and IBU at room temperature and without

43

any prior ice chilling (Fig. 10.). Some samples were also analyzed after 1 and 2 h of being at room temperature and the results showed no change in the concentration of SPS and IBU as well. This is the reason why all experiments were carried out accordingly without using chemical quenchers like MeOH and $NaNO_2$ as needed especially for degradation reaction based on chemical persulfate activation [78]. The pH at the beginning and by the end of each experiment was almost stable. It was measured by a pH/Ion meter (Thermo Orion, USA) equipped with an ultra-combination pH electrode (Ross). Control tests were conducted in parallel in the absence of SPS for each experiment and no significant IBU loss was noticed. Data presented are averaged value of 4 replicate samples (duplicate experiments and duplicate analyses). The calculated average uncertainties for all measurements were less than 5% which is typical under homogeneous conditions.
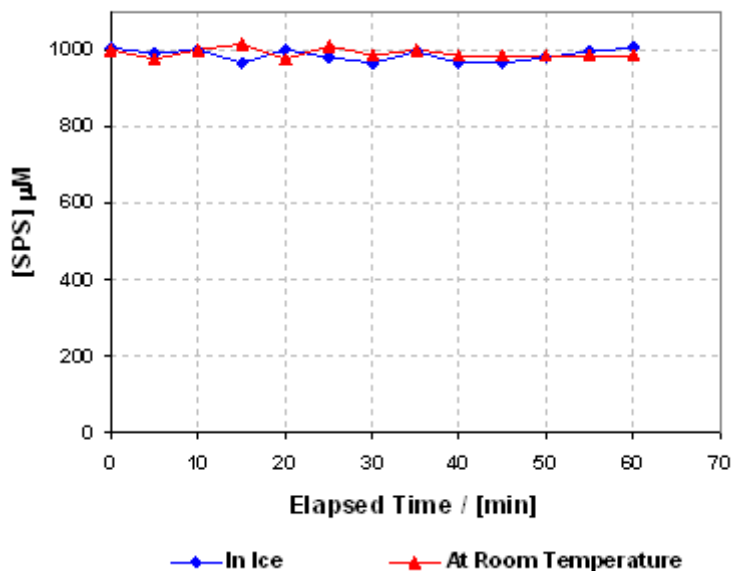
Fig. 10. Decline curves showing the degradation of IBU in IBU/SPS/PB system. The upper curve represents the concentration of IBU in scarified samples chilled in ice. The lower curve shows the concentration of IBU in scarified samples kept at room temperature. Experimental conditions: $[IBU]_0 = 20.36$ μM, $[SPS]_0 = 1.0$ mM, $[I]_{PB} = 0.09$ M, T = 60°C.

B. Results and discussion

1. Effect of temperature on IBU degradation
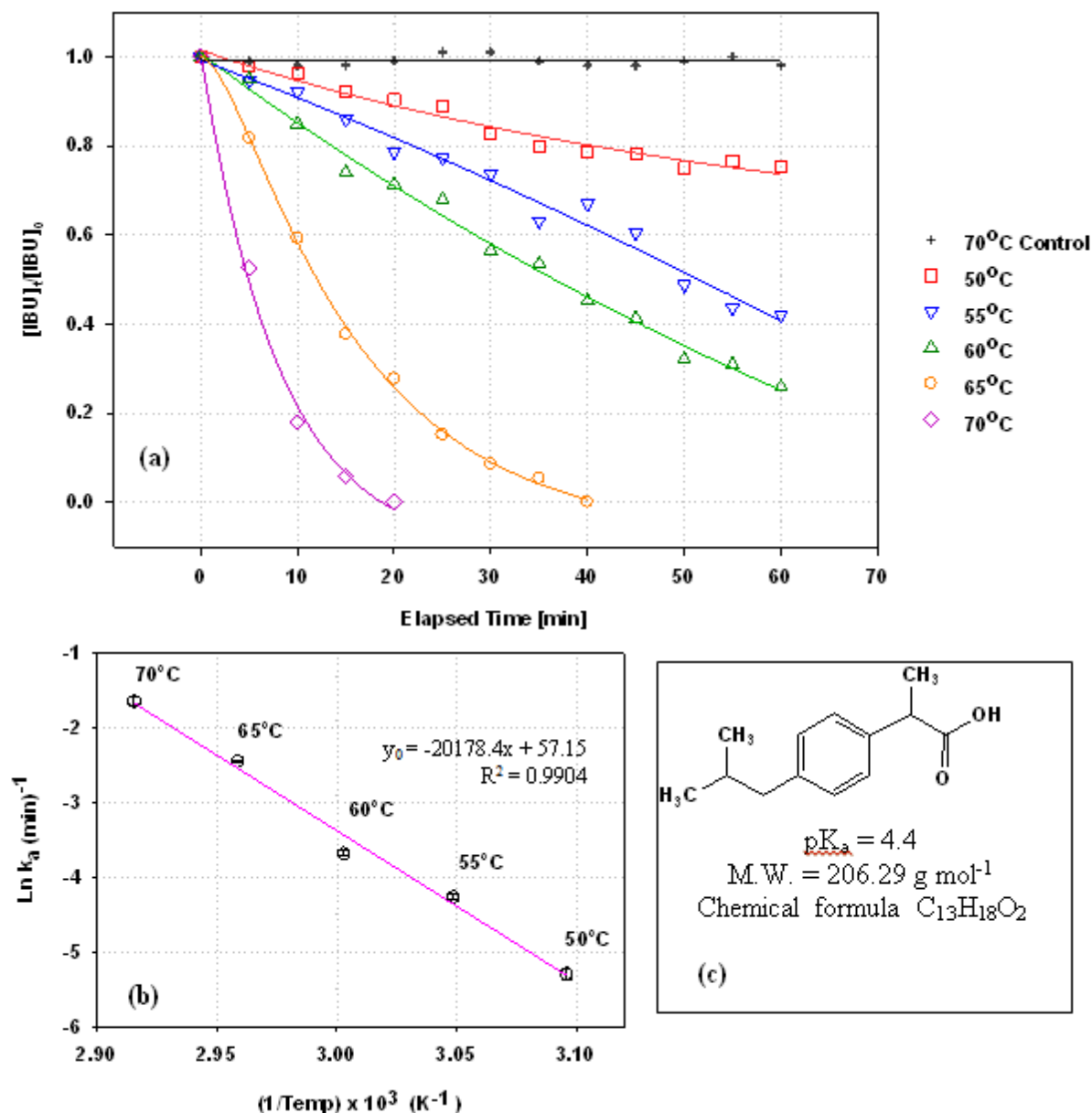
Fig. 11. (a) Temperature effect on SPS oxidation of IBU. Solid lines are exponential decay fitting functions. (b) Arrhenius plot for IBU degradation using the observed degradation rate constant k_a obtained from the slope of $Ln([IBU]_t/[IBU]_0)$ vs time. (c) Structure and selected physicochemical properties of IBU. Experimental conditions: $[I]_{PB} = 0.09$ M, pH = 7.0, $[IBU]_0 = 20.36$ µM, $[SPS]_0 = 1.00$ mM. The control was done at 70^oC without SPS. The error bars are not represented since the average uncertainties on 4 replicates were less than 5%.

Fig. 11.a. represents the pseudo-first order decline curves of SPS oxidized IBU under different temperatures. IBU chemical structure and physicochemical properties are presented in Fig. 1c. The results obtained show clearly that IBU degradation is temperature dependent. As the temperature of the reactor increases, IBU degrades faster. Complete removal is observed for reactions carried out at 70 °C and 65 °C over 20 min and 40 min, respectively. However, partial but significant degradation occurred after 60 min of treatment: 75%, 60% and 12% of degradation is reached at 60 °C, 55 °C and 50 °C, respectively. This observation is typical for all thermal activated persulfate oxidation reactions where more sulfate radicals SO_4^- (and indirectly hydroxyl radicals $OH^\cdot$) are generated at higher temperatures resulting in faster organic contaminants degradation. This was the case for ter-butyl ether [79], trichloroethylene and [36] volatile organic compounds [79], chlorinated ethenes [37] tetrachloroethylene [76] and bisoprolol [10] (Ghauch and Tuqan, 2012) treated in thermally activated SPS solutions in the range of 40–70 °C. The half-lives of IBU calculated from the pseudo-first order equation ($t_{1/2} = \ln2/k_{a1}$) extended from 3.6 min at 70 °C to 138 min at 50 °C. As for the other parameters summarized in Table 6 one can also notice almost a stable pH of the solution ($pH_{final} \sim pH_{initial}$) indicating that PB capacity has not been broken in spite of the production of acid species through SPS transformation. Finally, Table 6 shows also a significant increase in the degradation rate constant of about 2.5 folds (average) for each 5 °C increase of the chemical reactor.

Table 6. Rate constants of heat-assisted SPS oxidation of IBU in phosphate-buffered solutions under various temperatures and fixed ionic strength $[I]^a$.

[IBU]$_0$ (μM)	Temperature	pH$_{initial}$	pH$_{final}$	k_{a1} x 10^{-3} (mM min^{-1})	Half-life (min)^b
20.36	50	6.85	6.86	5.3	138.6
20.36	55	6.82	6.85	14.5	49.5
20.36	60	6.87	6.80	24.9	27.7
20.36	65	6.83	6.83	86.2	8.1
20.36	70	6.82	6.80	192.0	3.6

^{a} [SPS]$_0$ = 1 mM, $[I]_{PB}$ = 0.09 M.

^{b} Calculated from the pseudo-first order kinetics law where $t_{1/2}$ = Ln2/k_{a1}.

The thermal activated reaction showed also excellent fitting with the Arrhenius equation: $k_{\alpha1}$ = A exp$^{-Ea/RT}$ where A is the Arrhenius constant, E_A is the activation energy, R is the universal gas constant (8.314 kJ/mol K) and T the temperature (K). As it can be seen from Fig. 11b, the calculated Arrhenius constant A is about 57.2 (±3.4) kJ mol^{-1}, and the apparent activation energy E_A calculated from the slope of the linear plot of ln($k_{\alpha1}$) vs. (1/T) is about 168(±9.5) kJ mol^{-1}. The uncertainties reported for A and E_A were determined using the LINEST function of Microsoft excel. This calculated E_A is higher than the one reported by Ghauch and Tuqan [10] during the degradation of Bisoprolol pharmaceutical (E_A = 119.8(±10.8) kJ mol^{-1}) indicating the more recalcitrant character of IBU for persulfate oxidation.

2. pH effect on IBU degradation

Fig. 12 shows the pH effect on the degradation rate of IBU by thermally activated SPS under a fixed ionic strength of about $[I]_{PB} = 0.09$ M. Buffered solutions were prepared as stock solutions of pH 4.0, 7.0 and 9.0 then added to the heated IBU vials.
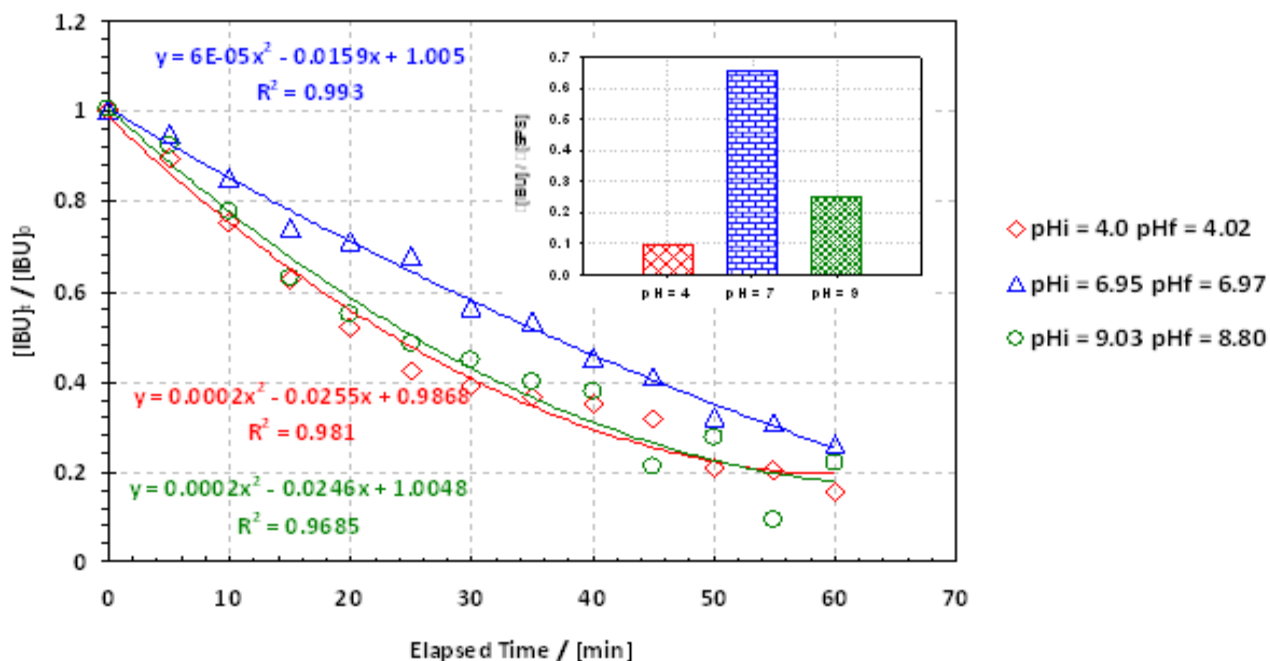
Fig. 12. (a) pH effect on IBU degradation. Solid lines are fitting curves. The inset represents the RSE at pHs 4.0, 7.0 and 9.0. Experimental conditions: $[IBU]_0 = 20.36$ μM, $[SPS]_0 = 1.00$ mM, $[I]_{PB} = 0.09$ M, Temperature = 60°C.

As it can be noticed (Fig. 12), SPS thermal oxidation of IBU at all studied pHs leads to significant degradation after only 1 h of reaction time. At pH 4.0 for example, a maximum of 85% degradation is achieved while at pHs 7.0 and 9.0, 75% and 78% were reached, respectively. Under acidic conditions, autocatalysis is more likely to happen along with production of sulfate radicals [80] resulting to higher IBU degradation. Similar results on acid catalysis were observed by Liang et al. [36] and Antoniou and coworkers [81], [82] and [83] who found that phosphate

and sulfate ions did not inhibit the degradation of aromatic compounds at acidic pH values. On the other hand, Liang and coworkers [36] showed, at pretty similar ionic strength ($[I]_{PB} = 0.1$ M), that persulfate oxidation of trichloroethylene (TCE) is also pH dependent. For example, the lowest k_{obs} calculated from pseudo-first order kinetics was for experiments done at pH 4 ($k_{obs} = 9.63 \times 10^2 \, h^{-1}$) followed by those at pH 9 ($k_{obs} = 11.48 \times 10^2 \, h^{-1}$) and pH 7 ($k_{obs} = 12.51 \times 10^2 \, h^{-1}$). Accordingly, based on the literature, the pH value of the solution can differently affect organic contaminants degradation and therefore common pH effect cannot be expected. In this study, self-quenching of $SO_4^{\bullet-}$ seems to be insignificant through acid-catalysis [28] because of the low concentration of SPS used (e.g. 1 mM leading low density of $SO_4^{\bullet-}$) and the fast reaction of $SO_4^{\bullet-}$ with IBU. At pH 9.0, the degradation rate of IBU seems not to be influenced by the presence of hydroxyl species partially responsible of the quenching of $SO_4^{\bullet-}$.

$$SO_4^{\bullet-} + H_2O \rightarrow SO_4^{2-} + OH^{\bullet} + H^+ \qquad \text{(Eq. 14)}$$

$$SO_4^{\bullet-} + OH^- \rightarrow SO_4^{-2} + OH^{\bullet} \qquad \text{(Eq. 15)}$$
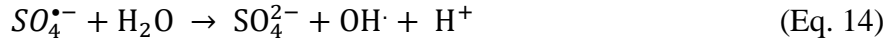
At pH 7.0, IBU degradation is comparable to that of pH values 4.0 and 9.0 however the corresponding decline curve presents a better fitting into polynomial regression than those reported for the other pHs. The best correlation coefficient obtained (R^2) is for pH 7.0 (0.9930) followed by pH 4.0 (0.9810) than pH 9.0 (0.9685). However, in order to decide whether acidic, neutral or basic pH is the optimum one for subsequent experiments in term of kinetics modeling, the amount of remaining SPS was monitored and the reaction stoichiometric efficiency (RSE) was evaluated by the end of the reaction. As it can be seen from the inset of Fig. 12, the optimum pH for IBU thermal oxidation is pH = 7.0 (RSE = 0.65) followed by pH = 9.0 (RSE = 0.25) and

pH = 4.0 (RSE = 0.09). The higher RSE found at pH = 7.0 is due to the fact that most of the $SO_4^{\bullet-}$ produced are exhibiting direct oxidation of IBU by electron transfer or by hydrogen abstraction through $OH^{\bullet}$ indirectly produced (Eq. (15)). However, the lowest RSE reported (RSE = 0.09) is for pH 4.0 where more $SO_4^{\bullet-}$ are produced through acidic catalysis [27] and [74] for almost the same number of IBU molecules degraded. In this case, few $SO_4^{\bullet-}$ are being involved in the oxidation of IBU while the rest could slightly react with phosphate species or they might react with each other as radical-to-radical reactions instead of radical-to-IBU reactions [84]. As for pH 9.0, it has been shown that $SO_4^{\bullet-}$ produced can also react with hydroxyl species yielding therefore more SPS consumption for less IBU degradation. As a result, buffered IBU solutions of pH 7.0 have been adopted for further investigations.

3. Reaction order and kinetics

The rate of a chemical reaction usually depends on the concentration of reactnts and the temperature under which the reaction is carried out. A common example can be given for a reaction of the form $aA + bB \rightarrow cC + dD$ under constant temperature for which the general rate is defined as [85]:

$$r = -\frac{dA}{dt} \equiv k\,[A]^a[B]^b \qquad \text{(Eq. 16)}$$

Based on IBU degradation, the reaction rate law of SPS oxidation of IBU can be related to the concentrations of SPS and IBU as follow:

$$r = -\frac{d[IBU]}{dt} \equiv k[IBU]^a[SPS]^b \qquad \text{(Eq. 17)}$$

where $r = -\frac{d[IBU]}{dt}$ is the rate constant for IBU degradation; k is the overall rate constant; a and b are the reaction orders in IBU and in SPS respectively. In order to elucidate the reaction orders in IBU and SPS in the aim of elaborating a kinetics law of SPS thermally oxidized IBU, the reaction will be conducted with an excess of the oxidant SPS in such a way that [SPS] remains almost constant, which means that $[SPS]_0 \ggg [IBU]_0$. Under such conditions, Eq. (6) can be simplified as shown below (Eq. 18):

$$r = -\frac{d[IBU]}{dt} \equiv k_a \, [IBU]^a \text{ where } k_a \equiv k[SPS]^b \qquad \text{(Eq. 18)}$$

In case the reaction follows pseudo first order kinetics, where [SPS] is almost constant, b will be equal to 1 and therefore $k_a = k_{a1} = k[SPS]$.

3.1. Effect of IBU concentration under fixed SPS concentration (case 1)

Table 7. Kinetic parameters for the determination of reaction orders for thermally activated persulfate oxidation of IBU at 60°C in IBU and in SPS.

$[IBU]_0$ x 10^{-3} (mM)	$[SPS]_0$ (mM)	$[SPS]_0/[IBU]_0$ molar ratio	Half-life $t_{1/2}$ (min)	K_a x 10^{-4} (mM min^{-1})
First set of experiments: determination of reaction order *a* in IBU				
7.33	1	136.4	17.08	2.15
10.18	1	98.23	20.97	2.43
12.63	1	79.17	24.28	2.6
20.36	1	49.11	36.89	2.76
Second set of experiments: determination of reaction order *b* in SPS				
20.36	1	49.11	36.89	2.76
20.36	1.6	78.58	25.14	4.05
20.36	2	98.23	18.46	5.51
20.36	2.8	137.52	13.69	7.44

Table 7 summarizes the different concentrations used as well as the obtained $[SPS]_0/[IBU]_0$ ratios for reactions undertaken at 60 °C in PB solution of circumneutral pH (pH 6.8-7.0). The first set of experiments was done by fixing $[SPS]_0$ to 1.0 mM while varying $[IBU]_0$ from 7.33 to 20.36 µM (case **1**). The second set of experiments (case **2**) was carried out by fixing $[IBU]_0$ to 20.36 µM and varying $[SPS]_0$ from 1.0 to 2.8 mM. In case **1**, the resulting $[SPS]_0/[IBU]_0$ molar ratios ranged from highest of 136.4 to the lowest molar ratio of 49.1. Such molar ratios (>10/1) are in agreement with the recommendation of Espenson [86] where one of the reactant remains almost constant. It is also very well known, in order to get a more accurate kinetics study, to collect samples at earlier stage of the reaction. This can help in minimizing side reactions that can happen between the transformation and end-products with the oxidative

species e.g. $SO_4^{\bullet-}$, $OH^\bullet$. However, such fact might not happen if the oxidation reaction is very fast and powerful yielding rapid mineralization of organic contaminants (OCs). The normalized IBU concentrations $[IBU]_t/[IBU]_0$ at each reaction time are illustrated in Fig. 14. Data analysis using a polynomial regression showed excellent correlation coefficients (R^2) greater than 0.99 even at longer reaction time extending over 60 min. Polynomial regressions obtained for shorter reaction times (<60 min, data not shown) did not affect significantly the correlation coefficients indicating therefore the efficient oxidation character of the reaction and may be the non-accumulation of transformation products. In fact, one might expect the presence of hydroxylated or sulfonated IBU derivatives upon oxidative attack of $OH^\bullet$ and $SO_4^{\bullet-}$ on the benzene ring or $OH^\cdot$ on the aliphatic chains[87] and [88]. However, no transformation products were noticed in all chromatograms of LC/MS analysis even at higher IBU concentration (e.g. 91.8 µM). IBU presents a molecular ion $[M–H]^-$ at 204.9 m/z with a fragment at 161.1 m/z corresponding to decarboxylation $[M–H–CO_2]^-$ (Fig. 13).
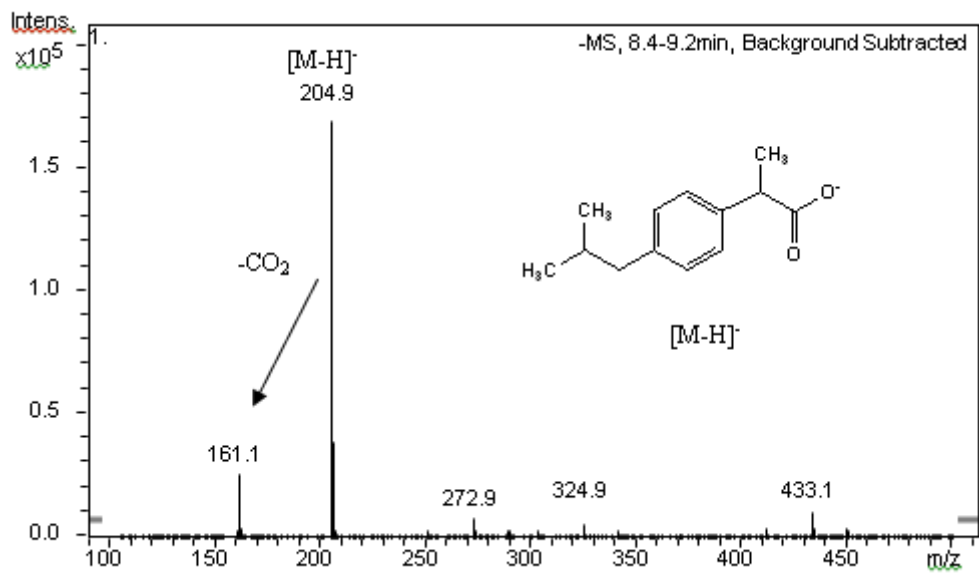
Fig. 13. (-)ESI mass spectrum of IBU showing the molecular ion at 204.9 m/z and the decarboxylated fragment after neutral loss of CO_2 at 161.1 m/z.
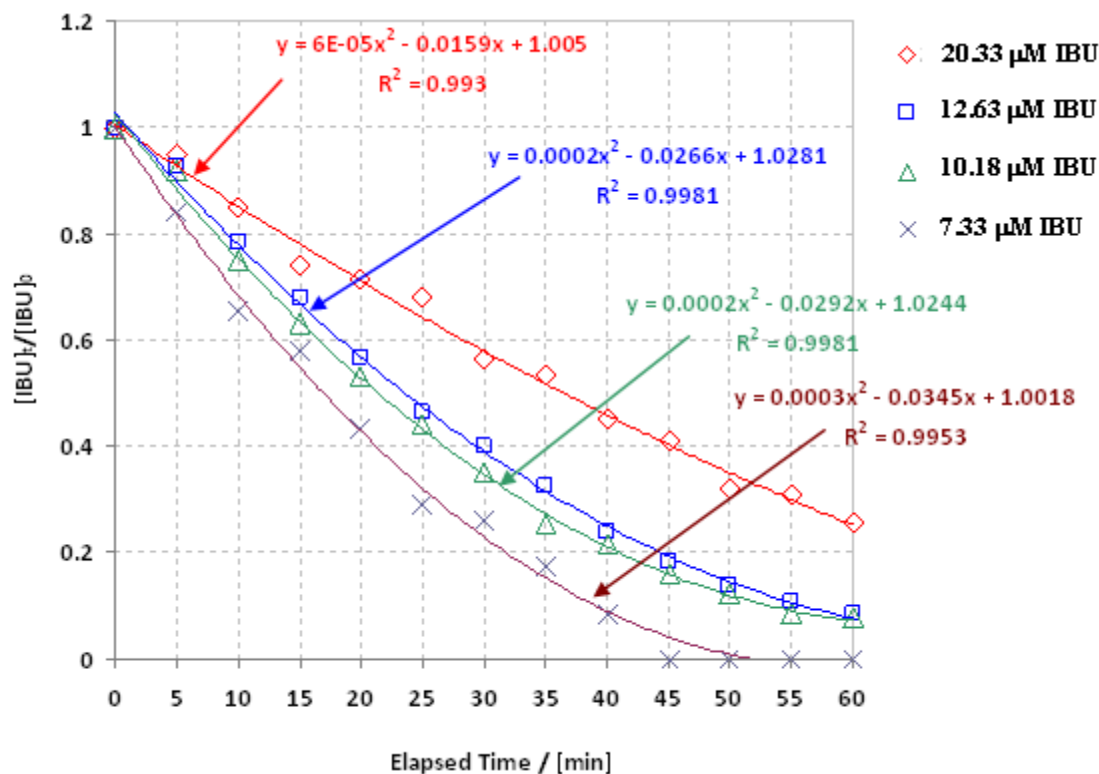
Fig. 14. (a) Normalized measured IBU concentrations and fits of the polynomial regression analysis. Experimental conditions: $[I]_{PB} = 0.09$ M, pH = 7.0, Temperature = 60°C, $[IBU]_0 = 7.33$-20.36 μM, $[SPS]_0 = 1.00$ mM.

Accordingly, it seems that transformation products are not within the detection limit of the LC/MS and that at least part of IBU has been mineralized by the action of $SO_4^{\bullet-}$ and $OH^{\bullet}$ available into the solution [89]. Additional analysis using UV/Vis spectroscopy on the whole IBU treated solution showed complete transformation of the UV/Vis spectrum in which the characteristic absorbance band 215–225 nm of IBU vanished completely. However, a hyperchromic shift is noticed at 263 nm accompanied with a hypsochromic shift ($\lambda = 255$ nm). The latter was unstable because it was followed at an advanced treatment time (2 h) by a serious decrease in its absorbance. This observation could be an indicator of the formation of non-stable transformation products followed by at least partial mineralization of IBU. Table 7 summarizes

55

also the half-lives ($t_{1/2}$) calculated from the resulting polynomial equations shown next to the decline plots of Fig. 12. These half-lives can be used for the determination of the reaction rate law as an alternative method of the method of initial rates commonly employed (method **1**) [90]. The latter is most likely an estimation over a very short time of the initial rate before any significant change in the concentration of the reactant and additional formation of by-products have occurred. Because preliminary results showed absence of by-products due to their very low concentration or to their non existence, the method of half-lives (method **2**) based on the half-life of a reaction as a function of the initial concentration of one reactant when the other is kept abundant is evaluated. Method **2** has been successfully used for the determination of the reaction rate law of TCE degradation by thermally activated SPS at 40 °C [74]. The results obtained demonstrated that the degradation of TCE was zero order in TCE and therefore independent of the initial concentration of TCE. It has been shown that half-life periods were more suitable for the elucidation of a reaction order than the method of initial rates. The time for IBU concentration to decrease by half its initial concentration correlated with reaction order a can be expressed as follows [91]:

$$t_{1/2} = \{2^{(a-1)} - 1\} / \{k_a \, (a-1)[IBU]_0^{(a-1)}\} \qquad \text{(Eq. 19)}$$

Assuming that $a \neq 1$, the half-life can be written as part of a function of $[IBU]_0$ as follows:

$$t_{1/2} = F(a, k_a)/\{[IBU]_0^{(a-1)}\} \qquad \text{(Eq. 20)}$$

Yielding

$$\ln\left(t_{\frac{1}{2}}\right) = \ln\{F(a, k_a)\} - (a-1)\ln[IBU]_0 \qquad \text{(Eq. 21)}$$

After taking logarithms of both sides of Eq. (20). The half-lives of IBU were calculated using equations obtained via polynomial regression analysis (Table 7, Fig. 14). Fig. 15 illustrates the relationship between $\ln(t_{1/2})$ and $\ln[IBU]_0$ in accordance with Eq. (21). The expression gives excellent linearity with a correlation coefficient $R^2 = 0.9917$, and the slope is 0.76 (± 0.05), which is equal to $-(a-1)$. Consequently, the reaction order with respect to IBU is ~ 0.25. This result is different than the one reported by Liang and Bruell [29] who found a zero order reaction ($a = 0.03$) in TCE under thermally activated SPS degradation. This discrepancy might be due to experimental conditions in terms of [PB]:[SPS]:[organic molecule] ratio. For example, the ratios used by Liang and Bruell [75] were about [0.45]:[1.0]:[0.012] and [1.48]:[1.0]:[0.010] showing phosphate buffer content equals to half or 1.5 times SPS content. However in IBU case, the ratios used were about [7.1]:[1.0]:[0.007] and [20]:[1.0]:[0.007] showing a PB content 7–20 times greater than SPS. This can explain the fractional order (1/4) obtained in IBU especially if radical-PB reactions are likely to happen even at lower rate than radical-IBU reactions. Accordingly, the elucidation of a common kinetics law for organic compounds of different chemical structures is difficult to be established and a case by case study is required under similar experimental conditions (e.g. probe concentration, temperature activation, buffer capacity, etc.). Another aspect of Fig. 14 is that by late stage of the reaction, the polynomial fitted lines do not exhibit curvature as the one reported during the degradation of TCE by SPS [75]. The authors considered only initial data for polynomial fittings in contrast to the present case of IBU where data have been considered throughout the total reaction time (up to 60 min). This did not affect at all the correlation coefficients of the polynomial regression that are found close to unity. On the other hand possible pseudo-first order behavior may be adopted because good correlations have been obtained when data are fitted with the first order model

$(0.95 < R^2 < 0.98)$. Nevertheless, both method of data analysis showed similar results. For example, increases in $t_{1/2}$ (from 17.08 to 36.89 min) occurred with increases in $[IBU]_0$ (from 7.33×10^{-3} to 20.30×10^{-3} mM). This tendency is not usually observed especially for reactions with two reactants where an increase in the concentration of any of the two species will result in an increase of the reaction rate or a decrease in $t_{1/2}$. In the case of IBU degradation, the concentration of SPS is almost constant and IBU degradation seems to follow a pseudo-zero order reaction with an average rate constant of $(2.5 \pm 0.3) \times 10^{-4}$ mM min^{-1} calculated by applying the derived $t_{1/2}$ equation (Eq.22) using the zero-order kinetics model.

$$k_a = [IBU]_0/2t_{1/2} \qquad (22)$$
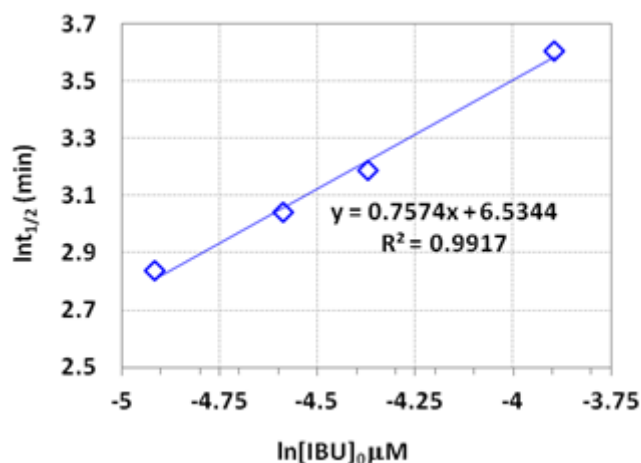
Fig. 15. Plot of ln(t1/2) vs. ln[IBU]$_0$. A slope of 0.7574 = -(a-1). Experimental conditions: $[I]_{PB}$ = 0.09 M, pH = 7.0, temperature = 60 °C, $[IBU]_0$ = 7.33–20.36 μM, $[SPS]_0$ = 1.0 mM.

3.2. Effect of SPS concentration under fixed IBU concentration (case 2)

The second set of experiments (case **2**) was carried out by fixing the concentration of IBU to 20.36 μM and varying the concentration of SPS from 1.0 to 2.8 mM. Case **2** experiments have been designed since it is impossible to undertake reactions keeping the concentration of IBU in great excess compared to that of SPS as it was in case **1** experiments (SPS in great excess). This

58

is due to the limited solubility of IBU in water estimated to 21 mg L^{-1} (101.8 μM) compared to that of SPS. The purpose of those experiments was to determine the reaction order b in SPS. Under these conditions, the resulting [SPS]$_0$/[IBU]$_0$ molar ratios are the same as those mentioned above (Section B.1). A rearrangement of Eqs. (17) and (18) yields the following relationships:

$$k_a = k[SPS]_t^b \approx k[SPS]_{t=0}^b \qquad \text{(Eq. 23)}$$

Taking logarithms of both sides of Eq. (23) yields:

$$\ln_{ka} = \ln k + b \ln[SPS]_{t=0} \qquad (Eq.\ 24)$$

The data of case **2** experiments plotted with normalized [IBU]$_t$/[IBU]$_0$ analysis shows excellent polynomial regression fittings with also correlation coefficients R^2 > 0.99 as it can be noticed from Fig. 16. The calculated k$_a$ values using Eq. (22) are reported in Table 8. A plot of ln(k$_a$) vs. ln[SPS]$_0$ shows excellent linearity with a correlation coefficient R^2 = 0.9912 (Fig. 17). According to Eq. (13), the slope obtained (slope = 0.9789) corresponds to the reaction order b with respect to SPS. Therefore, the reaction order of IBU oxidation reaction in SPS seems to be first order. This result is not in accordance with previous research work where SPS, used as an initiator for polymerization reactions, showed fractional reaction order of about 1/1.54 in SPS [90]. Furthermore, a more recent study done by Liang and Bruell [75] showed a reaction order in SPS of about 1/1.25 when TCE was treated in thermally activated SPS solutions (T = 40 °C). In this study, the reaction orders with respect to IBU and SPS were found to be 1/4

and 1.0, respectively which are slightly different than previous orders reported in other SPS oxidation reactions. This can be due to the probe used, the activation temperature and most probably to the ratios between reactants as previously described. The average overall rate constant of the reaction can be determined from the y intercept of the straight line of Fig.17 which is equal to 2.71×10^{-4} mM$^{1-(a+b)}$ min^{-1}. Consequently, the kinetics reaction law between SPS and IBU would be described by the following equation (Eq. 25):

$$r = -\frac{d[IBU]}{dt} = k[IBU]^a[SPS]^b = \left(2.71 \times 10^{-4} mM^{1-(a-b)^{-1}} min \right) \times [IBU]^{0.25}[SPS]^1 \quad \text{(Eq. 25)}$$

This law could be used to describe the degradation of IBU under specific conditions described in this work. However it would be interesting to check the validity of this law on pharmaceutical molecules of the same family (e.g. ketoprofen, naproxen) under similar conditions in order to confirm if such kinetics law can be expanded to other pharmaceuticals.
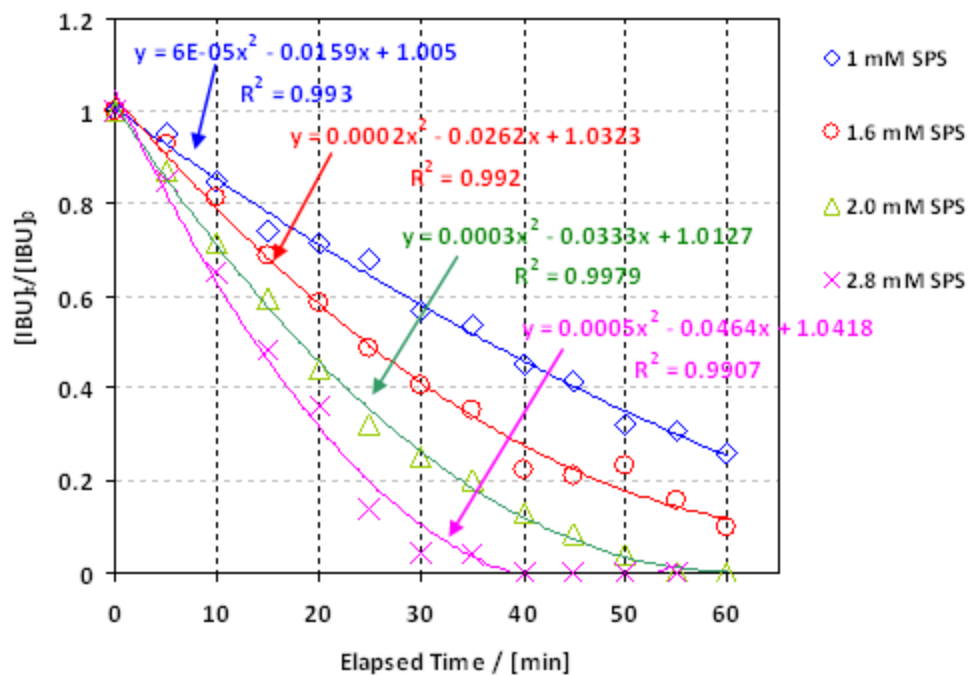
Fig. 16. Normalized measured IBU concentrations and fits of the polynomial regression analysis. Experimental conditions: $[I]_{PB} = 0.09$ M, pH = 7.0, temperature = 60 °C, $[IBU]_0 = 20.36$ µM, $[SPS]0 = 1.0$-2.8 mM.
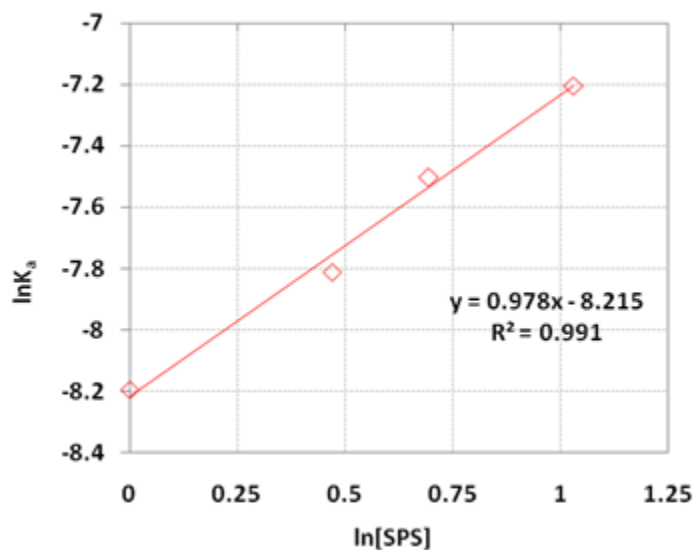
Fig. 17. Plot of ln(ka) vs. ln[SPS]. The slope obtained (0.9789) is the reaction order in SPS. All data are relative to experiments undertaken in Fig. 16. Experimental conditions: $[I]_{PB} = 0.09$ M, pH = 7.00, temperature = 60 °C, $[IBU]0 = 20.36$ µM, $[SPS]0 = 1.0$-2.8 mM.

4. Study of predominant oxidant in SPS/IBU/PB system ($SO_4^{•-}$/OH$^•$)

One of the most important advantages in using SPS for the oxidation of OC in aqueous systems is its ability to produce after activation $SO_4^{•-}$ and OH$^·$, the former being more selective. HO$_•$ is known to undergo by hydrogen abstraction while $SO_4^{•-}$ is more specific for electron transfer reactions [44]. A better understanding on the contribution of each type of those radicals in degrading IBU is evaluated by using radical scavengers like ethanol (EtOH) and tert-butyl alcohol (TBA) [36], [81], [82], [83] and [27]. Three aqueous PB ($[I]_{PB} = 0.09$ M) systems (Alcohol scavenger/SPS/IBU) were designed with the following ratios: system **1**(0/100/1), system **2** (40,000/100/1) and system **3** (40,000/100/1). Under those conditions, the concentration of the alcohol scavenger (800 mM) is 400 times greater than the concentration of the oxidant (2 mM) and 40 times greater than the concentration of phosphate species. This was designed in order to sufficiently quench the generated radicals instead of reacting with IBU probe at 20.36 μM (high scavenger density). The results obtained are summarized in Fig. 18. As it can be noticed, in the absence of alcohol (System **1**), almost full IBU degradation (lower curve) takes place mostly due to the action of both radicals $SO_4^{•-}$ and OH$^•$. However, in the presence of EtOH (System **2**), the scenario is reversed where negligible IBU degradation is noticed (~8%, upper curve). This can be explained by the consumption of almost all radicals ($SO_4^{•-}$ and OH$^•$) by EtOH as it is described by the high rate constants of the below reactions [27]. Therefore, a negligible amount of radicals could react with IBU to assume only 8% oxidation.

$$EtOH + OH^· \sim 1.2 - 2.8 \times 10^9 \ M^{-1}s^{-1}$$

$$EtOH + SO_4^- \sim 1.6 - 7.7 \times 10^7 \ M^{-1}s^{-1}$$

$$t - BuOH + OH^· \sim 3.8 - 7.6 \times 10^8 \ M^{-1}s^{-1}$$

$$t - BuOH + SO_4^- \sim 4.0 - 9.1 \times 10^5 \ M^{-1}s^{-1}$$
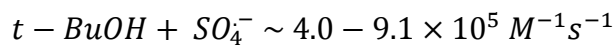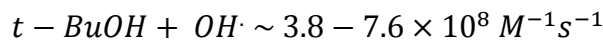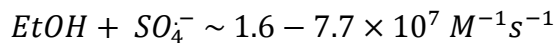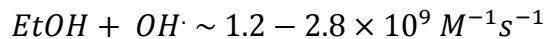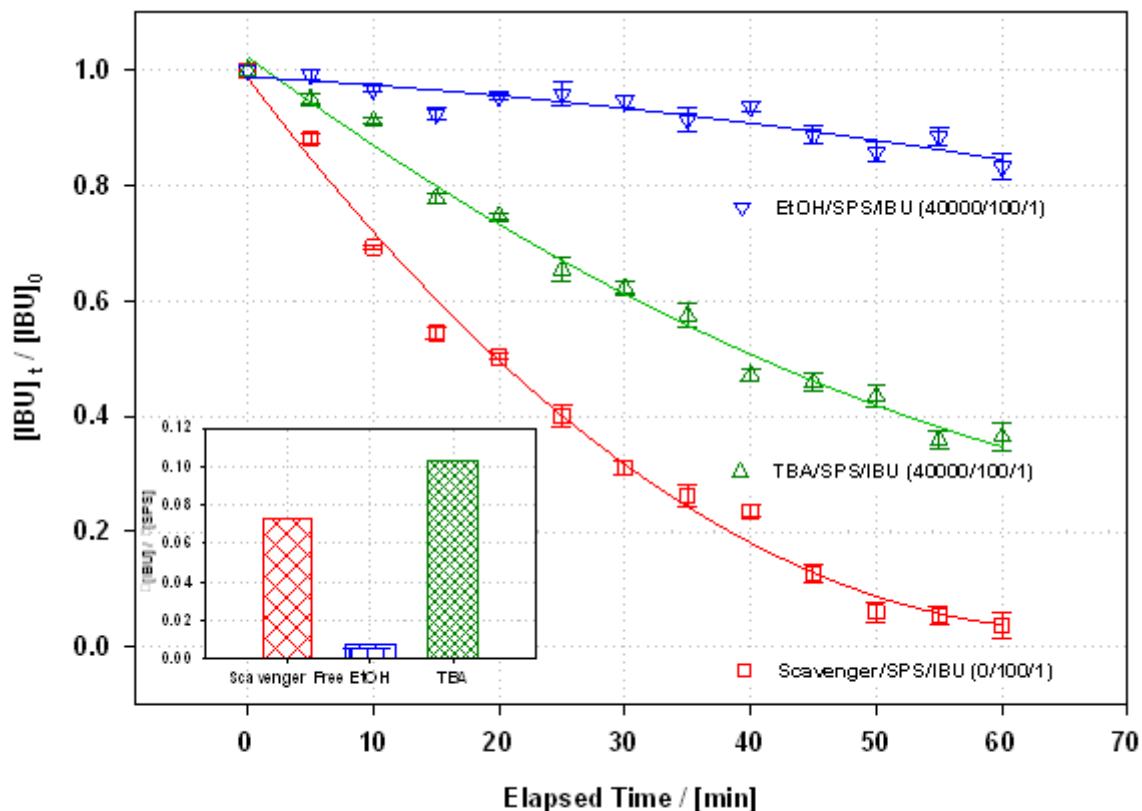
Fig. 18. Effect of EtOH and TBA as radical scavengers on the degradation of IBU at 60 _C. The solid lines are fitting functions. The inset shows the reaction stoichiometric efficiency (RSE) for the different systems at 60 min of reaction time. Experimental conditions: $[IBU]0 = 20.36$ lM, $[SPS]0 = 2.0$ mM and $[I]PB = 0.09$ M. The numbers between brackets next to the studied systems correspond to the molar ratio of species into the system.

In the presence of TBA (system **3**), however, the degradation process occurs to an extent of 65% (mid curve). In this case, the $OH^{\bullet}$ produced react with TBA while $tSO_4^{\bullet-}he$ will be poorly quenched by TBA and consequently most of them will react with IBU. This explanation is justified after calculation of the RSE at 60 min of reaction for the three systems. The inset of Fig. 18 shows clearly a non-significant RSE (<1.0%) for system **2** using ethanol as scavenger due to poor IBU degradation (only 8%) and a very high SPS consumption attributed to the high reaction rates of EtOH with both $SO_4^{\bullet-}$ and $OH^{\bullet}$ radicals. In system **1** (alcohol free solution), the

63

calculated RSE is about 7.5% while in system **3** (presence of TBA) it reached 10.5%. The latter being the highest RSE found can explain the selectivity of $SO_4^{\bullet-}$ in oxidizing IBU in the presence of TBA. However in alcohol free solution, $SO_4^{\bullet-}$ and $OH^{\cdot}$ are both involved in the oxidation of IBU. This can increase the number of $SO_4^{\bullet-}$ consumed and therefore decreasing the RSE (from 10.5% in system **3** to 7.5% in system **1**). Under the current conditions and regardless of phosphate species interferences with sulfate and hydroxyl radicals, one might estimate that $SO_4^{\bullet-}$ is more responsible of IBU degradation than $OH^{\bullet}$. IBU oxidation seems to be more affected by $SO_4^{\bullet-}$ than Bisoprolol (BIS) being treated under similar conditions to the exception of PB content ([PB] = 50 μM) [10]. In fact the latter has the same concentration of Bis (50 μM) with a molar ratio [phosphate]:[SPS]:[organic molecule] of about [0.05]:[1.0]:[0.05] while in the current case PB content is 980 times greater than IBU with a molar ratio of about [10]:[1.0]:[0.0102]. As a result, phosphate species might play a role in the whole oxidation reaction based on the reaction rate constants of $SO_4^{\bullet-}$ with phosphate species ($H_2PO_4^-$ and HPO_4^{2-}) as reported in Section 2.3.1. The higher selectivity of SO_4^- towards IBU is demonstrated by its higher% removal in TBA systems. While in the current study an estimation of 65% removal of IBU was attributed to $SO_4^{\bullet-}$, the later was only responsible of 51% removal in the case of BIS [10]. This might be due to the stable pH value throughout the TAP treatment because of the higher ionic strength used (e.g. $[I]_{PB} = 0.09$ M for IBU instead of $[I]_{PB} \sim 10^{-4}$ M for BIS) and the chemical structure of the probes studied. In fact, BIS presents aliphatic chains bonded to the benzene ring. Those chains are more reactive with $OH^{\cdot}$ than $SO_4^{\bullet-}$ due to the presence of more available α-hydrogen atoms. However, IBU has less aliphatic chains which favor more its reaction with $SO_4^{\bullet-}$ through electron transfer mechanism.

5. Chapter conclusion

It was demonstrated that thermally activated persulfate can effectively oxidize recalcitrant pharmaceuticals like IBU over a reasonable time period (e.g. min to h) at pH 7.0 with a high reaction stoichiometric efficiency (e.g. RSE = 0.65) compared to that of pHs 4.0 and 9.0 at $60^{\circ}C$. The oxidation reaction showed excellent Arrhenius behavior with activation energy of about 168 (± 9.5) kJ mol^{-1}. Reactions in the presence of radical quenchers (EtOH and TBA) showed the implication of both radicals $OH^{\bullet}$ and $SO_4^{\bullet-}$ in oxidizing IBU. Results showed also that IBU degradation can be explained by pseudo-first order model however a deep investigation into the reaction order yielded a more accurate kinetics rate equation that can be described by the following equation:

$$-\frac{d[IBU]}{dt} = (2.71x10^{-4}mM^{1-(a+b)}\min^{-1})x[IBU]^{0.25}[SPS]^{1}$$

With the limits of the experimental conditions applied here. The oxidation reaction exhibited a fractional order 0.25 with respect to IBU demonstrating that a change in $[IBU]_0$ at a fixed $[SPS]_0$ would result in different IBU degradation rates. Furthermore, the elaborated kinetics model showed that the reaction is first order with respect to SPS therefore an increase in $[SPS]_0$ for a fixed $[IBU]_0$ will result in faster IBU degradation rate.

CHAPTER IV
DEGRADATION OF NAPROXEN VIA HEATED PERSULFATE IN AQUEOUS SOLUTION

A. Materials and Methods

1. Chemicals

Pharmaceutical grade Naproxen sodium (NAP), Sodium Persulfate (SPS) ($Na_2S_2O_8$, 99+%) and Acetic acid glacial (CH_3COOH, 99.5+%) were purchased from Sigma-Aldrich (China), Chem-Lab (Belgium) and Surechem Products LTD (UK), respectively. Sodium dihydrogen phosphate dihydrate ($H_2NaO_4P\cdot2H_2O$, 99+%) and disodium hydrogen phosphate (Na_2HPO_4, 99+%) were acquired from Fluka (Netherlands) and Merck (Germany), respectively. Potassium iodide (KI) (puriss, 99-100.5%) and potassium dihydrogen phosphate (KH_2PO_4) were obtained from Riedel-de-Haen (Germany). Acetonitrile (CH_3CN) and methanol (CH_3OH) were both of HPLC grade and purchased from Sigma (USA).

2. Chemical analysis

2.1 HPLC-DAD-FLD-MSD

NAP was analyzed using an Agilent 1100 Series liquid chromatography (LC). The LC system is composed of a quaternary pump equipped with a vacuum degasser, thermostated autosampler and column compartment in addition to a diode array detector (DAD) and a fluorescence detector (FLD) in series with an ion-trap mass spectrometry detector (MSD). A C_{18} reverse phase column (5 μm; 4.6 i.d. × 250 mm long) attached to a pre-column guard HS C_{18} (5 μm; 4.6 i.d. × 20 mm long, Discovery, Supleco, USA) was used for the separation of pharmaceutical molecules and all derivatives. Both column and column guard were maintained at 30°C throughout the analysis. The mobile phase consisted of acetonitrile (55%) and 0.04% (v/v) acetic acid glacial (45%) percolating through the column in an isocratic mode with a flow

rate of 1.0 mL min^{-1}. The sample injection volume was about 50 µL. The whole chromatography system was controlled by Agilent ChemStation software for LC and LC/MS systems version A.09.0.

For HE samples, the same HPLC system was used however with gradient elution in order to better separate pharmaceuticals inside. Mobile phase was composed of (A) 50 mM potassium dihydrogen phosphate (KH_2PO_4) and (B) acetonitrile. The gradient was run as follows: At time 0-4.5 min 85% of mobile phase A and 15% of mobile phase B; at t = 12.5 min 80% A and 20% B; at t = 18 min 75% mobile phase A and 25% mobile phase B; finally at t = 27-45 min 55% of mobile phase A and 45% mobile phase B.

2.2. GC-MS

MS analyses were performed on a thermo scientific GC-MS equipped with a POLARIS Q Ion Trap MS detector, a Thermo Finnigan autosampler and XCalibur software (USA) in order to identify NAP transformation products. The conditions were as follows: EI = 70 eV, manifold temperature 473 K, dwell time 100 µs and scan range of 50-500 m/z. Separation was done on Agilent DB-23 column (30 m length, 0.25 mm internal diameter and 0.25µm film thickness) flushed with Helium as carrier gas. The injection volume was about 2 µL. System temperature was programed to start at 373 K for 2.5 min followed by a 6 K/min increase up to 523 K then held for 15 min.

2.3. Persulfate analysis

Persulfate anion concentration was determined spectrophotometriclly using a 1 mm path length on a Nanodrop 2000c UV-VIS spectrophotometer (Thermo scientific) as per procedure developed by Liang and Bruell [35]. When $[SPS]_0 \leq 1.0$ mM the absorbance of the complex was measured at $\lambda = 352$ nm. However for $[SPS]_0 > 1.0$ mM absorbance was measured at $\lambda = 400$

nm. SPS calibration curves were performed with a range of concentrations of 5-1000 µM. The limit of detection of SPS under these conditions was less than 5.0 µM [91].

2.4. Total organic carbon

TOC measurements were conducted using Sievers 5310C laboratory TOC analyzer by General Electric (USA). The system measures the amount of carbon dioxide produced upon oxidation through a percolating specific membrane by difference of conductivity.

2.5. Solid phase extraction

Solid phase extraction (SPE) was carried out on a Supelco Visiprep SPE cell. SPE cartridges used were Supelclean LC-18 SPE tube with 500 mg bed weight and 6 mL volume. All extractions were done at a rate of 50 drops/min as recommended by the supplier. Prior to sample extraction, SPE cartridges were conditioned by passing 5 mL of ACN with a flow rate of 50 drops/min. The % recovery was tested by passing 1 mL of a 20 ppm NAP solution with the same flow rate through the cartridge and extracted with 10 mL ACN. The extract was then purged with N_2 gas until all solvent has evaporated. The residues were dissolved in 1 mL of MeOH and injected into the HPLC to measure NAP concentration using the calibration curve. The % recovery was always found to be greater than 98%. As for the collected samples, the same procedure was followed and aliquots were injected either into the HPLC/MS or the GC/MS especially for by-products identification.

3. Experimental setup

All reagents were prepared at high concentration stock solution from which dilutions were made. The stock solutions were prepared as follows: 20 mg of NAP sodium were dissolved in 1 L of DI water and left to stir over night. The NAP stock solution was filtered using a 0.45

μm PTFE filter and kept at 4°C for a period no longer than 1 week. SPS stock solution was prepared by dissolving 2.3810 g of solid SPS in 100 mL deionized water so as to give a 0.100 M stock solution. As for the stock of phosphate buffer (PB) solution, a 0.200 M solution of pH = 7.50 was prepared by dissolving 3.1698 g and 3.343 g of NaH_2PO_4 and Na_2HPO_4, respectively in 100 mL deionized water. KI solution used for persulfate complexation was prepared by dissolving 25 g of KI in 250 mL of carbonated deionized water. SPS, PB and KI stock solutions were prepared on a daily basis.

For the work done on the HE, 10 L were collected at 6:00 a.m. from the final sewage hole of the hospital located just before the waste water is introduced into the Beirut municipal sewage system. The HE was collected in a PTFE bottle and immediately went through several steps of pre-treatment. Gravity filtration using cotton was done in order to remove any large solid waste in the water. Suction filtration through a 0.45 μm filter was performed to remove fine particles. Ultra-centrifugation for 30 min at 15,000 RPM (Sorvall Discovery 100SE Ultracentrifuge, Hitachi) was performed to remove any particles less than 0.45 μm in size which remained suspended in solution. The clear water remaining was then decanted and stored in an amber bottle at 4°C for a maximum period of a week. A new 10 L water sample was collected again at the same time when needed and treated similar to what has been described above.

All reactions were performed in 20 mL Pyrex vials and predetermined volumes of each stock solution were added to reach the final desired concentrations e.g. $[NAP]_0 = 50$ μM, $[SPS]_0 = 1.0$ mM and $[PB] = 50$ μM. Vials were placed in a temperature controlled water bath with the required temperature preset (range 40-70°C). At the desired times a vial was removed from the water bath and the reaction was thermally quenched by cooling the vial to 4°C in an ice bath. Experiments were performed over a period of 2 h and the pH was measured at the start and end

of each reaction using a pH/Ion meter (Thermo Orion, USA) equipped with an ultra-combination pH electrode (Ross). Control experiments were performed in the absence of SPS and all experiments were done in triplicate.

B. Results and discussion

1. Temperature effect
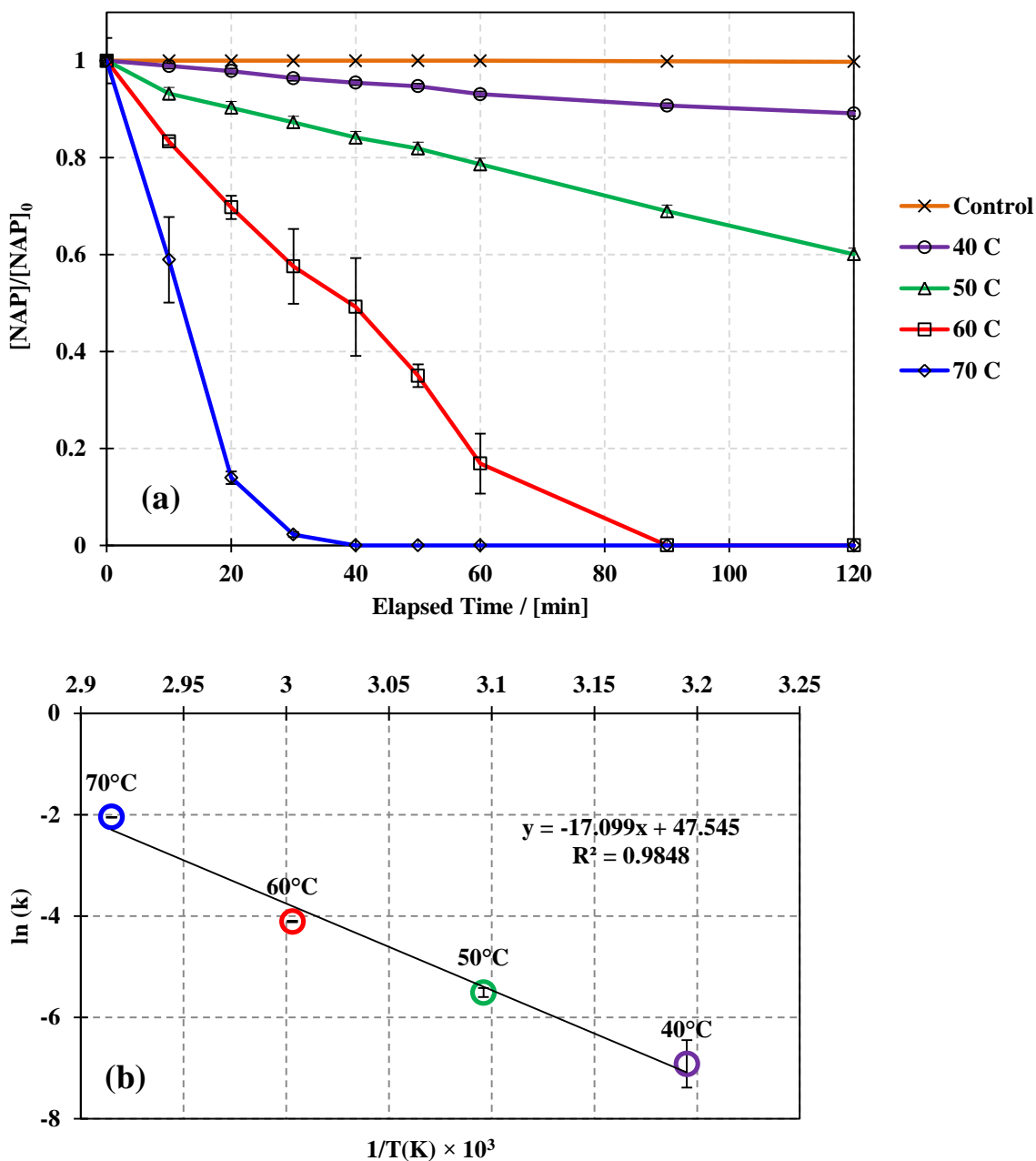
Fig. 19. (a) Temperature effect on the degradation of NAP via thermally activated persulfate.

Solid lines are not fitting functions; they are used in order to connect data. Experimental

conditions: $[NAP]_0 = 50$ µM, $[SPS] = 1.0$ mM, PB at pH = 7.50. Error bars representing standard deviation are calculated at 95% confidence level. (b) Arrhenius plot for the temperature effect experiments. Uncertainties were calculated from standard deviation on the slope determined after using the LINEST function of Microsoft excel.

Table 8. k_{obs} calculated at different temperatures

Temperature (°C)	k_{obs} (mM min^{-1})	R^2
40	9.90×10^{-4}	0.9844
50	4.05×10^{-3}	0.9874
60	2.69×10^{-2}	0.9837
70	1.29×10^{-1}	0.9893
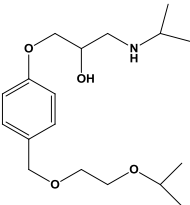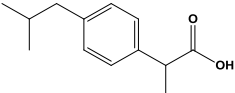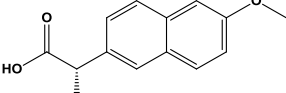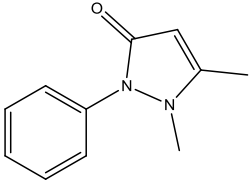
As it can be seen from Fig. 19a, the degradation rate of NAP solution is temperature dependent. All reactions undertaken at different temperatures (40, 50, 60 and 70°C) fit well the pseudo first-order kinetics with a correlation coefficient R^2 always greater than 0.9800. The corresponding observed degradation rate constants (k_{obs}) calculated from the slope of the plots of Ln($[NAP]/[NAP]_0$) vs Time ranged between 9.90×10^{-4} mM min^{-1} for the lowest temperature (40°C) and 1.29×10^{-1} mM min^{-1} for the highest temperature (70°C) as summarized in Table 8. Fig. 19b shows the Arrhenius plot for Naproxen degradation at different temperatures. Since Ln(k_{obs}) decreases linearly when plotted against 1/T, the systems can be fitted into the Arrhenius model (Eq. (26)) with good linearity showing a correlation coefficient of about $R^2 = 0.9848$.

$$Ln\ (k_{obs}) = Ln\ (A) - \frac{E_A}{RT} \qquad (26)$$

where A is the pre-exponential factor found from the intercept of the Arrhenius plot, E_A is the

activation energy, T is the temperature in Kelvin and R the universal gas constant (R = 8.314 J

$mol^{-1} K^{-1}$).

Using this model, the activation energies (E_A) was found equal to 155.03 ($\pm$26.4) kJ mol^{-1} (Table

9). This value is less than the one obtained for ibuprofen (IBU) (168.0 ($\pm$9.5) kJ mol^{-1}) and

greater than that of bisoprolol (BIS) b-blocker (119.8 ($\pm$10.8) kJ mol^{-1}) making from IBU the

most recalcitrant pharmaceutical [92] followed by NAP, (BIS) [10] and antipyrine [50]. The

latter having the lowest activation energy of 16.55 kJ mol^{-1} can be easily explained by the

presence of a 5-member ring pyrazole cycle very vulnerable to oxidation by hydrogen

abstraction through $OH^{\bullet}$ and/or electron transfer (ET) through $SO_4^{\bullet-}$. However, oxidation via

$SO_4^{\bullet-}$ is more favored in that case because of the presence of nonbonding electrons on the

nitrogen atoms as well as on oxygen atoms. As for the other compounds, one can notice that

molecules identified with more ether functions showed the lowest E_A. e.g. BIS. This can be

explained by the presence of oxygen atoms forming ether groups in side chains which are

vulnerable to oxidative radicals (abstraction of nonbonding electrons from oxygen atoms by

$SO_4^{\bullet-}$), more than molecules of comparable structure however exempted from ether groups [93].

Table 9. Comparison between the chemical and physical properties of NAP and other pharmaceuticals from previous work, as well as the experimental observed degradation rates (k_{obs}) and the calculated activation energies (E_a).

	Bisoprolol	Ibuprofen	Naproxen	Antipyrine
Medicinal property	β-blocker Hypertension	Non-steroidal Anti-inflammatory	Non-steroidal Anti-inflammatory	Analgesic and Antipyretic
Chemical Formula	$C_{18}H_{31}NO_4$	$C_{13}H_{18}O_2$	$C_{14}H_{14}O_3$	$C_{11}H_{12}N_2O$
Molecular weight (g/mL)	325.44	206.29	230.259	188.226
Chemical Structure				
Solubility (mg/L)	2,240	21	15.9	51,900
pKa	9.5	4.91	4.15	1.4
Density (g/mL)	1.033	1.029	1.197	1.190
Melting point (°C)	100	75-78	152-155	113
k_{obs} at 60°C (x 10^{-2} min^{-1})	8.47[1]	2.49[2]	1.64	54.5[3]
E_a (kJ.mol^{-1})	119.8(±10.8)	168.0(±9.5)	155.0(±26.4)	16.55

[1]Ghauch et al. [10]

[2]Ghauch et al. [92]

[3]Calculated from k_{obs} reported in s^{-1}; Tan et al. [50]
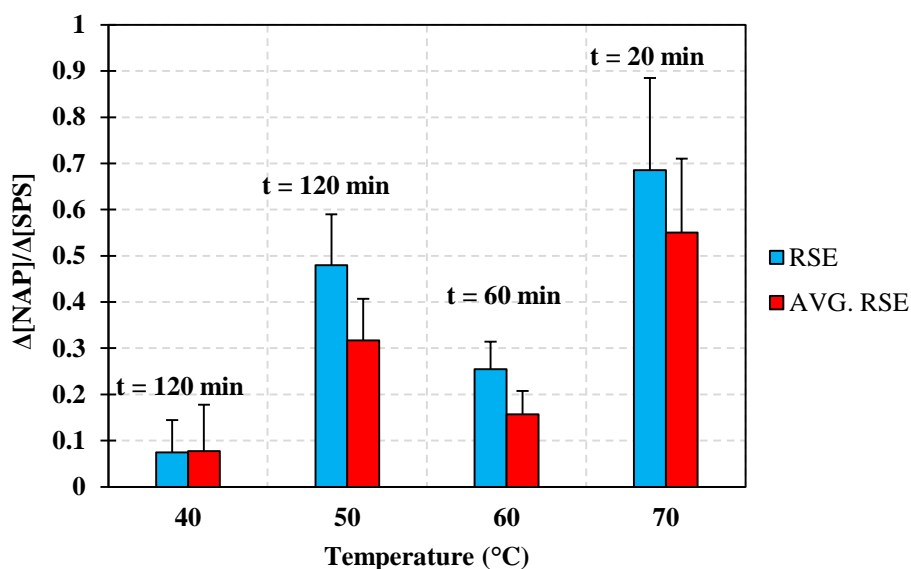
Fig. 20. Maximum and average RSE values noticed at different reaction times under different temperatures. The calculated RSEs are from data collected in Fig. 19. Error bars representing standard deviation are calculated at 95% confidence level.

Fig. 20 summarizes the maximum and average values of the reaction stoichiometric efficiencies (RSEs) obtained for all oxidation reactions undertaken at different temperatures e.g. 40-70°C. The RSE is the number of NAP moles degraded over the number of SPS moles consumed during a specific time interval [$RSE = \frac{\Delta n(NAP)}{\Delta n(SPS)}$]. As it can be noticed, the calculated RSEs (maxima and averages) follow the same trend in terms of reaction temperature. For example, the maximum RSEs are noticed at 70°C (RSE = 68%) and 50°C (48%) while the minimum RSEs obtained are for reactions occurring at 40°C (RSE = 7.5%) and 60°C (24%). Compared to previous work done on different pharmaceuticals however under similar conditions, NAP showed lesser RSE at 60°C. For example the calculated RSEs for BIS and IBU after 1 hour of reaction were about 65% and 70%, respectively [10, 92]. This observation has important input

on the interpretation of the kinetics law and the role of dissolved species involved in the oxidation mechanisms. As mentioned in Table 9, k_{obs} of NAP is the smallest one (k_{obs} = 1.64 x 10^{-2} min^{-1}) followed by IBU (k_{obs} = 2.49 x 10^{-2} min^{-1}) and BIS (k_{obs} = 8.47 x 10^{-2} min^{-1}) under pseudo-first order kinetics model. Accordingly, it is not surprising to notice lesser RSE for NAP at 60°C because of its chemical structure more susceptible to $SO_4^{\bullet-}$ than $OH^{\bullet}$. BIS and IBU showed almost equal affinity (45-55%) toward $SO_4^{\bullet-}$ and $OH^{\bullet}$ as well [10, 92] in contrast to NAP whose affinity to $SO_4^{\bullet-}$ was much stronger (90% for $SO_4^{\bullet-}$ against only 10% for $OH^{\bullet}$) as per quenching experiments data (section 3 of this chapter). Therefore, more PS is consumed for lesser NAP degradation dropping thereby the RSE value from 65-70% to less than 30%. Therefore RSE parameter with respect to PS consumed cannot be used a key factor to evaluate TAP effectiveness especially with pharmaceutical probes of different structures and properties. Details on the most active oxidant toward NAP are provided in section B of this chapter.

2. Persulfate dosage and effect on mineralization

Previous studies showed that although some pharmaceutical active ingredients undergo thermal persulfate oxidation however, acceptable mineralization yields were not reached unless higher concentrations of persulfate are being used [92]. In this work a comparative study was done so as to demonstrate complete mineralization of NAP in two different matrices. Experiments were undertaken on NAP dissolved in (i) UP water and (ii) HE matrix at 70°C. The results showed that any SPS:NAP molar ratio above (20:1) was enough to fully degrade NAP however at different contact times. For example, NAP totally disappeared after 60, 30, 20, 10 and 10 min of reaction for SPS concentration of about 1.0, 2.5, 5.0, 7.5 and 10.0 mM, respectively (Fig. 21a). Although full degradation was reached, this was however not sufficient to reach significant NAP mineralization as per TOC analysis (Fig. 21b). Accordingly, SPS

concentration was increased in increments from 1.0 mM to 10 mM yielding an upper limit molar ratio SPS:NAP of about 200:1. As it can be noticed from Fig. 21b, at 1.0 mM SPS no mineralization was observed unfortunately. However, a minimum acceptable molar ratio SPS:NAP of about (1:50) was needed in order to exhibit little mineralization to not exceed 10%. As the concentration of SPS increases from 2.0 to 7.5 mM, one can notice a linear mineralization trend with correlation coefficients R^2 of about 0.9911 and 0.9964 for UP water and HE systems, respectively. However, the linear dynamic range in the case of the HE system (2.5-10.0 mM) is greater than the one noticed for UP water system (2.5-7.5 mM). Furthermore, mineralization of NAP in UP water is more significant e.g. 42% and 90% against 30% and 65% for UP water and HE, at 5.0 and 7.5 mM SPS, respectively. This can be attributed to the matrix effect of the HE potentially containing a large spectrum of pharmaceuticals and a mixture of dissolved ions. Those might quench $SO_4^{-\bullet}$ and $OH^{\bullet}$ minimizing therefore the reaction efficacy and % RSE of the reaction. Fig. 21b shows also that above a critical SPS concentration limit e.g > 10 mM, the matrix effect becomes negligible and full mineralization is reached as well even in HE matrix. Furthermore, one can also predict, from data of Fig. 21b, that full NAP mineralization in UP water matrix occurred at [SPS] = 8.0 mM and this based on the corresponding linearity response curve. Recall that oxic solutions favor more organic contaminants' mineralization in activated PS/H_2O systems as it has been recently demonstrated in SPS chemically activated systems [32] making from dissolved oxygen an important parameter to maintain in SPS-based AOPs.
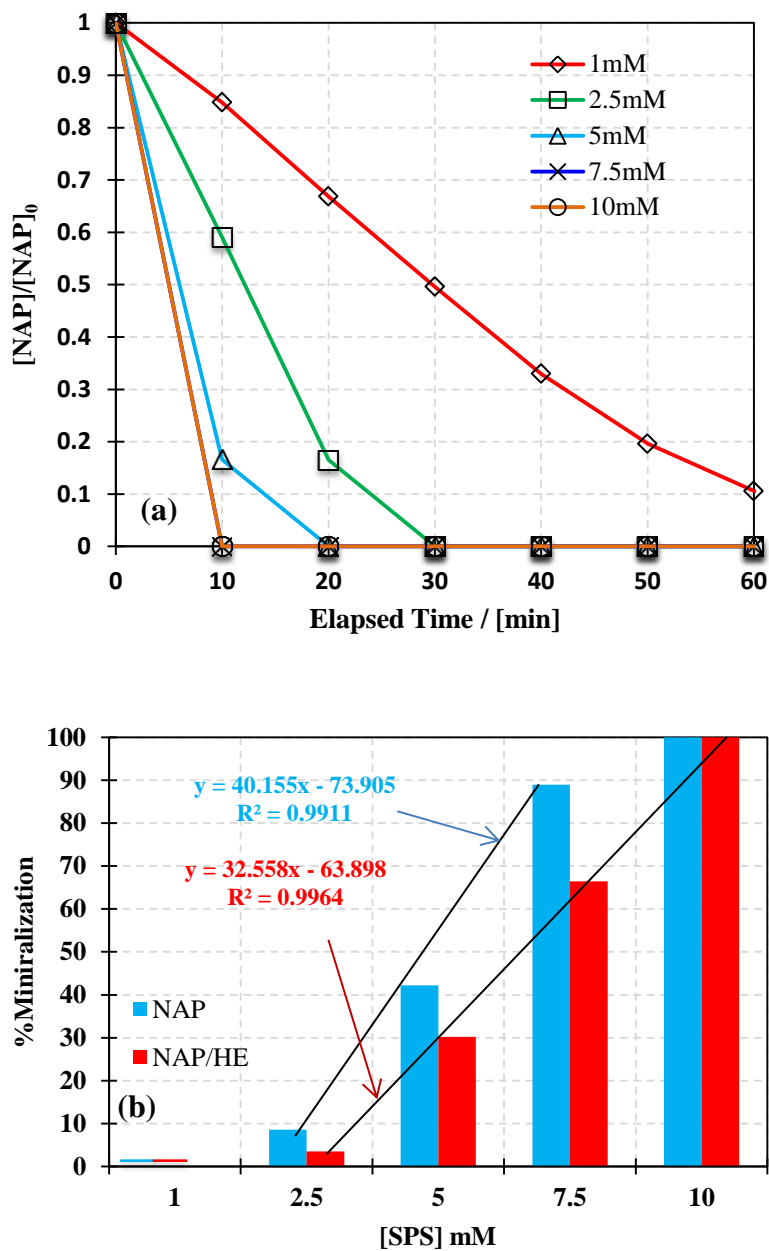
Fig. 21. (a) Time course degradation of NAP as a function of [PS] increasing additive. Curves corresponding to 7.5 and 10.0 mM are overlapping. (b) % mineralization of NAP in ultra-pure water and in hospital effluents (HE) based on TOC measurements. The inline correspond to the linear mineralization trend obtained for a specific range of SPS concentration: 2.5-7.5 mM for UP water and 2.5-10.0 mM in HE matrix. Experimental conditions are $[NAP]_0 = 50 \ \mu M$, $[PB] = 50 \ \mu M$, $pH = 7.00$, $T = 70 \ °C$.

To further support the results showing full NAP mineralization, conductivity measurements were performed on solutions of NAP dissolved in UP water matrix (Table 10). The results showed an increase in the conductivity of the original NAP solution of about 47 microS/cm. This additional conductivity observed after 2 h of heat at 60^oC in a PB solution demonstrated the leaching in solution of ionic fragments originated from NAP molecule. Those fragments were not identified however could be similar to those found in persulfate-like AOPs e.g. glyoxylic acid, oxalic acid, formic acid, etc. [93]. This was also true for the HE treated under similar conditions however at 70^oC where an increase of about 120 microS/cm was noticed. Such increase in conductivity values is probably due to the activation of more persulfate species in solution (at 70^oC) yielding therefore degradation of other organic molecules and their transformation products into ionic species present in the HE. The powerful oxidants recognized to be $SO_4^{-\bullet}$ and $OH^{\bullet}$ thermally generated in solution are responsible for this high mineralization yield. However, in order to check the contribution of each of them into the oxidation process, experiments were conducted in the presence of alcohols having different affinities towards generated radicals.

Table 10. Conductivity of different solutions used in the experiments

Systems /Solution	Concentration of species	Conductivity (microS/cm)
	μM	
NAP	50	12.1
NAP/SPS /PB	50/1,000/50	1245.5
NAP/SPS/PB[1]	50/1,000/50	1292.8
HE[2]	na	520
HE/NAP/SPS	na/50/1,000	1690
HE/NAP/SPS[3]	na/50/1,000	1810
	mg/L	
$MgNO_3$	5.0	11.6 (10.1)
$CaCl_2$	2.5	73.0 (70.7)
$CaSO_4$	50	25.5 (22.0)
$NaHCO_3$	160	161.2 (159.9)

[1] After 2 h of reaction at 60°C
[2] HE: Hospital Effluent (pHi = 7.51; pHf = 7.65, PB free)
[3] After 2 h of reaction at 70°C
Values between brackets are for conductivities of NAP-free solutions.
The conductivity of the UP water used was less than 0.5 microS/cm.

3. Investigations into predominant oxidant in SPS/NAP systems $SO_4^{•-}$ vs $OH^•$)

Previous studies demonstrated that SPS not only produces $SO_4^{•-}$ reacting ET mechanism once activated [94], but it also generates, upon reaction with water (Eq. 27), the highly reactive $OH^•$ being non-selective and reacting through hydrogen abstraction [94, 95, 40] . In 1977, Neta et al. [50] demonstrated that oxidation of organic molecules via $SO_4^{•-}$ is more specific to ET. However in the case of $OH^•$, the reaction taking place is occurring though hydrogen abstraction. Accordingly, in order to identify the species responsible the most for the removal of organic carbons in the studied systems, oxidation experiments were done using excess of ethanol (EtOH) and ter-butyl alcohol (TBA) as radicals' scavengers. EtOH scavenger is responsible for removing both $SO_4^{-•}$ and $OH^•$ radicals from the system (Eqs. 28, 29). Whereas TBA scavenger is more selective by removing first $OH^•$ from the system as it can be noticed from the difference in the

reaction rates provided by Eqs. 30 and 31 ($OH^\bullet$ is almost 1,000 times more reactive than $SO_4^{-\bullet}$ with TBA) [92, 94, 40]. Three different systems were tested: System **1** (Fig. 22a) was a scavenger free system (control): scavenger/SPS/NAP (0/100/1); System **2** (Fig. 22b) was the $SO_4^{-\bullet}$ and $OH^\bullet$ scavenging system: EtOH/SPS/NAP (40,000/100/1) and system **3** (Fig. 22c) was the $OH^\bullet$ scavenging system: TBA/SPS/NAP (40,000/100/1). In all scavenged systems, the concentration of the scavenger was set to be 400 times greater than that of SPS in order to secure high quenching yield compared to that of NAP.

$$SO_4^{-\bullet} + H_2O \rightarrow OH^\bullet + HSO_4^- \qquad (27)$$

$$EtOH + OH^\bullet \sim 1.2 - 2.8 \times 10^9 M^{-1}s^{-1} \qquad (28)$$

$$EtOH + SO_4^{-\bullet} \sim 1.6 - 7.7 \times 10^7 M^{-1}s^{-1} \qquad (29)$$

$$TBA + OH^\bullet \sim 3.8 - 7.6 \times 10^8 M^{-1}s^{-1} \qquad (30)$$

$$TBA + SO_4^{-\bullet} \sim 4.0 - 9.1 \times 10^5 M^{-1}s^{-1} \qquad (31)$$
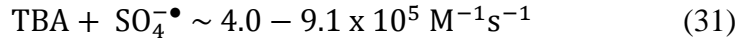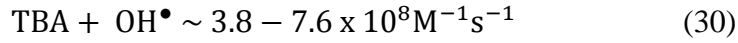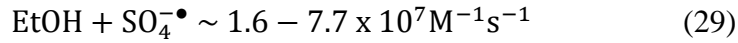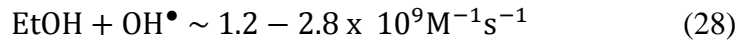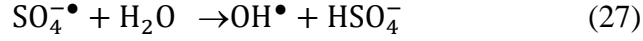
Fig. 21b shows clearly that when both radials are scavenged (System **2**), NAP degradation is less significant with respect to the scavenger free system e.g. 32% vs 82% after 60 min for the scavenged and non-scavenged systems, respectively (Fig. 22a). Nevertheless, when TBA is used, only $SO_4^{-\bullet}$ species remained in solution and achieved 90% NAP degradation at 60 min of reaction (Fig. 22c) to finally reach full degradation after 90 min of reaction (data not shown). This was not the case for BIS [10] and IBU [92] molecules for which both $SO_4^{-\bullet}$ and $OH^\bullet$ contributed an average of 42% and 58%, respectively to the oxidation reactions (Fig. 22c). In contrary to the previous results on BIS and IBU, the present study on NAP degradation suggests that even with the noticeable help of $OH^\bullet$, $SO_4^{-\bullet}$ is the most significant radical responsible for NAP removal. For example, in the absence of any $SO_4^{-\bullet}$ quencher, NAP was the most

recalcitrant pharmaceutical followed by IBU and BIS (Fig. 22a). However, once $OH^\bullet$ radicals were quenched by TBA (Fig. 22c), the degradation trend was reversed with BIS being the more recalcitrant pharmaceutical followed by IBU and NAP. Accordingly, this behavior towards the reactive oxidant in the medium can be attributed to the difference in the molecular structures and functional groups of NAP, IBU and BIS as can be seen in Table 9. For example, compared to BIS and IBU, NAP structure shows more electron rich environment e.g. presence of a naphthalene moiety, making it more susceptible to oxidation via ET reactions. However, BIS and IBU are less electron-rich entities and present abundance in hydrogen available atoms (four CH_3 groups in BIS and three CH_3 groups in IBU vs only one CH_3 group in NAP) that can undergo quickly hydrogen abstraction via $OH^\bullet$. This corroborates findings of Klefah et al. [97] who demonstrated that the CH_3 group on NAP molecule acts as a proton donor which in its turn enhances the decarboxylation step thereby NAP degradation.
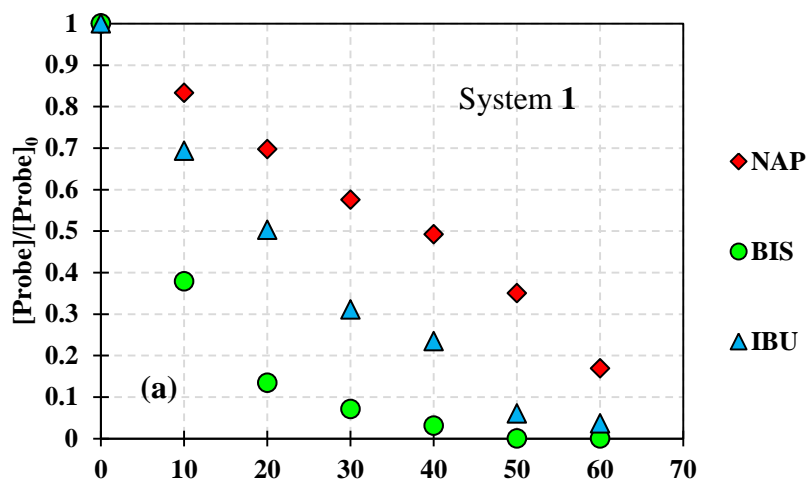
Fig. 22. (a) Scavenger free degradation of NAP, BIS[1] and IBU[2].
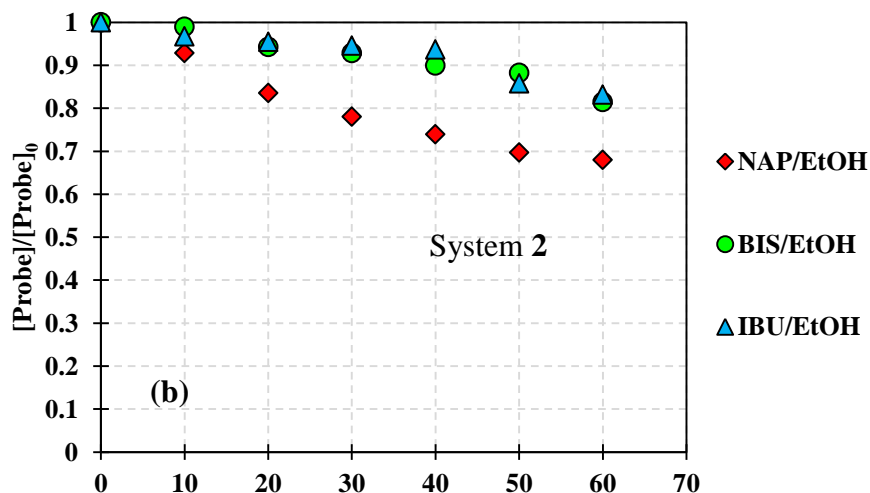
(b) Effect of EtOH radical scavenger on the removal of NAP, BIS[1] and IBU[2].
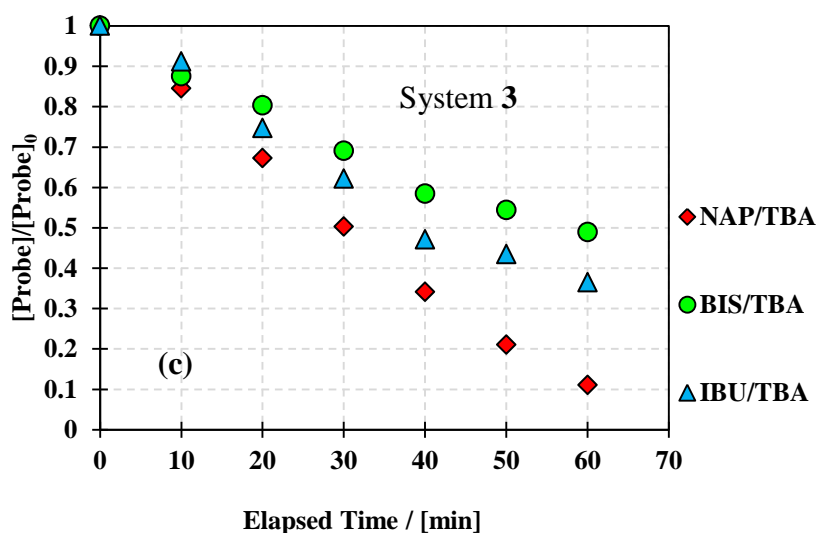
(c) Effect of TBA radical scavenger on the removal of NAP, BIS[1] and IBU[2]. Ratio of Scavenger:SPS:Probe was 40000:100:1 in all experiments.

Experimental conditions: T = 60°C, $[NAP]_0 = 50$ μM, $[BIS]_0 = 50$ μM, $[IBU]_0 = 23$ μM, $[SPS] = 1.0$ mM, PB at pH = 7.00.

[1] Ghauch et al. [10]
[2] Ghauch et al. [92]

83

Furthermore, a calculation of the % change in k_{obs} ($\Delta k_{obs} = ((k_{obs(with\ quencher)}/k_{obs(quencher-free)}) - 1) \times 100$) (Table 11) showed a decrease by -75.1% for NAP upon quenching with EtOH while an increase by +35.8% was noticed with TBA quencher and this compared to quencher-free NAP solution. This means that NAP degradation was positively affected by $OH^\bullet$ quenchers through TBA additive in contrast to BIS and IBU that showed a decrease in their degradation rate constant Δk_{obs} of about -85.8% and -66.8%, respectively. The improvement of NAP degradation kinetics reported in the presence of TBA might be related to the enhancement of NAP-$SO_4^{-\bullet}$ reaction rate in the absence of radical-radical quenching reactions between$OH^\bullet$and $SO_4^{-\bullet}$ (Eq. 32) since the former is being totally quenched by the alcohol additive e.g. TBA. On the other hand, Table 11 showed also that in all-radical quenching systems (EtOH additives) Δk_{obs} for NAP was the least affected value with only -75.1% decrease compared to -95.2% and -96.2% and that for IBU and BIS, respectively. This can be considered as an additional proof that NAP molecule is much more sensitive to $SO_4^{-\bullet}$ known by its selectivity toward electron rich moieties and its applicability to NAP molecules dissolved in complex matrices.

$$SO_4^{-\bullet} + HO^\bullet \rightarrow HSO_5^- \qquad (32)$$

Table 11. Comparison of NAP kinetics parameters as a function of alcohol additives (scavengers) and ion additives

Scavengers (mole ratios) (40,000/100/1)	$k_{obs} \times 10^{-2}$ $(min^{-1})^a$	$t_{1/2}{}^b$ (min)	R^2	% Δk_{obs}
Additive free	2.65 ± 0.09	24.07	0.9837	0
EtOH/SPS/NAP	0.66 ± 0.03	105.0	0.9628	-75.1
EtOH/SPS/BIS[c]	0.32 ± 0.03	216.1	0.9059	-96.2
EtOH/SPS/IBU[d]	0.26 ± 0.03	267.1	0.8380	-95.2
TBA/SPS/NAP	3.60 ± 0.03	19.3	0.9939	+35.8
TBA/SPS/BIS[d]	1.20 ± 0.04	57.8	0.9836	-85.8
TBA/SPS/IBU[e]	1.82 ± 0.03	38.2	0.9757	-66.8
Ion additives $(mg\ L^{-1})$	$k_{obs} \times 10^{-2}$ $(min^{-1})^a$	$t_{1/2}{}^b$ (min)	R^2	% Δk_{obs}
$CaCl_2$ (5.0) [e]	2.16 ± 0.06	37.27	0.9918	-18.49
$CaSO_4$ (50)	4.90 ± 0.66	16.35	0.9452	+84.9
$NaHCO_3$ (160)	4.29 ± 0.27	24.24	0.9816	+61.9
$MgNO_3$ (5.0)	6.74 ± 0.56	7.66	0.8289	+154.3
Drinking Water	4.60 ± 0.33	18.94	0.9775	+73.6

[a] k_{obs} are obtained from the slopes of the plots of Ln([NAP]/[NAP]$_0$) vs Time. Uncertainties were calculated from standard deviation on the slope determined after using the LINEST function of Microsoft excel.

[b] Calculated from the pseudo-first order equation where $t_{1/2} = Ln2/k_{obs}$.

[c] Data are from reference [10] where Δk_{obs} is calculated with respect to the k_{obs} of scavenger-free solution.

[d] Data are from reference [10] where Δk_{obs} is calculated with respect to the k_{obs} of scavenger-free solution.

[e] Concentration of additives (ppm).

4. Matrix effect

4.1. Case of inorganic additives

In real-life application of water treatment using TAP systems, several factors may interfere with the reaction rates and RSEs. In addition to humic acids [98], dissolved inorganic species in water can be one of those factors. As a method of studying the effect of these inorganic additives on NAP degradation in water, experiments were performed with the addition of $NaHCO_3$, $CaSO_4$, $CaCl_2$ and $Mg(NO_3)_2$ at concentrations mimicking those of natural/spring waters (Table 11). Each inorganic additive was added separately to NAP:SPS (1:20) systems and the reactor was heated to 60°C for oxidation reactions. The k_{obs} of these reactions were calculated at appropriate reaction times (before complete NAP vanishing) with respect to pseudo-first order kinetics and reported in Table 11. As it can be noticed, all additives showed an increase in k_{obs} values with respect to the additive-free solution (Fig. 23, dash line), except for $CaCl_2$.
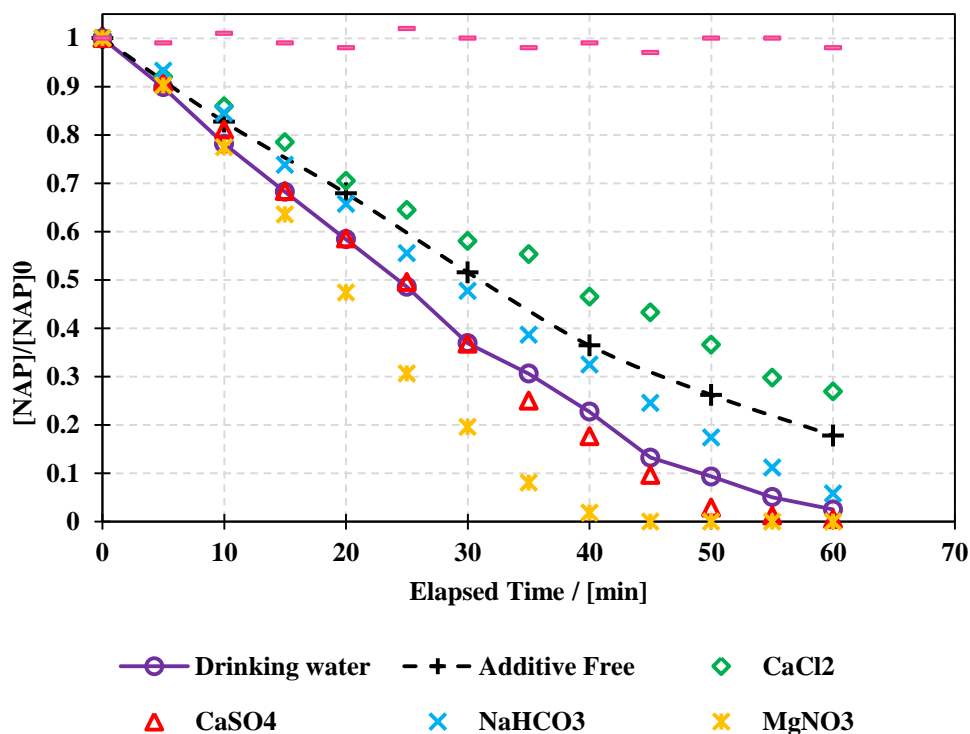
Fig. 23. Effect of inorganic additives on the removal of NAP. Experimental conditions: $[NAP]_0 = 50 \ \mu M$, $[SPS] = 1.0 \ mM$, PB at pH = 7.50.

The addition of $CaCl_2$ showed a decrease in Δk_{obs} value of about -18.49%. In fact, chlorides in solutions are the precursors of chlorine and dichlorine radicals e.g. $Cl^{\bullet}$ and $Cl_2^{\bullet-}$ responsible for side quenching reactions of $SO_4^{\bullet-}$ (Eqs. 33, 34). Therefore, less $SO_4^{\bullet-}$ are available for NAP oxidation.

$$SO_4^{\bullet-} + Cl^- \rightarrow Cl^{\bullet} + SO_4^{2-} \qquad k = 3.1 \times 10^8 \ L \ mol^{-1} \ s^{-1} \ at \ pH \ 6.8 \qquad (33)$$

$$Cl^{\bullet} + Cl^- \rightarrow Cl_2^{\bullet-} \qquad k = 2.1 \times 10^{10} \ L \ mol^{-1} \ s^{-1} \qquad (34)$$
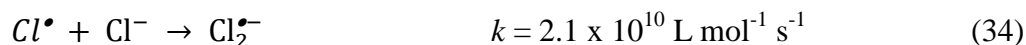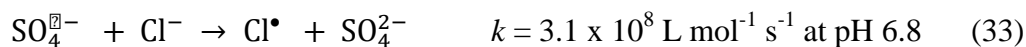
Although $Cl^{\bullet}$ and $Cl_2^{\bullet-}$ are known by their oxidative properties toward organic compounds, however in a slightly basic medium as it is the case here (7.50 < pH < 7.86), $Cl^{\bullet}$ is more reactive toward hydroxyl species than organic compounds (Eq. 35) [90, 100]. This most probably can

explain the slight decrease in the k_{obs} of NAP compared to a slight increase as previously reported for BIS [20] where the pH was relatively acidic ($6.70 < $ pH $ < 7.00$) favoring therefore the dissociation of $ClOH^{\bullet-}$ into $Cl^{\bullet}$ (Eq. 36). In addition, $Cl^{\bullet}$ might also be quenched by water however at a much slower rate compared to that of hydroxyl species (Eq. 37) [101, 47].

$$Cl^{\bullet} + OH^- \rightarrow ClOH^{\bullet-} \qquad\qquad k = 1.8 \text{ x } 10^{10}\,\text{L mol}^{-1}\,\text{s}^{-1} \qquad (35)$$

$$HOCl^{\bullet-} + H^+ \rightarrow Cl^{\bullet} + H_2O \qquad\qquad\qquad\qquad (36)$$

$$Cl^{\bullet} + H_2O \rightarrow ClOH^- + H^+ \qquad\qquad k = 1.6 \text{ x } 10^5\,\text{s}^{-1} \qquad (37)$$

On the other hand, the greater improvement among all additives was noticed with $MgNO_3$ exhibiting a Δk_{obs} value of about +154.3%. This is not surprising since Δk_{obs} improvement has already been noticed in a previous work under similar conditions however for BIS removal whose degradation was shown dependent on the presence of both $SO_4^{\bullet-}$ and $HO^{\bullet}$ equally [20]. In fact $SO_4^{\bullet-}$ can produce in the medium $NO_3^{\bullet}$ (Eq. 18) having a high redox potential ($E_{1/2} = 2.50$ V) for more NAP oxidation [41, 42].

$$SO_4^{\bullet-} + NO_3^- \rightarrow SO_4^{2-} + NO_3^{\bullet} \qquad k = 2.1 \text{ x } 10^6\,\text{L mol}^{-1}\,\text{s}^{-1} \text{ at pH 7-8} \qquad (38)$$
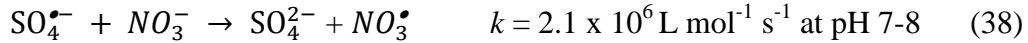
In the case of $CaSO_4$ additive, a lesser improvement has been noticed with a Δk_{obs} value of about +84.9%. In this case SO_4^{2-} generates $SO_4^{\bullet-}$ (Eq. 39) however in a steady state manner avoiding thereby $SO_4^{\bullet-}$ quenching keeping therefore high NAP oxidation yield.

$$SO_4^{\bullet-} + SO_4^{2-} \rightarrow SO_4^{\bullet-} + SO_4^{2-} \qquad\qquad (39)$$
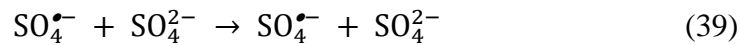
Finally the least improvement was noticed in $NaHCO_3$ spiked NAP solution ($\Delta k_{obs} = $ +61.9%). Basically, HCO_3^- species react with $SO_4^{\bullet-}$ to produce $CO_3^{\bullet-}$ radicals (Eq. 40). Those have also positive redox potential ($E_{1/2}^{red} = 1.50$ V) comparable to that of $NO_3^{\bullet}$ ($E_{1/2}^{red} = 2.50$ V), $SO_4^{\bullet-}$ ($E_{1/2}^{red} = 2.43$ V) and $Cl_2^{\bullet-}$ ($E_{1/2}^{red} = 2.09$ V) [44,47,101]. Accordingly, an enhancement in k_{obs} with regard to bicarbonate-free solution is not surprising especially if the selected probe e.g.

NAP has good affinity toward $CO_3^{\bullet-}$ in contrast to BIS that showed a decrease in its k_{obs} in bicarbonate-spiked solution [10]. In fact, BIS degradation, in contrast to NAP degradation, showed more implication of $HO^{\square\bullet}$ that is more quenched by HCO_3^- species (Eq. 20) [44].

$$SO_4^{\bullet-} + HCO_3^- \rightarrow SO_4^{2-} + CO_3^{\bullet-} + H^+ \qquad k = 8.5 \text{ x } 10^6 \text{ L mol}^{-1} \text{ s}^{-1} \qquad (40)$$

$$HO^{\bullet} + HCO_3^- \rightarrow CO_3^{\bullet-} + H_2O \qquad k = 1.6 \text{ x } 10^6 \text{ L mol}^{-1} \text{ s}^{-1} \qquad (41)$$
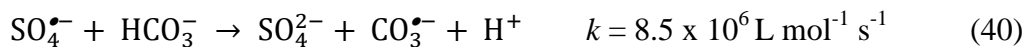
4.2 Case of drinking water and hospital effluent (HE)

TAP process was also applied to a NAP-spiked commercial mineral drinking water having almost a similar composition range in inorganic species as previously reported, however in a mixture. The mineral drinking water is assumed to not contain any organic species except the spiked NAP solution. Its composition as per its label denominates the following ions given in mg L^{-1}: $[Ca^{2+}]$ = 33; $[Mg^{2+}]$ = 16; $[SO_4^{2-}]$ = 12; $[NO_3^-]$ = 1.5; $[Cl^-]$ = 7 and $[HCO_3^-]$ = 150. The results showed complete degradation of NAP after 60 min of reaction time (Fig. 23, solid line) with an improved Δk_{obs} of about +73.6% as per comparison to an additive-free NAP solution (Table 11). Accordingly, little and even no quenching reactions occurred during the treatment of this solution which can be considered as an advantage for TAP application to drinking water supplies slightly charged in dissolves inorganic species.

In order to further explore the potential of TAP systems in degrading organic contaminants regardless of the matrix content, 20 mL sample of processed HE was spiked with 50 µM of NAP. Based on the TOC data of previous experiments (Fig. 21b), 10 mM of SPS were added to the spiked HE and treated for 2 h at 70°C. As can been seen in Fig. 24, the HPLC chromatographic peak of NAP (Retention time = 35 min) totally vanished after TAP treatment. In addition, other peaks corresponding to unknown organic compounds (indicated with a "*" on the chromatogram) most probably pharmaceuticals disappeared partially or totally demonstrating

that TAP can be considered as a universal treatment method for application to highly charged effluents like HE. Conductivity measurements done on the same solutions before and after TAP treatment showed an increase in the conductivity of about 120 microS/cm as previously reported (Table 10). This can also reflect to a certain extent that additional mineralization of organic contaminants occurred as well.
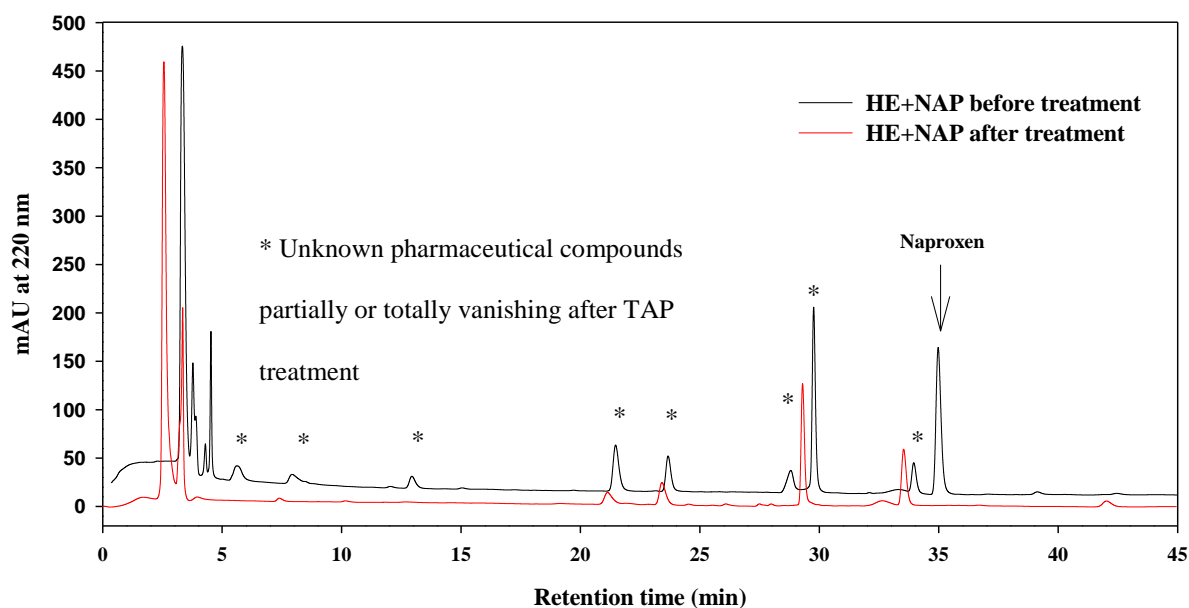

Fig. 24. HPLC-DAD spectrum of hospital effluent spiked with NAP before and after treatment with SPS. Experimental conditions: [NAP] = 50 µM; [SPS] = 10 mM; T = 70°C; Reaction time = 2 h.

5. Transformation products

Time course profiles for the disappearance of NAP and the appearance/disappearance of its transformation products are shown in Fig. 25. As it can be noticed, NAP totally disappeared after 40 min of reaction. At the same time, two of its by-products BP**1** and BP**2** reached a maximum of concentration in solution at 20 min of reaction then totally vanished at 50 min. However, a third by-product BP**3** showed an increase in its concentration up to 50 min followed by a significant decline maintained up to 2 h of reaction. Based on this observation, one can deduce that direct and successive oxidation reactions are very plausible so that BP**1** and BP**2** disappeared in favor of BP**3** considered the final transformation product before its total degradation at longer reaction time (data not shown). In order to confirm such hypothesis allowing therefore the elucidation of a degradation mechanism of NAP in TAP systems, HPLC/DAD/FLD/MS and GC/MS analyses were performed however in the absence of authentic standards. In HPLC/MS analysis, the atmospheric pressure photo-ionization head did show any response neither for NAP nor for its transformation products although in the presence of a dopant e.g. acetone, toluene. On the contrary, electrospray ionization (ESI) showed significant response for NAP and its transformation products in positive ionization (PI) mode (Fig. 27, Table 12) while only NAP was responsive in negative ionization (NI) mode (Fig. 26, Table 13). Accordingly, PI mode was adopted for the identification of transformation products. Furthermore, the GC/MS analysis done in electron impact mode, after SPE preparation, showed the MS spectra of NAP and two of its by-products (BP**1** and BP**3**) (Table 14) confirming thereby the identity of two transformation products previously analyzed by HPLC/MS.
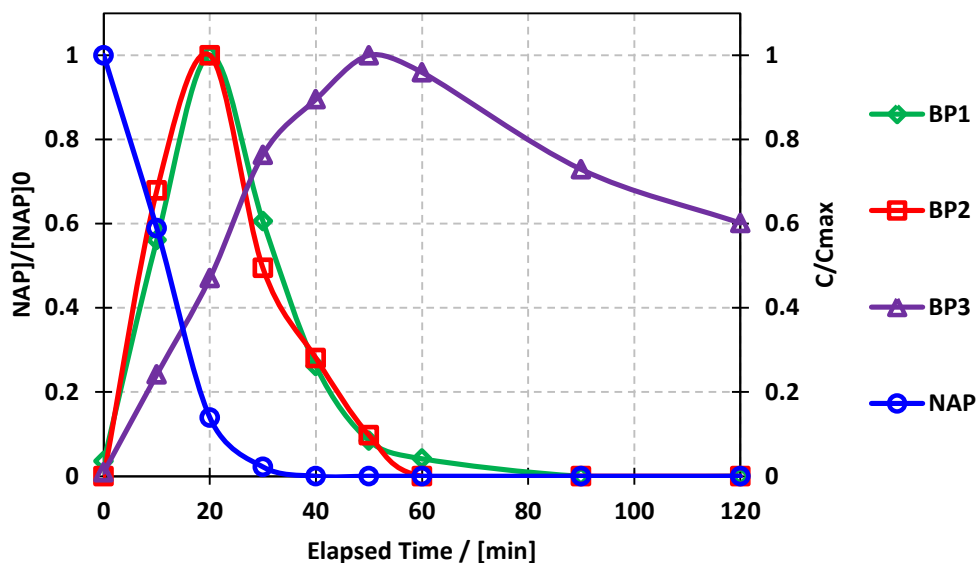
Fig. 25. (a) Simultaneous evolution of NAP and its transformation products in a PS spiked reactor over 2 h of treatment. Experimental conditions: $[NAP]_0 = 100$ μM, $[SPS] = 1.0$ mM, Temperature $= 70^{\circ}$C, PB at pH $= 7.50$.
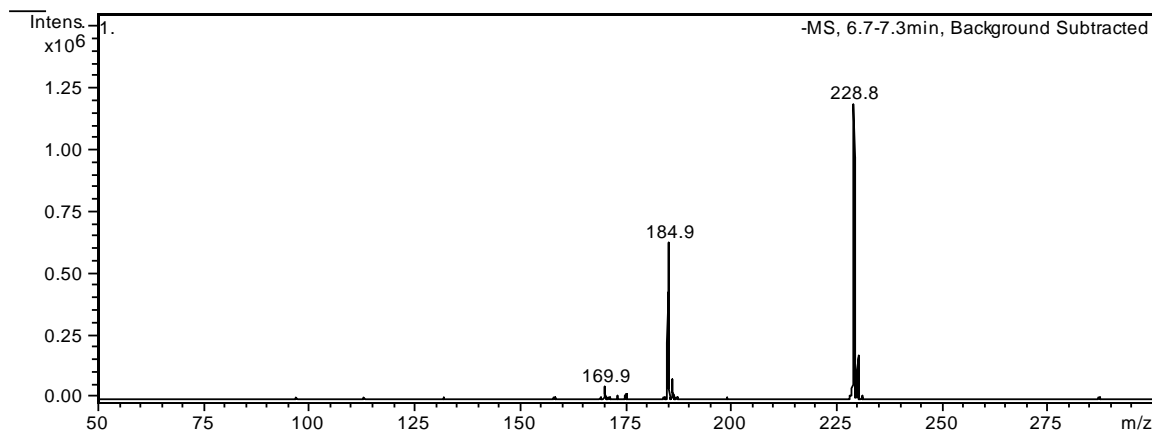
Fig. 26. (-) ESI/MS spectrum of NAP showing the molecular ion [M-H]⁻ as well as the corresponding fragments as per below.

Table 12. Proposed structures of the corresponding fragments of NAP upon ESI/MS analyses in Negative Ionization (NI) Mode.
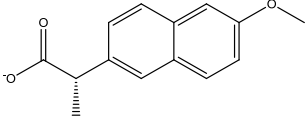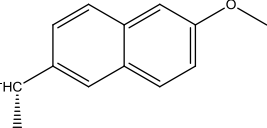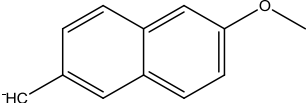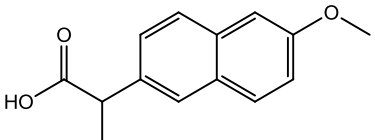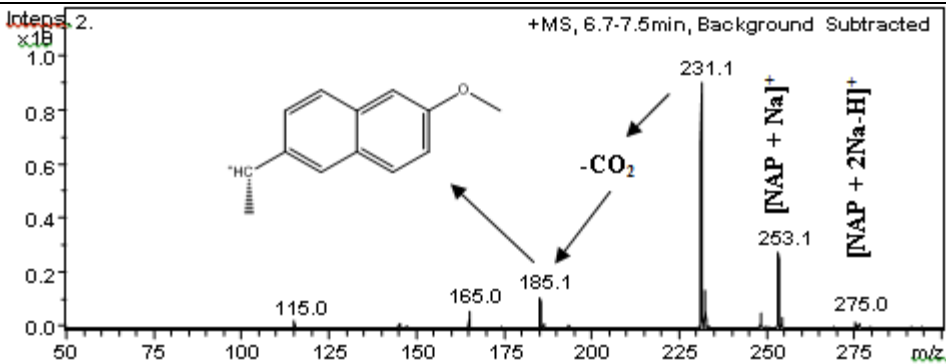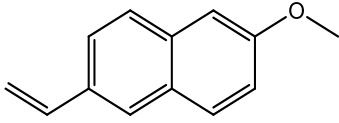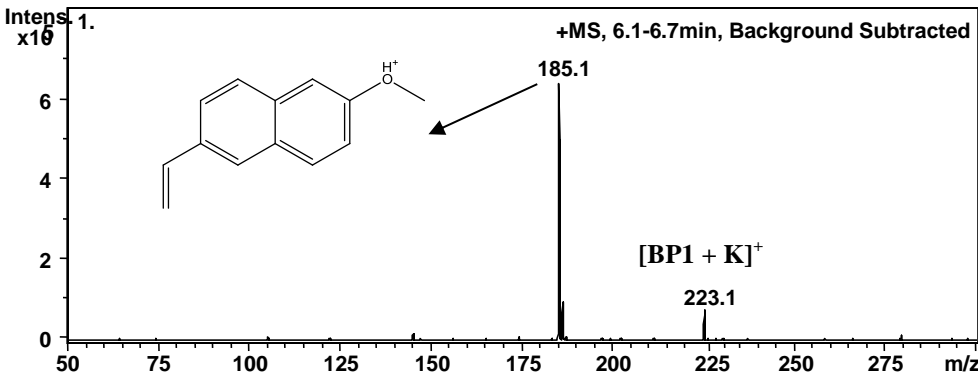
Ion	[M-H]⁻	[M-CO₂H]⁻	[M-CO₂-CH₃]⁻
Proposed structure			

Table 13. Proposed name of NAP degradation products and their corresponding analytical properties using GC/MS and HPLC/DAD/MS analyses upon solid phase extraction.

Name	MW	Proposed Structure	Rt (min)	(+)ESI/MS spectrum
Naproxen	230.26		6.72	
BP1	184.23		6.22	

BP2	200.23		7.77

Intens.
x10^3.

+MS, 7.6-8.2min, Background Subtracted

201.1 **[BP2 + H]**⁺

[-O]

[BP2 + Na]⁺
223.1

185.1

[BP2 + K]⁺ 269.1

239.1

83.5

145.0

62.3 74.3 105.1

50 75 100 125 150 175 200 225 250 275 m/z

BP3	200.23		9.45

Intens.
x10^4.

+MS, 9.6-10.7min, Background Subtracted

201.1 **[BP3 + H]**⁺

153.5
161.9

[BP3 + Na]⁺

69.0 80.3 112.4

223.1 252.0 292.6

50 75 100 125 150 175 200 225 250 275 m/z
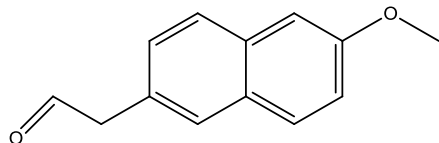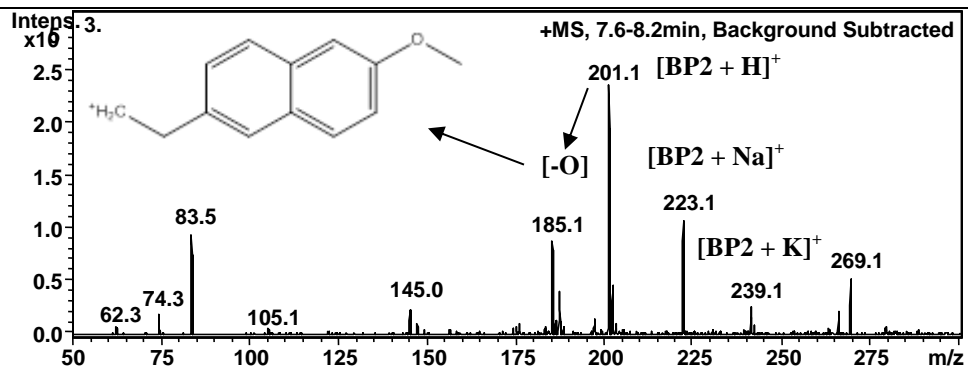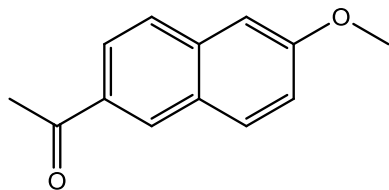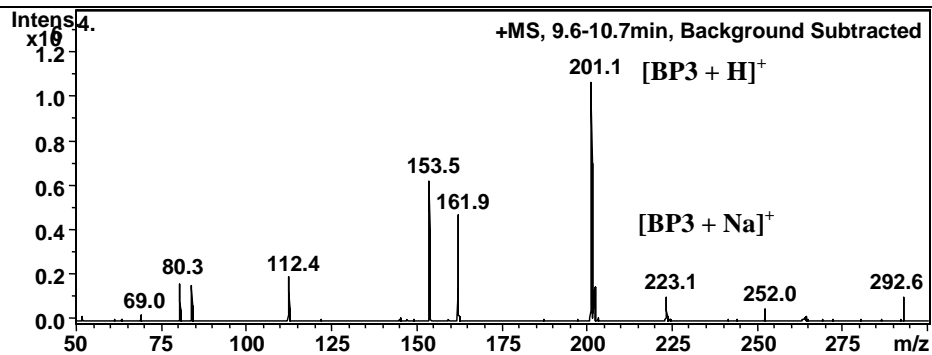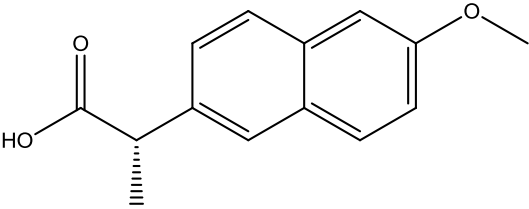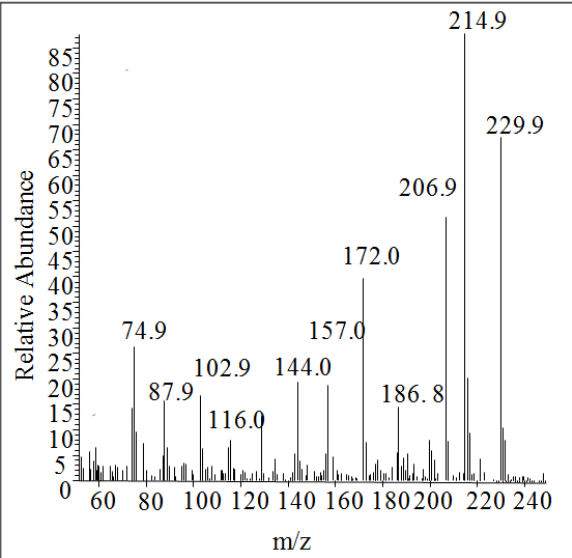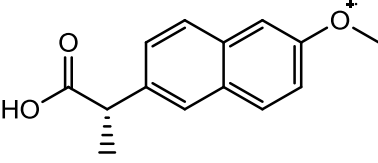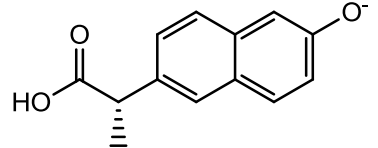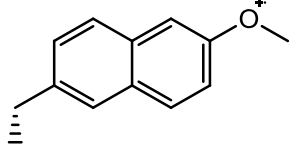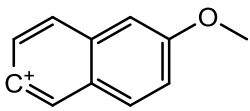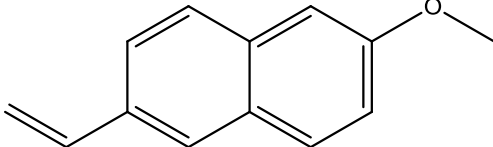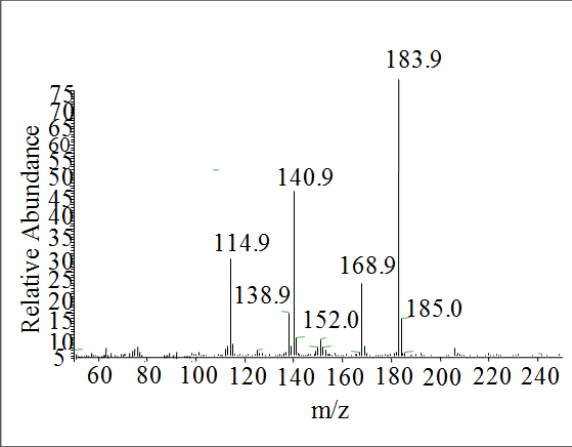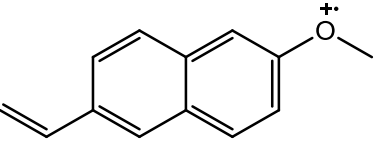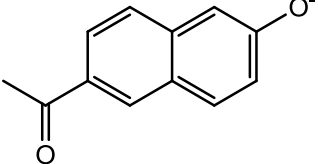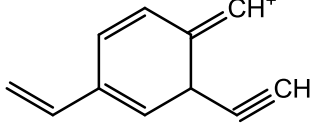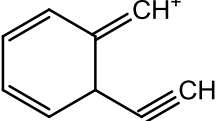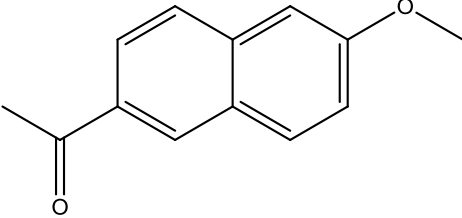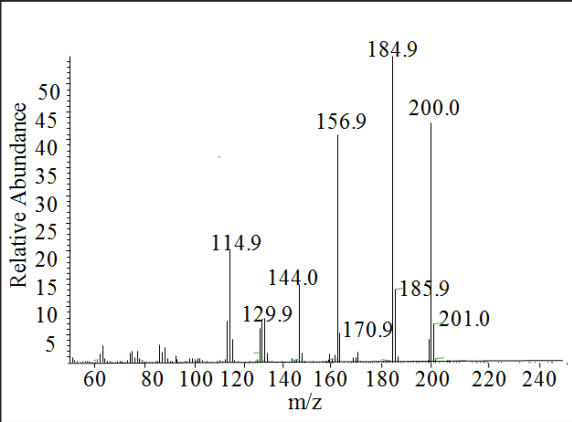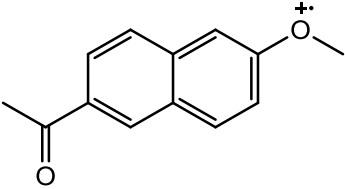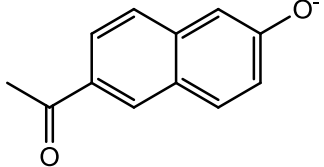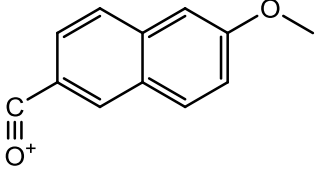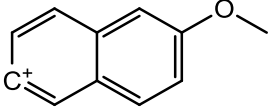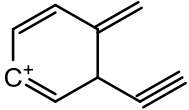
BP1: 2-Methoxy-6-vinylnaphthalene, BP2: 2-(6-methoxynaphthalen-2-yl)acetaldehyde, BP3: 1-(6-methoxynaphthalen-2-yl)ethanone.

Table 14. EI/MS spectra of NAP and its transformation products obtained upon SPE followed by GC/MS analysis as well as the proposed structures of the main encountered fragments.

Chemical structure of NAP and its transformation products	Mass Spectrum obtnained by EI	Chemical structures of corresponding ions / fragments	m/z
Naproxen Chemical Formula: $C_{14}H_{14}O_3$ Exact Mass: 230.09 Molecular Weight: 230.26			229.9
			214.9
			186.8
			157.0

BP 1 Chemical Formula: $C_{13}H_{12}O$ Exact Mass: 184.09 Molecular Weight: 184.23			183.9
			168.9
			140.9
			114.9

BP 3 1-(6-methoxynaphthalen-2-yl)ethanone Chemical Formula: $C_{13}H_{12}O_2$ Exact Mass: 200.08 Molecular Weight: 200.23			200.0
		 	184.9
			156.9
			114.9

5.1 UV/Vis and fluorescence analyses

Fig. 27 shows the TIC of NAP solution during TAP process at 20 min of reaction. Under the current analytical conditions, NAP was eluted at 7.1 min, BP**1**, BP**2** and BP**3** at 6.4, 7.9 and 10.15 min, respectively. The DAD results showed almost similar UV/VIS absorbance spectra for NAP, BP**1** and BP**2** with a very small blue shift (hypsochromic) of about $\Delta\lambda = 2$ nm ($\lambda_{max} = 232$ nm for NAP and 230 nm for BP**1** and BP**2**) that could explain the formation of a lesser conjugated molecule (Inset Fig. 27b). As for BP**3**, a red shift is obvious with two λ_{max} at 242 nm and 310 nm ($\Delta\lambda = 10$ nm and 35 nm) confirming thereby the formation of a more conjugated electronic system (Inset Fig. 27b). In an oxidative medium and in the presence of dissolved oxygen, the formation of a ketone moiety (C=O group) could take place. This corroborates previous findings [102-104] that reported the formation of BP**3** upon photolysis of NAP in oxic solution. On the other hand, BP**1** showed high fluorescence yield ($\lambda_{max\,(em)} = 360$ nm) compared to NAP ($\lambda_{max\,(em)} = 356$ nm) while BP**2** is much less fluorescent ($\lambda_{max\,(em)} = 355$ nm). However, BP**3** did not show any fluorescence and this at the same excitation wavelength e.g. $\lambda_{ex} = 230$ nm. Such observation can be considered as an advantage transforming the parent fluorescent compound (NAP) to non-fluorescent compound in terms of reduced photosensitivity [102]. However, in the absence of authentic standards, MS analysis was conducted in order to identify all transformation products based on their fragmentation patterns.

(a) Total Ion Chromatogram (+)

(b) HPLC/DAD Chromatogram, $\lambda_{detection}$ = 230 nm

(c) HPLC/FLD Chromatogram λ_{ex} = 230

(d) Extracted Ion Chromatogram at m/z 231

(e) Extracted Ion Chromatogram at m/z 185

(f) Extracted Ion Chromatogram at m/z 201

100
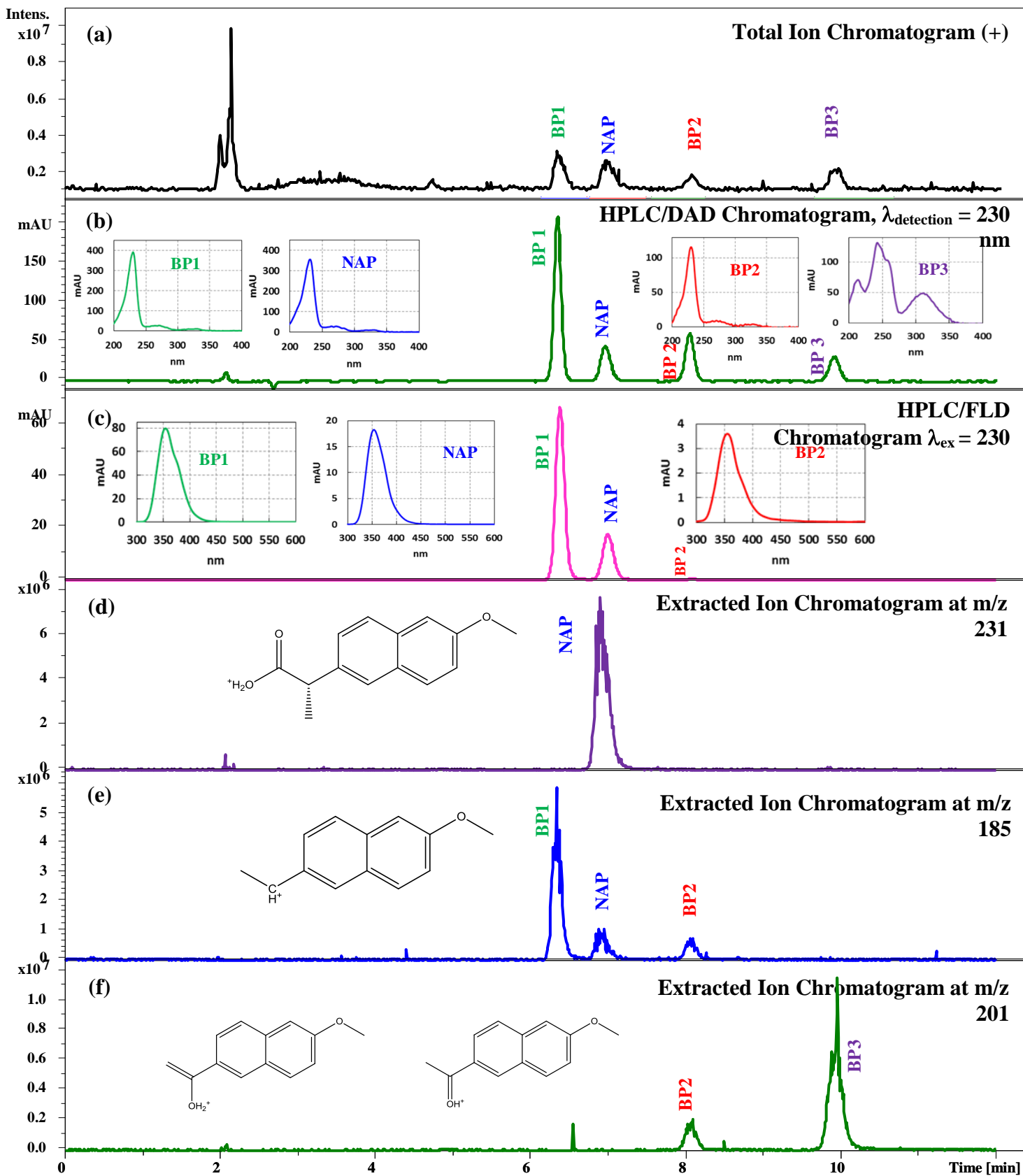
Fig. 27. (+) ESI/MS (a), UV/DAD (b) and UV/FLD (c) chromatograms and the corresponding extracted ion chromatomgrams (d-f) obtained by HPLC/ESI/MS in postive ionization mode on the NAP solution (100 μM) after 20 min of contact with SPS (1.0 mM) at 70°C in oxic solution at (231 ± 0.5), (185 ± 0.5) and (201 ± 0.5) m/z for NAP, BP 1 and BP 2 and BP 3, respectively. Insets represent the (i) UV/VIS absorbance (b) and fluoresence (c) spectra of NAP and its transformation products e.g. BP1, BP2 and BP3 and (ii) the chemical structures of the proposed positively ionized fragments (d-f).

5.2 HPLC/MS and GC/MS analyses

HPLC/MS spectra of NAP and all its transformation products are listed in Table 12. Under the current analytical conditions, NAP showed two adducts at m/z 253.1 and 275.0 corresponding to [M+Na]$^+$ and [M+2Na-H]$^+$, respectively. It also showed the base peak of the molecular ion [M+H]$^+$ at m/z 231.1 and the decarboxylated fragment [M-COOH]$^+$ at 185.1 m/z. BP**1** has a base peak molecular ion [M+H]$^+$ at 185.1 m/z corresponding to a decarboxylated NAP molecule (2-Methoxy-6-vinylnaphthalene) and a potassium adduct [M+K]$^+$ at m/z 223.1. BP**2** depicted a base peak molecular ion [M+H]$^+$ at m/z 201.1 and two adducts [M+Na]$^+$ and [M+K]$^+$ at 223.1 and 239.1 m/z, respectively. It also showed a fragment at 185.1 m/z that can be attributed to the loss of an oxygen atom (16 amu) from the oxidized aldehyde NAP derivative (2-(6-methoxynaphthalen-2-yl)acetaldehyde). BP**3** has the same molecular ion [M+H]$^+$ as BP**2** however it does not show the same fragmentation pattern and adducts which means a different structure (Isomer). For example, only sodium adduct [M+Na]$^+$ is noticed at 223.1 m/z while potassium adduct is absent. Furthermore, non-identified significant fragments e.g 161.9 and

101

153.5 m/z are present. Those can be attributed to some mass losses followed by molecule rearrangement in the mass analyzer. However, based on the UV/Vis analyses shown above, BP**3** should correspond to the ketone isomer providing more electron conjugation to the molecule. Accordingly, BP**2** and BP**3** are the result of oxidation of BP**1** after its decarboxylation.

In order to confirm this hypothesis and further investigate into the transformation products, GC/MS spectra summarized in Table 13 showed the corresponding molecular ions matching those obtained with the HPLC/MS analysis. For example, NAP showed a molecular ion at 229.9 m/z. It also shows a base peak at 214.9 m/z and a fragment at 186.8 m/z corresponding to the loss of a methyl group (CH_3; 15 amu) and a carboxylic moiety (COOH; 44 amu), respectively [46]. BP**1** showed a base peak molecular ion at 183.9 m/z and fragments at 168.9, 140.9 and 114.9 m/z corresponding to the losses of CH_3 (15 amu), CH_3CO (43 amu) and (C_4H_5O, 69 amu). BP**3** showed a molecular ion at 200 m/z, a base peak at 184.9 m/z and fragments at 156.9 and 114.9 m/z corresponding to the loss of the CH_3 (15 amu), CH_3CO (43 amu), and C_4H_4O (69 amu), respectively. BP**2**, however, was not detected by GC/MS. This could be due to the non-stability of the molecule at high temperature.

The obtained NAP by-products (BP**1**, BP**2** and BP**3**) were previously reported in the literature as the most common for NAP degradation disregarding of the oxidation method and reaction conditions. For example, Arany et al. [103] identified two of those transformation products (BP**1** and BP**3**) upon photolysis of NAP, whereas Marco-Urrea et al. [95] reported BP**2** as a result of NAP biodegradation Marotta and co-workers [104] demonstrated the formation of BP**3** however after hydroxylation of the decarboxylated NAP in photo-degradation reactions. In this work, no hydroxylated transformation products were identified which could be explained by the oxidation mechanism mostly relying on $SO_4^{\cdot-}$ instead of $HO^{\cdot}$.

5.3 NAP degradation scheme

According to the above investigations and previous data regarding the elucidation of TAP oxidation mechanisms [105, 106], a scheme of the degradation mechanism of NAP could be proposed as reported in Fig. 28. First, NAP molecule got ionized upon electron abstraction by $SO_4^{\bullet-}$ occurring on available lone pair of an oxygen atom to form NAP radical cation $[NAP]^{\bullet+}$. This is followed by decarboxylation yielding the formation of **BP1** which undergoes oxidative reaction in the presence of dissolved oxygen. The result of such oxidation is the production of an aldehyde (**BP2**) and a ketone (**BP3**). Finally, **BP3** did not persist in solution and disappeared as the reaction time is prolonged and sulfate radicals' precursor remains available in the reactive medium reaching therefore full mineralization.
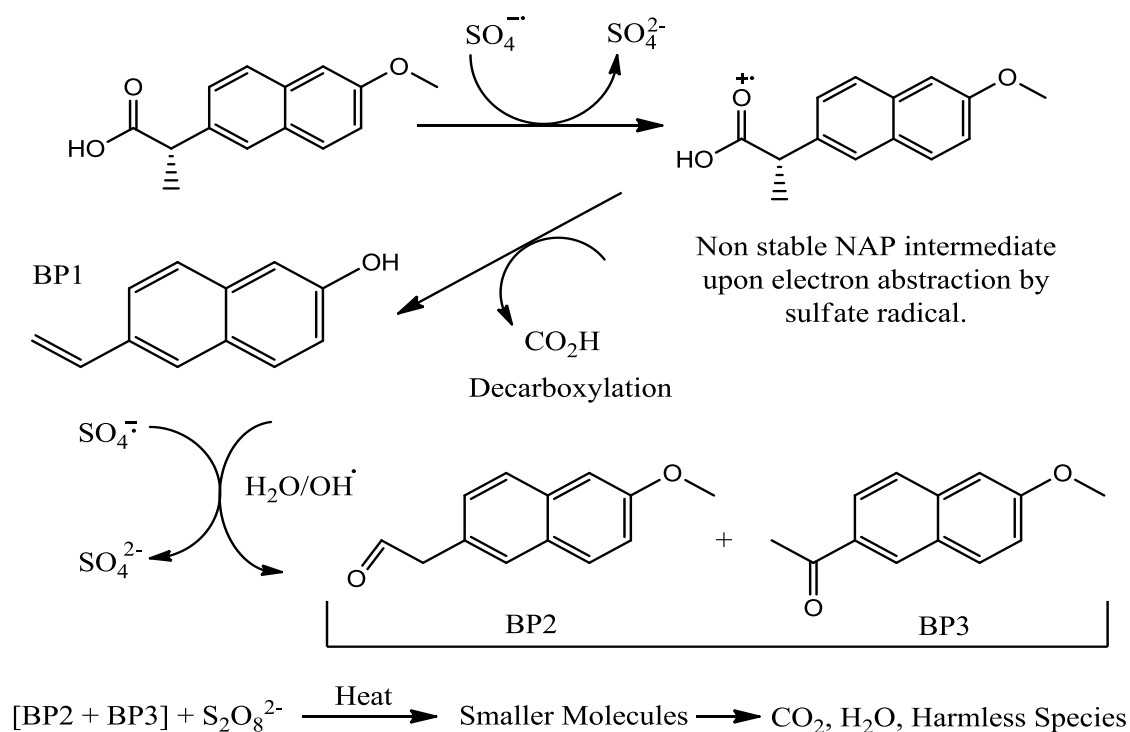
Fig. 28. Proposed degradation scheme of NAP in thermally activated persulfate solution.

5. Chapter conclusion

In this work, TAP system showed once more its effectiveness as strong oxidant to be used for water treatment technologies. In addition of being able to act under circumneutral pH conditions in clean matrices e.g. DI water, TAP system can also be a great oxidizer regardless of the aqueous matrix in which contaminants are dissolved. The results obtained showed full degradation of NAP in a highly charged non-treated HE. Complete mineralization of pharmaceutical wastes and HEs was obtained under decent conditions according to TOC data. These conditions include cricumneutral pH, short periods of reaction times and economically affordable temperatures e.g. case of solar energy. During all the experimental work, high RSEs were achieved (e.g. RSE up to 68% after 20 min of reaction at 70°C). Inorganic additives affected more or less the oxidation process. $MgNO_3$ improved by 154% NAP degradation rate while $CaCl_2$ decreased the degradation rate by 18.5%. All reactions showed a pseudo first-order degradation kinetics as well as good Arrhenius behavior. The highest achieved k_{obs} was found to be 1.286 mM min^{-1} at 70°C with an E_A of about 155.0($\pm$26.4) kJ mol^{-1}. In radical scavenging systems, it was seen that both radical species $HO^\bullet$ and $SO_4^{\bullet-}$ played a role in the oxidation process however $SO_4^{\bullet-}$ was the most dominant oxidant. This was attributed to the chemical structure of NAP rich in non-bonding electrons pairs. This observation was also comforted by the nature of the transformation products where no hydroxylated NAP species were detected upon HPLC/MS and GC/MS analyses. Results showed that after NAP decarboxylation (BP**1**), an aldehyde (BP**2**) and ketone (BP**3**) decarboxylated NAP compounds were identified; BP**3** being the most stable transformation product that totally vanished by the end of the reaction. Future development into potential synergistic effect of solar and chemical activation of PS in aqueous systems is under consideration toward field application for direct water reuse [107].

CHAPTER V

Conclusion

In this thesis, TAP has proven to be a very efficient method to be used in the removal of PPCPs from wastewater. In addition to its efficiency, TAP is considered to be an economical method, as well as energy efficient method. Throughout this study, TAP demonstrated its ability to operate under different sets of variables. Optimum reaction conditions were determined; nevertheless TAP functioned under a wide range of pH, temperatures, and SPS/Probe concentrations. Furthermore, TAP was able to function its oxidative properties in both lab induced contamination (DI water), and in matrix whether it be the case of mineral water or hospital effluent.

TAP did not only oxidize and fully degrade the probe molecule; it was also able to act on the emerging reaction by-products and full mineralization was achieved under optimum conditions. In addition to full mineralization, high %RSE was observed throughout the degradation reactions.

BIS was fully degraded in aqueous solution in under 1 h with a very sufficient reaction stoichiometric efficiency (at 50^oC RSE = 1.0 and 60^oC RSE > 0.8). It was found that relatively high temperatures (above 50°C) and neutral pH, are the optimum conditions needed for the removal of BIS from solution. Results showed also that BIS degradation can be explained by pseudo-first order model. Radical scavengers used (EtOH and TBA) showed that both the $SO_4^{\cdot-}$ and $HO^\cdot$ are responsible for the oxidation of BIS. When in matrix, it was found that only the

presence of HCO_3^- slightly affected the degradation rate of BIS. In addition to BIS, the emerging by-products were also oxidized.

IBU degradation was similar to that of BIS in terms of optimum reaction conditions (temperatures above 50°C and neutral pH). While IBU also followed a pseudo-first order model, further ivistigation into the reaction order produced the following kinetic equation:

$$-\frac{d[IBU]}{dt} = (2.71x10^{-4}mM^{1-(a+b)}\min^{-1})x[IBU]^{0.25}[SPS]^1$$

NAP removal using TAP was also fully achievable under optimum conditions with a noticeably high %RSE (e.g. RSE up to 68% after 20 min of reaction at 70°C). When in matrix, inorganic additives slightly affected the oxidation reaction both positively and negatively depending on the additive. For example $MgNO_3$ improved NAP oxidation by 154%, whereas $CaCl_2$ decreased the degradation of NAP by 18.4%. Scavenging experiments showed that, unlike BIS and IBU, the sulfate radical was the predominant species responsible for the oxidation process.

Future attempts should be carried out in order to check the validity of this kinetics model under different conditions as for example lower temperature (e.g. < 40°C) in order to reduce the operational cost and lesser ionic strength (e.g. $[I]_{PB} < 10^{-3}$ M) so as to minimize side reactions between radicals and inorganic species affecting therefore the reaction efficiency. Such process can be applied to small volumes of water charged with pharmaceutical compounds like hot spot effluents of hospitals and pharmaceutical industries.

References

[1] K. Fent, A.. Weston, D. Caminada, Ecotoxicology of human pharmaceuticals, Aquatic Toxicology 76 (2006) 122–159.

[2] Ginebreda A, Muñoz I, de Alda ML, Brix R, López-Doval J, Barceló D. Environmental risk assessment of pharmaceuticals in rivers: relationships between hazard indexes and aquatic macroinvertebrate diversity indexes in the Llobregat River (NE Spain). Environ Int 2010;36:153–62.

[3] Du B, Price AE, ScottWC, Kristofco LA, Ramirez AJ, Chambliss CK, et al. Comparison of contaminantsof emerging concern removal, discharge, and water quality hazards among centralized and on-site wastewater treatment system effluents receiving common wastewater influent. Sci Total Environ 2014;466–467:976–84.

[4] Schaider LA, Rudel RA, Ackerman JM, Dunagan SC, Brody JG. Pharmaceuticals, perfluorosurfactants, and other organic wastewater compounds in public drinking water wells in a shallow sand and gravel aquifer. Sci Total Environ 2014;468–469: 384–93.

[5] P.E. Stackelberg, E. Furlon, M. T.Meyer, S. Zaugg, Sci. Total Environ. 329 (2004) 99–113.

[6] J. Rivera-Utrilla M. Sánchez-Polo, M. Ferro-García, G. Prados-Joya, R. Ocampo-Pérez Chemosphere 93 (2013) 1268–1287.

[7] T. Heberer, Occurrence, fate, and removal of pharmaceutical residues in the aquatic environment: a review of recent research data. Toxicology Lett. 131 (2002) 5–17.

[8] S. Esplugas, D.M. Bila, L.G.T. Krause, M. Dezotti, Ozonation and advanced oxidation technologies to remove endocrine disrupting chemicals (EDCs) and pharmaceuticals and personal care products (PPCPs) in water effluents, J. Hazard. Mater. 149 (2007) 631-642.

[9] A.R. Ribeiro, O. Nunes, M. Pereira, A. Silva, An overview on the advanced oxidation processes applied for the treatment of water pollutants defined in the recently launched Directive 2013/39/EU Environ Int. 75 (2015) 33–51.

[10] A. Ghauch, A.M. Tuqan, Oxidation of bisoprolol in heated persulfate/H_2O systems: Kinetics and products, Chem. Eng. J. 183 (2012) 162-171.

[11] N. Sabri, K. Hanna, V. Yargeau, Chemical oxidation of ibuprofen in the presence of iron species at near neutral pH. Sci. Total Environ. 427–428 (2012) 382–389.

[12] J. Bound, K. Kitsou, N. Voulvoulis, Household disposal of pharmaceuticals and perception of risk to the environment. Environ. Toxicology Pharma. 21 (2006) 301–307.

[13] B. Escher, R. Baumgartner, M. Koller, K. Treyer, J. Lienert, C. McArdell, Environmental toxicology and risk assessment of pharmaceuticals from hospital wastewater. water res. 45 (2011) 75-92.

[14] R. Andreozzi, M. Raffaele, P. Nicklas, Pharmaceuticals in STP effluents and their solar photodegradation in aquatic environment. Chemosphere 50 (2003) 1319–1330.

[15] C. Mi`ege, M. Favier, C. Brosse, J. Canler, M. Coquery, Occurrence of betablockers in effluents of wastewater treatment plants from the Lyon area (France) and risk assessment for the downstream rivers. Talanta 70 (2006) 739–744.

[16] M.J. Gomez, M.J. Martinez Bueno, S. Lacorte, A.R. Fernandez-Alba, A. Aguera, Pilot survey monitoring pharmaceuticals and related compounds in a sewage treatment plant located on the Mediterranean coast, Chemosphere 66 (2007) 993-1002.

[17] C. Carlsson, A. Johansson, G. Alvan, K. Bergman, T. Kuhler, Are pharmaceuticals potent environmental pollutants? Part I: Environmental risk assessments of selected active pharmaceutical ingredients. Sci Total Environ 364 (2006) 67– 87.

[18] Z. Dong, D. Senn, R. Moran, J. Shine, Prioritizing environmental risk of prescription pharmaceuticals. Reg. Toxi. Pharma. 65 (2013) 60–67.

[19] S. Mompelat, B. Le Bot, O. Thomas, Occurrence and fate of pharmaceutical products and by-products, from resource to drinking water. Environ. Inter. 35 (2009) 803–814.

[20] W. Li, Occurrence, sources, and fate of pharmaceuticals in aquatic environment and soil. Environ. Pollution 187 (2014) 193-201.

[21] G. Buerge , H. Rudolfbuser, T. Poiger, M. Muller, Occurrence and Fate of the Cytostatic Drugs Cyclophosphamide and Ifosfamide in Wastewater and Surface Waters. Environ. Sci. Technol. 2006, 40, 7242-7250.

[22] Boreen, A.L., Arnold, W.A., McNeill, K., 2003. Photodegradation of pharmaceuticals in the aquatic environment: a review. Aquat. Sci. 65, 320e341.

[23] H. Yamamoto, Y. Nakamura, S. Moriguchi, Y. Nakamura, Y. Honda, I. Tamura, Y. Hirata, A. Hayashi, J. Sekizawa, Persistence and partitioning of eight selected pharmaceuticals in the aquatic environment: Laboratory photolysis, biodegradation, and sorption experiments. Water Res. (2009) 351-362.

[24] M. Koch, A. Dezi, M. Tarquini, L. Capurso, Prevention of non-steroidal anti-inflammatory drug induced gastrointestinal mucosal injury risk factors for serious complications. Digestive and Liver Disease, Volume 32, Issue 2, March 2000, Pages 138-151

[25] M. Pera-Titus[a], V. García-Molina[a], M. Baños, J. Giménez, S. Esplugas, Degradation of chlorophenols by means of advanced oxidation processes: a general review. Applied Catalysis B: Environmental 47 (2004) 219–256.

[26] A. Ribeiro, O. Nunes, M. Pereira, A. Silva, An overview on the advanced oxidation processes applied for the treatment of water pollutants defined in the recently launched Directive 2013/39/EU. Environment International 75 (2015) 33–51.

[27] G.P. Anipsitakis, D.D. Dionysiou, Radical Generation by the Interaction of Transition Metals with Common Oxidants, Environ. Sci. Technol. 38 (2004) 3705-3712.

[28] Arvin, E., Moller, M.S., Pedersen, L.-F.,Hydrogen peroxide decomposition kinetics in aquaculture water, *Aquacultural Engineering* (2014), http://dx.doi.org/10.1016/j.aquaeng.2014.12.004.

[29] Y. Seol, H. Zhang, F. W. Schwartz, A Review on In-Situ Chemical Oxidation and Heterogeneity. doi: 10.2113/9.1.37v. 9 no. 1 p. 37-49.

[30] R. Andreozzi, V. Caprio, A. Insola, R. Marotta, Advanced oxidation processes (AOP) for water purification and recovery. Catalysis Today 53 (1999) 51–59.

[31] S.-Y. Oh, S.-G. Kang, P.C. Chiu, Degradation of 2,4-dinitrotoluene by persulfate activated with zero-valent iron, Sci. Total Environ. 408 (2010) 3464-3468.

[32] G. Ayoub, A. Ghauch, Assessment of bimetallic and trimetallic iron-based systems for persulfate activation: Application to sulfamethoxazole degradation. Chem. Eng. J. 256 (2014) 280-292.

[33] P. Xie, J. Ma, W. Liu, J. Zou, S. Yue, X. Li, M. Wiesner, J. Fang, Removal of 2-MIB and geosmin using UV/persulfate: Contributions of hydroxyl and sulfate radicals. Water Res. (2015) 223-233.

[34] R.E. Huie, C.L. Clifton, Temperature dependence of the rate constants for reactions of the sulfate radical, SO4-, with anions, J. Phys. Chem. 94 (1990) 8561-8567.

[35] C. Liang, C.F. Huang, N. Mohant, R.M. Kurakalva, A rapid spectrophotometric determination of persulfate anion in ISCO, Chemosphere, 73 (2008), pp. 1540–1543.

[36] C. Liang, Z.S. Wang, C.J. Bruell, Influence of pH on persulfate oxidation of TCE at ambient temperatures, Chemosphere, 66 (2007), pp. 106–113.

[37] R.H. Waldemer, P.G. Tratnyek, R.L. Johnson, J.T. Nurmi, Oxidation of chlorinated ethenes by heat-activated persulfate: kinetics and products, Environ. Sci. Technol., 41 (2007), pp. 1010–1015.

[38] C. Liang, C.F. Huang, N. Mohanty, C.J. Lu, R.M. Kurakalva, Hydroxypropyl-β-cyclodextrin-mediated iron-activated persulfate oxidation of trichloroethylene and tetrachloroethylene, Ind. Eng. Chem. Res., 46 (2007), pp. 6466–6479.

[39] P. Maruthamuthu, P. Neta, Phosphate radicals. Spectra, acid–base equilibria, and reactions with inorganic compounds, J. Phys. Chem., 82 (1978), pp. 710–713.

[40] G.P. Anipsitakis, D.D. Dionysiou, Radical generation by the interaction of transition metals with common oxidants, Environ. Sci. Technol., 38 (2004), pp. 3705–3712.

[41] Minisci, A. Citterio, Electron-transfer processes: peroxydisulfate, a useful and versatile reagent in organic chemistry, Acc. Chem. Res., 16 (1983), pp. 27–32.

[42] G.P. Peyton, The free-radical chemistry of persulfate-based total organic carbon analyzers, Mar. Chem., 41 (1993), pp. 91–103.

[43] R.E. Huie, C.L. Clifton, Temperature dependence of the rate constants of reactions of the sulfate radical, $SO_4^{•-}$, with anions, J. Phys. Chem., 94 (1990), pp. 8561–8567.

[44] G.V. Buxton, A.J. Elliot, Rate constant for reaction of hydroxyl radicals with bicarbonate ions, Radiat. Phys. Chem., 27 (1986), pp. 241–243.

[45] G.V. Buxton, M. Bydder, G.A. Salmon, J.E. Williams, The reactivity of chlorine atoms in aqueous solutions. Part III. The reaction of $Cl^{•}$ with solutes, Phys. Chem. Phys., 2 (2000), pp. 237–245.

[46] H.W. Jacobi, F. Wicktor, H. Herrmann, R. Zellner, A laser flash photolysis kinetic study of reactions of the Cl_2 radical anion with oxygenated hydrocarbons in aqueous solution, Inter, J. Chem. Kinet., 31 (1999), pp. 169–181.

[47] B. Venkatachalapathy, P. Ramamurthy, Reactions of nitrate radical with amino acids in acidic aqueous medium: a flash photolysis investigation, J. Photochem. Photobiol. A, 93 (1996), pp. 1–5.

[48] M. Exner, H. Herrmann, R. Zellner, Laser-based studies of reactions of the nitrate radical in aqueous solution, Ber. Bunsen. Ges., 96 (1992), pp. 470–477.

[49] M. Skoumal, P.L. Cabot, F. Centellas, C. Arias, R.M. Rodriguez, J.A. Garrido, E. Brillas, Mineralization of paracetamol by ozonation catalyzed with Fe^{2+}, Cu^{2+} and UVA light, Appl. Catal. B: Environ., 66 (2006), p. 228

[50] C. Tan, N. Gao, Y. Deng, W. Rong, S. Zhou, N. Lu, Degradation of antipyrine by heat activated persulfate, Sep. Purif. Technol. 109 (2013) 122-128.

[51] R. Hirsch, T.A. Ternes, K. Haberer, A. Mehlich, F. Ballwanz, K.L. Kratz, Determination of antibiotics in different water compartments via liquid chromatography–electrospray tandem mass spectrometry J. Chromatogr. A, 815 (1998), pp. 213–223.

[52] T.A. Ternes, Occurrence of drugs in German sewage treatment plants and rivers, Water Res., 32 (1998), pp. 3245–3260.

[53] D. Ashton, M. Hilton, K.V. Thomas, Investigating the environmental transport of human pharmaceuticals to streams in the United Kingdom, Sci. Total Environ., 333 (2004), pp. 167–184.

[54] M.D. Hernando, M. Mezcua, A.R. Ferńandez-Alba, D. Barceĺo, Environmental risk assessment of pharmaceutical residues in wastewater effluents, surface waters and sediments, Talanta, 69 (2006), pp. 334–342.

[55] M. Ramil, T. El Aref, G. Fink, M. Scheurer, T.A. Ternes, Fate of beta blockers in aquatic-sediment systems: sorption and biotransformation, Environ. Sci. Technol., 44 (2010), pp. 962–970.

[56] S.D. Kim, J. Cho, I.S. Kim, B.J. Vanderford, S.A. Snyder, Occurrence and removal of pharmaceuticals and endocrine disruptors in South Korean surface, drinking, and waste waters, Water Res., 41 (2007), pp. 1013–1021.

[57] A.M. Comerton, R.C. Andrews, D.M. Bagley, C. Hao, The rejection of endocrine disrupting and pharmaceutically active compounds by NF and RO membranes as a function of compound and water matrix properties, J. Membr. Sci., 313 (2008), pp. 323–335.

[58] N. Nakada, H. Shinohara, A. Murata, K. Kiri, S. Managaki, N. Sato, H. Takada, Removal of selected pharmaceuticals and personal care products (PPCPs) and endocrine-disrupting chemicals (EDCs) during sand filtration and ozonation at a municipal sewage treatment plant, Water Res., 41 (2007), pp. 4373–4382.

[59] H. Tekin, O. Bilkay, S.S. Ataberk, T.H. Balta, I.H. Ceribasi, F.D. Sanin, F.B. Dilek, U. Yetis, Use of Fenton oxidation to improve the biodegradability of a pharmaceutical wastewater, J. Hazard. Mater., 136 (2006), pp. 258–265.

[60] A. Ghauch, H. Baydoun, P. Dermesropian, Degradation of aqueous carbamazepine in ultrasonic/Fe^0/H_2O_2 systems, Chem. Eng. J., 172 (2011), pp. 18–27.

[61] Ghauch, H. Abou Assi, A. Tuqan, Investigating the mechanism of clofibric acid removal in Fe^0/H_2O systems, J. Hazard. Mater., 176 (2010), pp. 48–55.

[62] Noubactep, S. Caré, F. Togue-Kamga, A. Schöner, P. Woafo, Extending service life of household water filters by mixing metallic iron with sand, Clean Soil Air Water, 38 (2010), pp. 951–959.

[63] F. Méndez-Arriaga, R.A. Torres-Palma, C. Pétrier, S. Esplugas, J. Gimenez, C. Pulgarin, Ultrasonic treatment of water contaminated with ibuprofen, Water Res., 42 (2008), pp. 4243–4248.

[64] T.E. Doll, F.H. Frimmel, Fate of pharmaceuticals-photodegradation by simulated solar UV-light, Chemosphere, 52 (2003), pp. 1757–1769.

[65] H. Tungudomwongsa, J. Leckie, T. Mill, Photocatalytic oxidation of emerging contaminants: kinetics and pathways for photocatalytic oxidation of pharmaceutical compounds, J. Adv. Oxid. Technol., 9 (2006), pp. 59–64.

[66] M. Lahti, A. Oikari, Microbial transformation of pharmaceuticals naproxen, bisoprolol, and diclofenac in aerobic and anaerobic environments, Arch. Environ. Contam. Toxicol., 61 (2011), pp. 202–210.

113

[67] A. Piram, A. Salvador, C. Verne, B. Herbreteau, R. Faure, Photolysis of β-blockers in environmental waters, Chemosphere, 73 (2008), pp. 1265–1271.

[68] J. Benner, E. Salhi, T. Ternes, U. von Gunten, Ozonation of reverse osmosis concentrate: kinetics and efficiency of beta blocker oxidation, Water Res., 42 (2008), pp. 3003–3012.

[69] S. Beier, S. Koster, K. Veltmann, H. Fr Schroder, J. Pinnekamp, Treatment of hospital wastewater effluent by nanofiltration and reverse osmosis, Water Sci. Technol., 61 (2010), pp. 1691–1698.

[70] K.C. Huang, Z. Zhao, G.E. Hoag, A. Dahmani, P.A. Block, Degradation of volatile organic compounds with thermally activated persulfate oxidation, Chemosphere, 61 (2005), pp. 551–560.

[71] Liang, C.F. Huang, Y.J. Chen, Potential for activated persulfate degradation of BTEX contamination, Water Res., 42 (2008), pp. 4091–4100.

[72] D.A. House, Kinetics and mechanism of oxidations by peroxydisulfate, Chem. Rev., 62 (1962), pp. 185–203.

[73] I.M. Kolthoff, I.K. Miller, The chemistry of persulfate. I. The kinetics and mechanism of the decomposition of the persulfate ion in aqueous medium, J. Am. Chem. Soc., 73 (1951), pp. 3055–3059.

[74] C. Liang, C.J. Bruell, M.C. Marley, K.L. Sperry, Thermally activated persulfate oxidation of trichloroethylene (TCE) and 1,1,1-trichloroethane (TCA) in aqueous systems and soil slurries, Soil Sediment Contam., 12 (2003), pp. 207–228.

[75] C. Liang, C.J. Bruell, Thermally activated persulfate oxidation of trichloroethylene: experimental investigation of reaction orders, Ind. Eng. Chem. Res., 47 (2008), pp. 2912–2918.

[76] J. Costanza, G. Otano, J. Callaghan, K.D. Pennell, PCE oxidation by persulfate in the presence of solids, Environ. Sci. Technol., 44 (2010), pp. 9445–9450.

[77]   J.R. Pugh, in: Situ Remediation of Soils Containing Organic Contaminants Using the Electromigration of Peroxysulfate ions. U.S. Patent 5976,348, 1999.

[78]   A. Rastogi, S.R. Al-Abed, D.D. Dionysiou, Sulfate radical-based ferrous–peroxymonosulfate oxidative system for PCBs degradation in aqueous and sediment systems, Appl. Catal. B: Environ., 85 (2009), pp. 171–179.

[79]   K.C. Huang, Z. Zhao, G.E. Hoag, A. Dahmani, P.A. Block, Degradation of volatile organic compounds with thermally activated persulfate oxidation, Chemosphere, 61 (2005), pp. 551–560.

[80]   R.L. Johnson, P.G. Tratneyk, R. O'Brien Johnson, Persulfate persistence under thermal activation conditions, Environ. Sci. Technol., 42 (2008), pp. 9350–9356.

[81]   M.G. Antoniou, U. Nambiar, D.D. Dionysiou, Investigation of the photocatalytic degradation pathway of the urine metabolite, creatinine: the effect of pH, Water Res., 43 (2009), pp. 3956–3963.

[82]   M.G. Antoniou, P.A. Nicolaou, J.A. Shoemaker, A.A. de la Cruz, D.D. Dionysiou, Detoxification of water contaminated with the cyanotoxin, microcystin-LR, by utilizing thin TiO2 photocatalytic films, Appl. Catal. B-Environ., 91 (2009), pp. 165–173.

[83]   M.G. Antoniou, A.A. de la Cruz, D.D. Dionysiou, Degradation of microcystin-LR using sulfate radicals generated through photolysis, thermolysis, and electron transfer mechanisms, Appl. Catal. B- Environ., 96 (2010), pp. 290–298.

[84]   A. Tsitonaki, B. Petri, M. Crimi, H. Mosbaek, R.L. Siergist, P.L. Bjerg, In situ chemical oxidation of contaminated soil and groundwater using persulfate: a review, Cr. Rev. Environ. Sci. Technol., 40 (2010), pp. 55–91.

[85]   Yang. Deng, Casey M. Ezyske Sulfate radical-advanced oxidation process (SR-AOP) for simultaneous removal of refractory organic contaminants and ammonia in landfill leachate, Water Res., 45 (2011), pp. 6189–6194.

[86]   J.H. Espenson, Chemical Kinetics and Reaction Mechanisms, McGraw-Hill book Co., New York (1981).

[87]   G. Palmisano, M. Addamo, V. Augugliaro, T. Caronna, A. Di Paola, E. Garcia Lopez, V. Loddo, G. Marci, L. Palmisano, M. Schiavello, Selectivity of hydroxyl radical in the partial oxidation of aromatic compounds in heterogeneous photocatalysis, Catal. Today, 122 (2007), pp. 118–127.

[88]   V.C. Mora, J.A. Rosso, D.O. Mártire, M.C. Gonzalez, Phenol depletion by thermally activated peroxydisulfate at 70 °C, Chemosphere, 84 (2011), pp. 1270–1275.

[89]   F. Vicente, A. Santos, A. Romero, S. Rodriguez, Kinetic study of diuron oxidation and mineralization by persulphate: Effects of temperature, oxidant concentration and iron dosage method, Chem. Eng. J., 170 (2011), pp. 127–135.

[90]   K.I. Seo, I.J. Chung, Reaction analysis of 3,4-ethylenedioxythiophene with potassium persulfate in aqueous solution by using a calorimeter, Polymer, 41 (2000), pp. 4491–4499.

[91]   Tsitonaki, B. Petri, M. Crimi, H. Mosbæk, R. Siegrist, P.L. Bjerg, Critical Reviews in In situ chemical oxidation of contaminated soil and groundwater using persulfate: A review, Environ. Sci. Technol. 40 (2010) 55-91.

[92]   A. Ghauch, A.Tuqan, N. Kibbi, Ibuprofen removal by heated persulfate in aqueous solution: A kinetics study, Chem. Eng. J. 197 (2012) 483-492.

[93]   Gurol, M. D. & Vatistas, R. Oxidation of phenolic compounds by ozone and ozone/UV radiation: A comparative study, Water Res. 21 (1987) 895-903.

[94]   G.P. Anipsitakis, D.D. Dionysiou, M.A. Gonzalez, Cobalt-mediated activation of peroxymonosulfate and sulfate radical attack on phenolic compounds: implications of chloride ions, Environ. Sci. Technol. 40 (2006) 1000-1007.

[95]   E. Marco-Urrea , M. Pérez-Trujill, P. Blánquez, T. Vicent, G. Caminal, Biodegradation of the analgesic naproxen by Trametes versicolor and identification of intermediates using HPLC-DAD-MS and NMR, Bioresource Technol. 101 (2010) 2159-2166.

[96]   P. Neta, V. Madhavan, H. Zemel, R. Fessenden, J. Am. Chem. Soc. Rate Constants and Mechanism of Reaction of $SO_4^{-\bullet}$ with Aromatic Compounds. 1977, pp. 163-164.

[97]   A.K. Klefah, M. Eriksson, L. A. Eriksson, Theoretical study of the phototoxicity of naproxen and the active form of nabumetone, J. Phys. Chem. A, 112 (2008) 10921-10930.

[98]   X. Xu , S. Li , Q. Hao, J. Liu, Y. Yu, H. Li, Activation of persulfate and its environmental application, Int. J. Environ. Bioen. 1 (2012) 60-81.

[99]   H. V. Lutze, N. Kerlin, T. C. Schmidt, Sulfate radical -based water treatment in presence of chloride: Formation of chlorate, inter-conversion of sulfate radicals into hydroxyl radicals and influence of bicarbonate, Water Res. 2014, doi: 10.1016/j.watres.2014.10.006.

[100]   P. Neta, R. E. Huie, A. B. Ross, Rate constants for reactions of inorganic radicals in aqueous solutions, J. Phys. Chem. Ref. Data, Vol. 17, No3, 1988.

[101]   G.G. Jayson, B.J. Parsons, Some simple, highly reactive, inorganic chlorine derivatives in aqueous solution, J. Chem. Soc. Faraday Trans. I 69 (1973) 1597-1607.

[102]   W. Cory, A. DeSantis, C. Ulmer, Photodegradation of Naproxen and Ibuprofen and the Formation of Ecotoxic Photoproducts in Natural Water Systems. IWA specialty conference on Natural Organic Matter, Costa Mesa, CA, USA, July 27-29, 2011.

[103]   E. Arany, R.K. Szabó, L. Apáti, T. Alapi, I. Ilisz,P. Mazellier, A. Dombi, K. Gajda-Schrantz, Degradation of naproxen by UV, VUV photolysis and their combination, J. Hazard. Mater. 262 (2013) 151-157.

[104]   R. Marotta, D. Spasiano, I. Di Somma, R. Andreozzi, Photodegradation of naproxen and its photoproducts in aqueous solution at 254 nm: A kinetic investigation, Water Res. 47 (2013) 373-383.

[105]   A. Ghauch, , G. Ayoub, S. Naim,. Degradation of sulfamethoxazole by persulfate assisted micrometric Fe^0 in aqueous solution. Chem. Eng. J. 228, (2013) 1168-1181.

[106]   A. Ghauch, A. Tuqan, N. Kibbi, S, Geryes, Methylene blue discoloration by heated persulfate in aqueous solution, Chemical Eng. J. 213 (2012) 259-271.

[107]   C. Gadipelly, A. Pérez-González, G.D. Yadav, I. Ortiz, R. Ibáñez, V.K. Rathod, K.V. Marathe, Pharmaceutical industry wastewater: Review of the technologies for water treatment and reuse, Ind. Eng. Chem. Res., 29 (2014) 11571-11592.

[108]   K.C. Huang, G.E. Hoag, P. Chedda, B.A. Woody, G.M. Dobbs, Kinetics and mechanism of oxidation of tetrachloroethylene with permanganate, Chemosphere, 46 (2002), p. 815.

[109]   H.S. Fogler, Elements of Chemical Reaction Engineering, Prentice Hall, Inc., Englewood Cliffs, NJ (1998).

[110]   D.W. Kolpin, E.T. Furlong, M.T. Meyer, E.M. Thurman, S.D. Zaugg, L.B. Barber, H.T. Buxton, Environ. Sci. Technol., 36 (2002), pp. 1202–1211.

[111]   D.W. Kolpin, M. Skopec, M.T. Meyer, E.T. Furlong, S.D. Zaugg, Urban contribution of pharmaceuticals and other organic wastewater contaminants to streams during differing flow conditions, Sci. Total Environ., 328 (2004), pp. 119–130.

[112]   G.R. Boyd, H. Reemtsma, D.A. Grimm, S. Mitra, Pharmaceuticals and personal care products (PPCPs) in surface and treated waters of Louisiana, USA and Ontario, Canada, Sci. Total Environ., 311 (2003), pp. 135–149.

[113]   T. Takagi, C. Ramachandran, M. Bermejo, S. Yamashita, L.X. Yu, G.L. Amidon, A provisional biopharmaceutical classification of the top 200 oral drug products in the United States, Great Britain, Spain, and Japan, Mol. Pharmacol., 3 (2006), pp. 631–643.

[114]   T.A. Ternes, N. Herrmann, M. Bonerz, T. Knacker, H. Siegrist, A. Joss, A rapid method to measure the solid-water distribution coefficient (K–d) for pharmaceuticals and musk fragrances in sewage sludge, Water Res., 38 (2004), pp. 4075–4084.

[115]   J.L. Santos, I. Aparicio, E. Alonso, Occurrence and risk assessment of pharmaceutically active compounds in wastewater treatment plants: a case study: Seville city (Spain), Environ. Int., 33 (2007), pp. 596–601.

[116]   C. Miege, J.M. Choubert, L. Ribeiro, M. Eusebe, M. Coquery, Removal efficiency of pharmaceuticals and personal care products with varying wastewater treatment processes and operating conditions – conception of a database and first results, in: Kohl, Andrea (Ed.), Proceedings in Fifth IWA Specialized Conference on Assessment and Control of Micropollutants/Hazardous Substances in Water. Micropol & Ecohazard. DECHEMA e.V., Frankfurt/Main, Germany, 2007, pp. 220–225.

[117]   R.L. Meyrs, The 100 Most Important Chemical Compounds: A Reference Guide, 2007.

[118]   P.H. Roberts, K.V. Thomas, The occurrence of selected pharmaceuticals in wastewater effluent and surface waters of the lower Tyne catchment, Sci. Total Environ., 356 (2006), pp. 143–153.

[119]   F. Méndez-Arriaga, R.A. Torres-Palma, C. Pétrier, S. Esplugas, J. Gimenez, C. Pulgarinm Ultrasonic treatment of water contaminated with ibuprofen, Water Res., 42 (2008), pp. 4243–4248.

[120]   F. Méndez-Arriaga, S. Esplugas, J. Giménez, Degradation of the emerging contaminant ibuprofen in water by photo-Fenton, Water Res., 44 (2010), pp. 589–595.

[121]   R.K. Szabó, Cs. Megyeri, E. Illés, K. Gajda-Schrantz, P. Mazellier, A. Dombi, Phototransformation of ibuprofen and ketoprofen in aqueous solutions, Chemosphere, 84 (2011), pp. 1658–1663.

[122]   M. Pérez, F. Torrades, X. Domènech, J. Peral, Removal of organic contaminants in paper pulp effluents by AOPs: an economic study, J. Chem. Technol. Biotechnol., 77 (2002), pp. 525–532.

[123]   R. Andreozzi, V. Caprio, A. Insola, R. Marotta, R., Advanced oxidation processes (AOP) for water purification and recovery, Catal. Today, 53 (1999), pp. 51–59.

[124]   R.H. Waldemer, P.G. Tratnyek, R.L. Johnson, J.T. Nurmi, Oxidation of chlorinated ethenes by heat-activated persulfate: kinetics and products, Environ. Sci. Technol., 41 (2007), pp. 1010–1015.

[125]   A.E. Kabeel, S.A. El-Agouz, Review of researches and developments on solar stills, Desalination, 276 (2011), pp. 1–12.

[126]   M.M. Huber, S. Canonica, G.Y. Park, U.V. Gunten, Oxidation of pharmaceuticals during ozonation and advanced oxidation processes, Environ. Sci. Technol., 37 (2003), pp. 1016–1024.

[127]   A. Tsitonaki, B.F. Smets, P.L. Bjerg, Effects of heat-activated persulfate oxidation on soil microorganisms, Water Res., 42 (2008), pp. 1013–1022.

[128]   V.C. Mora, J.A. Rosso, G.C. Le Roux, D.O. Mártire, M.C. Gonzalez, Thermally activated peroxydisulfate in the presence of additives: a clean method for the degradation of pollutants, Chemosphere, 75 (2009), pp. 1405–1409.

[129]   K.C. Huang, R.A. Couttenye, G.E. Hoag, kinetics of heat-assisted persulfate oxidation of methyl ter-butyl ether (MTBE), Chemosphere, 49 (2002), pp. 413–420.

[130]   T. Ishimoto, R. Nagumo, T. Ogura, T. Ishihara, B. Kim, A. Miyamoto, M. Koyamaa, Chemical degradation mechanism of model compound, $CF_3(CF_2)_3O(CF_2)_2OCF_2SO_3H$, of PFSA polymer by attack of hydroxyl radical in PEMFCs, J. Electrochem. Soc. 157 (2010) B1305-B1309.

[130]   T. Kosjek, E. Heath, A. Krbavcic, Determination of non-steroidal anti-inflammatory drug (NSAIDs) residues in water samples, Environ. Int. 31 (2005) 679-685.

[131]   J.L. Zhoua, Z.L. Zhanga, E. Banks a, D. Grovera, J.Q. Jiangb, Pharmaceutical residues in wastewater treatment works effluents and their impact on receiving river water, J. Hazard. Mater. 166 (2009) 655-661.

[132]   M. Isidori, Ma. Lavorgna, A. Nardelli, A. Parrella, L. Previtera, M. Rubino, Ecotoxicity of naproxen and its phototransformation products, Sci. Total Environ. 348 (2005) 93-101.

[133]   Ma, G. Liu, W. Lv, K, Yao, X. Zhang, H. Xiao, Photodegradation of naproxen in water under simulated solar radiation: mechanism, kinetics, and toxicity variation, Environ. Sci. Pollut. Res. Int. 13 (2014) 7797-804.

[134]   F. Javier Benitez, J.L. Acero, F.J. Real, G. Roldán, Ozonation of pharmaceutical compounds: Rate constants and elimination in various water matrices, Chemosphere 77 (2009) 53-59.

[135]   J. Im, J. Heo, L.K. Boateng, N. Her, J.R.V. Flora, J. Yoon, K. Zoh, Y. Yoon, Ultrasonic degradation of acetaminophen and naproxen in the presence of single-walled carbon nanotubes, J. Hazard. Mater. 254-255 (2013) 284-292.

[136]   E. Felis, D. Marciocha, J. Surmacz-Gorska, K. Miksch, Photochemical degradation of naproxen in the aquatic environment, Water Sci Technol. 12 (2007) 281-286.

[137]   B. Zheng, Z. Zheng, J. Zhang, Q. Liu, J. Wang, X. Luo, L. Wang, Degradation kinetics and by-products of naproxen in aqueous solutions by gamma irradiation, Environ. Eng. Sci. 29 (2012) 386-391.

[138]   M. Qurie, M. Khamis, F. Malek, S. Nir, S. A. Bufo, J. Abbadi, L. Scrano, R. Karaman. Stability and removal of naproxen and its metabolite by advanced membrane wastewater treatment plant and micelle-clay complex, Clean - Soil, Air, Water 41 (2013) 1-7.

[139]   F.J. Benitez, J.L. Acero, F.J. Real, G. Roldan, F. Casas, Comparison of different chemical oxidation treatments for the removal of selected pharmaceuticals in water matrices, Chem. Eng. J. 168 (2011) 1149-1156.

[140]   L. Rein, A. Welch, Toxicity of Combinations of Naproxen and its Photodegradants to Toad Tadpoles. Society for integrative and comparative biology, College of Charleston, Meeting Abstract, P3.100, 2015.

[141]   A. Long, Y. Lei, H. Zhang. In situ chemical oxidation of organic contaminated soil and groundwater using activated persulfate process. Prog. Chem. 26 (2014) 898-908.

[142]   D. Zhao, X. Liao, X. Yan, S.G. Huling, T. Chai, H. Tao, Effect and mechanism of persulfate activated by different methods for PAHs removal in soil, J. Hazard. Mater. 254-255 (2013) 228-235.

[143]   X.R. Xu, X.Z. Li, Degradation of azo dye Orange G in aqueous solutions by persulfate with ferrous ion, Sep. Purif. Technol. 72 (2010) 105-111.

[144]   P. Rao, M.S.H. Mak, T. Liu, K.C.K. Lai, I.M.C. Lo, Effects of humic acid on arsenic(V) removal by zero-valent iron from groundwater with special references to corrosion products analyses, Chemosphere 75 (2009) 156-162.

[145]   S. Selkea, M. Scheurella, M.R. Shahb, H. Hühnerfussa, Identification and enantioselective gas chromatographic mass-spectrometric separation of O-desmethylnaproxen, the main metabolite of the drug naproxen, as a new environmental contaminant, J. Chromatogr. A, 1217 (2010) 419-423.

[146]   X. Wu, X. Gu, S. Lu, M. Xu, X. Zang, Z. Miao, Z. Qiu, Q. Sui, Degradation of trichloroethylene in aqueous solution by persulfate activated with citric acid chelated ferrous ion, Chem. Eng. J. 2014 (255) 585-592.

[147]   C. Gadipelly, A. Pérez-González, G.D Pharmaceutical industry wastewater: Review of the technologies.